

ALMA MATER STUDIORUM | UNIVERSITÀ DI BOLOGNA

**DOTTORATO DI RICERCA IN  
INGEGNERIA CIVILE, CHIMICA, AMBIENTALE E DEI MATERIALI**

CICLO | 30°

SETTORE CONCORSUALE | 08/A2

SETTORE SCIENTIFICO DISCIPLINARE | ING-IND 28

**INFRASTRUCTURE MAINTAINANCE  
AND COUNTERMEASURES PLANNING  
IN COMPLEX GEOLOGICAL  
AND GEOMORPHOLOGICAL SETTINGS**

PRESENTATA DA GIACOMO TEDESCO

COORDINATORE  
PROF. LUCA VITTOARI

SUPERVISORE  
PROF. STEFANO BONDUÀ  
CO-SUPERVISORE  
PROF.SSA LISA BORGATTI

ESAME FINALE ANNO 2018

Intentionally blank page

# INDEX

1	INTRODUCTION .....	1
2	SAN LORENZO TUNNEL .....	1
2.1	AREA GEOGRAPHY .....	1
2.2	STUDY SITE .....	3
2.3	GEOLOGICAL SETTINGS.....	5
2.4	HYDROLOGICAL SETTINGS.....	14
2.5	CLIMATE SETTINGS .....	19
2.6	PASSO DELLA MORTE LANDSLIDE.....	21
2.7	INFRASTRUCTURE .....	21
3	INVESTIGATION AND MONITORING.....	26
3.1	PRESENT WORK INVESTIGATIONS .....	26
3.2	SITE MONITORING.....	29
3.2.1	GNSS .....	30
3.2.2	SYNTHETIC APERTURE RADAR.....	30
3.2.3	INCLINOMETERS .....	31
3.2.4	PIEZOMETERS .....	33
3.2.5	INSTRUMENTED HYDRAULIC SECTIONS.....	34
3.3	STRUCTURAL HEALTH MOITORING .....	41
3.3.1	SAN LORENZO LINING SEGMENTS 26-29 .....	41
3.3.2	DRAINAGE TUNNEL LINING .....	45
4	MATERIAL CHARACTERIZATION.....	46
4.1	LAB TESTING .....	46
4.1.1	SAMPLES CORING .....	48
4.1.2	SOUND WAVE VELOCITY.....	49
4.1.3	UNIAXIAL COMPRESSIVE STRENGTH AND ELASTIC PARAMETERS.....	50
4.1.4	TRIAXIAL TEST.....	54
4.1.5	TENSILE STRENGTH .....	55
4.1.6	X-RAY DIFFRACTION.....	55
5	SLOPE MODEL .....	57
5.1	SLIP SURFACE SIMULATION STRATEGY .....	57
5.2	MODEL DEFINITION.....	58
5.3	SENSITIVITY ANALISYS .....	62
5.4	FINAL MODEL.....	67
6	CONCLUSIONS .....	72
6.1	PROPOSED COUNTERMEASURES .....	72
7	REFERENCES .....	75

8	APPENDIX .....	79
8.1	CONDUITS AND DRAINAGE TUNNEL WATER DISCHARGE .....	79
8.2	INSRUMENTATION INSTALLED SINCE 1999.....	81
8.3	SAN LORENZO LAYBY STANDARD SECTION.....	83
8.4	X RAY DIFFRACTION.....	84
8.5	SAN LORENZO MONITORING HOMEPAGE.....	85
8.6	SENSITIVITY ANALYSIS DISPLACEMENTS.....	86

# FIGURES INDEX

Figure 2-1 Geographical map.....	2
Figure 2-2 Commemorative stone of the Passo della Morte ambush at the old tunnel entrance.....	3
Figure 2-3 1910s and nowadays, it can be see the original NR52 route blasted as consequence of Caporetto retreat.....	3
Figure 2-4 Sancrovint post-glacial landslide in the neighborhood of Passo della Morte: on the left (A) an aerial view, on the right (B) the deposit of coarse debris deluged by the Tagliamento river bank erosion .....	4
Figure 2-5 Simplified geological-geomorphological map (modified after Marcato 2007) .....	6
Figure 2-6 Geological-geomorphological map legend (modified after Marcato 2007) .....	7
Figure 2-7 Stratigraphic column (modified after Marcato 2007) .....	8
Figure 2-8 Geomorphological map legend (modified after Marcato 2007) legend in Figure 2-6.....	10
Figure 2-9 Geological section AA' (modified after Marcato 2013) .....	11
Figure 2-10 Geological section BB' (modified after Marcato 2013) .....	11
Figure 2-11 Geological section FF' (modified after Marcato 2013) .....	12
Figure 2-12 Cima Corso landslide, Passo della Morte is the nowadays active portion .....	13
Figure 2-13 Landslides mapped at Passo della Morte area.....	14
Figure 2-14 Hydrological map .....	16
Figure 2-15 Hydro-geological section AA' .....	17
Figure 2-16 Lefranc test in G4I borehole.....	18
Figure 2-17 Climate setting at Passo della Morte, from the top: daily temperature, snow cover, cumulated and hourly rainfall .....	20
Figure 2-18 Passo della Morte landslide evolution .....	21
Figure 2-19 San Lorenzo (NR52) road tunnel standard section.....	22
Figure 2-20 Drains pattern into the drainage tunnel .....	24
Figure 2-21 On the left: damage on concrete lining at pk 300 (segments from 26 to 29) after the heavy rainfall event on late 1996. On the right: a 3D reconstruction of the crack in the final lining at segment 27-29 (2012 photos) .....	25
Figure 3-1 Instrumentation installed since 1999 .....	26
Figure 3-2 Discontinuities mapped in the landslide area (2016 field survey) .....	27
Figure 3-3 Survey of the dolomite pillars area. From the top: photogrammetric survey on left (A), open fractures on right (B), pics localization (middle-left), sinkholes (C), severely fractured area in the I20 neighborhoods (D), open fracture (E).....	28
Figure 3-4 Monitoring network directly used in the current study.....	29
Figure 3-5 GPS benchmarks displacement (2002-2018).....	30
Figure 3-6 GB-InSAR displacements (campaign 2004-2005) [2].....	31
Figure 3-7 I-16 displacements and P20 groundwater table level (2012-2018) .....	32
Figure 3-8 Correlation between slip surface deformation and severe fractured rock mass water discharge .....	32
Figure 3-9 P20 and P23 water tables rising after the heavy rainfall on November 2014 and slope movement activations (I-16 on landslide 3, I-15 on landslide 2) .....	33
Figure 3-10 I-20 and P-20 water tables (2017-2018).....	34
Figure 3-11 Severely fractured rock-mass and San Lorenzo conduits discharge (2014-2018) .....	36
Figure 3-12 Spring pk 857 m water discharge.....	37
Figure 3-13 From the top: cumulated rainfall, electric conductivity at spring pk 857, at drainage adit, into San Lorenzo tunnel, hourly rainfall (black) and snow cover (red). For the location, see Figure 3-4. ....	39
Figure 3-14 Inspection of the tunnel lining wetting condition, classified in wet, moist and dry.....	40
Figure 3-15 Structural monitoring on lining segments 26-29 of the San Lorenzo tunnel .....	41

Figure 3-16 Monitoring instruments at tunnel lining segment 26-29. Clockwise: crackmeter F23 on lining joint, (B) crackmeter F06 on the roof, (C) clinometer C03 on the roof, optical fiber on the roof (D), reference fiber loop installation loop (E) .....	42
Figure 3-17 Deformations in the road tunnel lining. Instruments are grouped by the displacements magnitude, up to 0.2 mm (A), 0.6 mm (B) and 8 mm (C, 2014-2018. Screenshot of the online monitoring portal).....	43
Figure 3-18 Rotations in the road tunnel lining. Top-down: (A) rotations perpendicular to the tunnel axis, (B) rotations parallel to the tunnel axis (2014-2018. Screenshot of the online monitoring portal).....	44
Figure 3-19 Proposed static scheme of the tunnel lining at the landslide crossing (segments 26-29) .....	44
Figure 3-20 Structural monitoring in the drainage tunnel lining.....	45
Figure 3-21 Deformations in the drainage tunnel lining (2017-2018. Screenshot of the online monitoring portal).....	45
Figure 4-1 G6P (P10) core log boxes and testing localizations .....	47
Figure 4-2 Unit weight.....	48
Figure 4-3 Sample coring: a visible lens of water sensitive material (left), muddy drilling fluid, i.e. water (right).....	48
Figure 4-4 Open fracture in a dolomite specimen intercepted during coring stage .....	49
Figure 4-5 Sound wave velocity .....	49
Figure 4-6 Young modulus calculated with different formulae and derived from lab testing.....	50
Figure 4-7 Uniaxial Compressive Strength.....	51
Figure 4-8 Uniaxial compression tests equipped with strain gauges .....	52
Figure 4-9 Uniaxial test on dolomite (A) and chaotic silty clay (B) .....	53
Figure 4-10 Poisson ratio .....	53
Figure 4-11 Triaxial test .....	54
Figure 4-12 Tensile strength from indirect (Brazilian) test .....	55
Figure 4-13 Indirect tensile test (Brazilian) sample failures. Developed ruptures look completely (A) or partially (B) not dependent from the cemented cracks. ....	55
Figure 4-14 Disturbance zones around an underground opening (by Perras & Diederichs [53])....	56
Figure 4-15 Mineralogy by X ray diffraction analysis of sample from G4I borehole (depth 4 m)....	56
Figure 5-1 Slip surface intercepted during the drainage tunnel excavation, note the thickness of 2 m ca.....	58
Figure 5-2 Inclinomometer S2N (same location I-16) .....	59
Figure 5-3 Interface elements in Flac3D: rheological scheme (after Flac3D manual [54], A) and present model application (B) .....	60
Figure 5-4 Flac3D grid (mesh) construction details .....	61
Figure 5-5 Comparison between geological and modeled sections.....	62
Figure 5-6 Sensitivity analysis on the landslide slip surface, i.e. interface elements.....	63
Figure 5-7 Sensitivity analysis on the landslide body materials .....	64
Figure 5-8 Sensitivity analysis on general model settings .....	65
Figure 5-9 Weathered chaotic silty clay material at the Passo della Morte slip surface daylighting at the landslide toe.....	67
Figure 5-10 Displacements pre (A) and post (B) an extreme rainfall event, i.e. slip surface dry (A) and wet (B) .....	68
Figure 5-11 Section including I16 as reference, displacements pre (A) and post (B) an extreme rainfall event, i.e. slip surface dry (A) and wet (B) .....	69
Figure 5-12 Simulated displacement profiles at I16.....	70
Figure 5-13 Activation phases.....	71
Figure 6-1 Drainage tunnel effect: water table level at P23, landslide 2 area .....	72
Figure 6-2 Dewatering expected effectiveness of the drainage tunnel extension .....	73
Figure 6-3 Proposed countermeasure works.....	74

Figure 8-1 Conduits discharge (2014-2018).....	79
Figure 8-2 Drainage adit discharge (2014-2018).....	80
Figure 8-3 San Lorenzo tunnel standard layby section.....	83
Figure 8-4 X ray diffraction on G4I sample.....	84
Figure 8-5 Home-page of the CNR-ANAS monitoring online portal.....	85
Figure 8-6 Sensitivity analysis absolute displacements. Top-down: on slip surface (interface) and landslide body properties.....	86
Figure 8-7 Sensitivity analysis absolute displacements on model settings variation.....	87

## TABLE INDEX

Table 2-1 Permeability classes.....	17
Table 3-1 Pre-web portal displacement recorded by CNR in place inclinometers.....	32
Table 4-1 Calculated friction angle and cohesion from triaxial test data interpretation.....	54
Table 5-1 Slip surface reference points at Passo della Morte (Figure 3-1 and Figure 3-4).....	57
Table 5-2 Mesh (grid) regions settings.....	60
Table 5-3 Material properties used in Flac3D modeling.....	66
Table 8-1 Instrumentation installed, since 1999.....	81

# 1 INTRODUCTION

This dissertation presents the geological, hydro-geological and geo-mechanical characterization of a large landslide threatening a strategic infrastructure.

In the second chapter, the studied site is widely described. Site geography and strategic relevance of the valley segment is explained. The geological settings of the area are described together with the groundwater circulation. The landslide phenomenon is then reported, followed by the local climate settings. The remaining sections treat about the infrastructure.

The third chapter the monitoring instrumentation installed at Paso della Morte is listed. Inclinerometers and piezometers measures are compared in order to find a correlation between extreme rainfalls, rapid snowmelt events and landslide activation. A specific section treats the topographic benchmarks displacements.

Fourth, the lab tests carried out on the slope materials is presented. Initially, the borehole selection is explained. Triaxial, uniaxial, point load, Brazilian and sound wave velocity tests results are presented in a subsection each. The chapter is closed by a mineralogical analysis, which support other assumption done in the modeling related to the slip surface properties.

In the fifth chapter, the numerical simulations done are presented. Initially, the slip surface geometrical construction is shown. Then, a slip surface modelling strategy using no-thick elements is explained. The sensitivity analysis carried out on the model settings and mechanical parameters is later discussed in a specific subsection. Finally, a comparison between calculated and measured displacements is done.

In the end, a series of countermeasure works are proposed based on the field observation, monitoring data and numerical simulation results.

## 2 SAN LORENZO TUNNEL

### 2.1 AREA GEOGRAPHY

Passo della Morte study area is a narrow pass in the Upper Tagliamento valley, between the municipalities of Forni di Sotto and Ampezzo (Figure 2-1). Those villages are part of the Udine province, which represent the most extended provincial district of the Friuli Venezia Giulia (FVG) Region, North-East of Italy.

The site is placed on the South slope of 2100 m-high mount Tinisa (Figure 2-1). This peak stays at the Northern edge of a series of relatively high crests evolving in North-West direction forming a kind of ridge, i.e. Mt. Zauf (2246 m a.s.l.), Mt. Bivera (2474 m) ending at Mt. Tiarfin (2413 m). The Sauris Lake is localized 8 km on North, its formation is due to a dam on the Lumiei stream built by Allied prisoner of war during the Second World War [1]. The main watercourse in the area is the Tagliamento River, which flows in the homonymous Valley just few hundred meters to the South of the site of interest. The Northern slopes of the Mt. Tinisa - Mt. Bivera ridge are facing on the Lumiei Valley.

In the segment of the Tagliamento valley object by this study, several areas affected by slope instability phenomena have been mapped [2] (Figure 2-13). The so-called Passo della Morte landslide is the principal active movement; it is classified as a rock block slide with an overall volume of 24million cubic meters. As a consequence of the Tagliamento glacier melting at the end of the last glacial age, the lacking of lateral support is considered a predisposing factor for the enhancement of landslide activity over this area. The presence of plastic clay substratum underlying rigid rock units, i.e. dolomite and limestone, plays a key role in the area geomorphological process. The conceptual model of the Passo della Morte landslide kinematics can be summarized in a cycle: the clay-rich units lose their strength when they are wettened; this causes deformation and displacement in the overlying dolomite rock mass [3].

The study area is crossed by the National Road 52 (NR52). Twenty years ago, the NR52 old route on the slope was abandoned because of sporadic rock falls threatened the vehicles and people. During 1990es, a new project moved the path of NR52 underground for around 2200 m, into the so-called San Lorenzo tunnel. Unfortunately, this road tunnel cross the Passo della Morte landslide. Since the construction phase, it was not possible guarantying a sufficient serviceability level because of frequent seepage and damage on the concrete structures (Figure 2-21) apparently caused by the Passo della Morte landslide(Figure 2-13). In early 2000s, parts of the lining were reconstructed in independent segment of 12 meters, which was heavily armored. The countermeasures included a drainage adit, running few meters on the North and 30 m below the San Lorenzo tunnel.

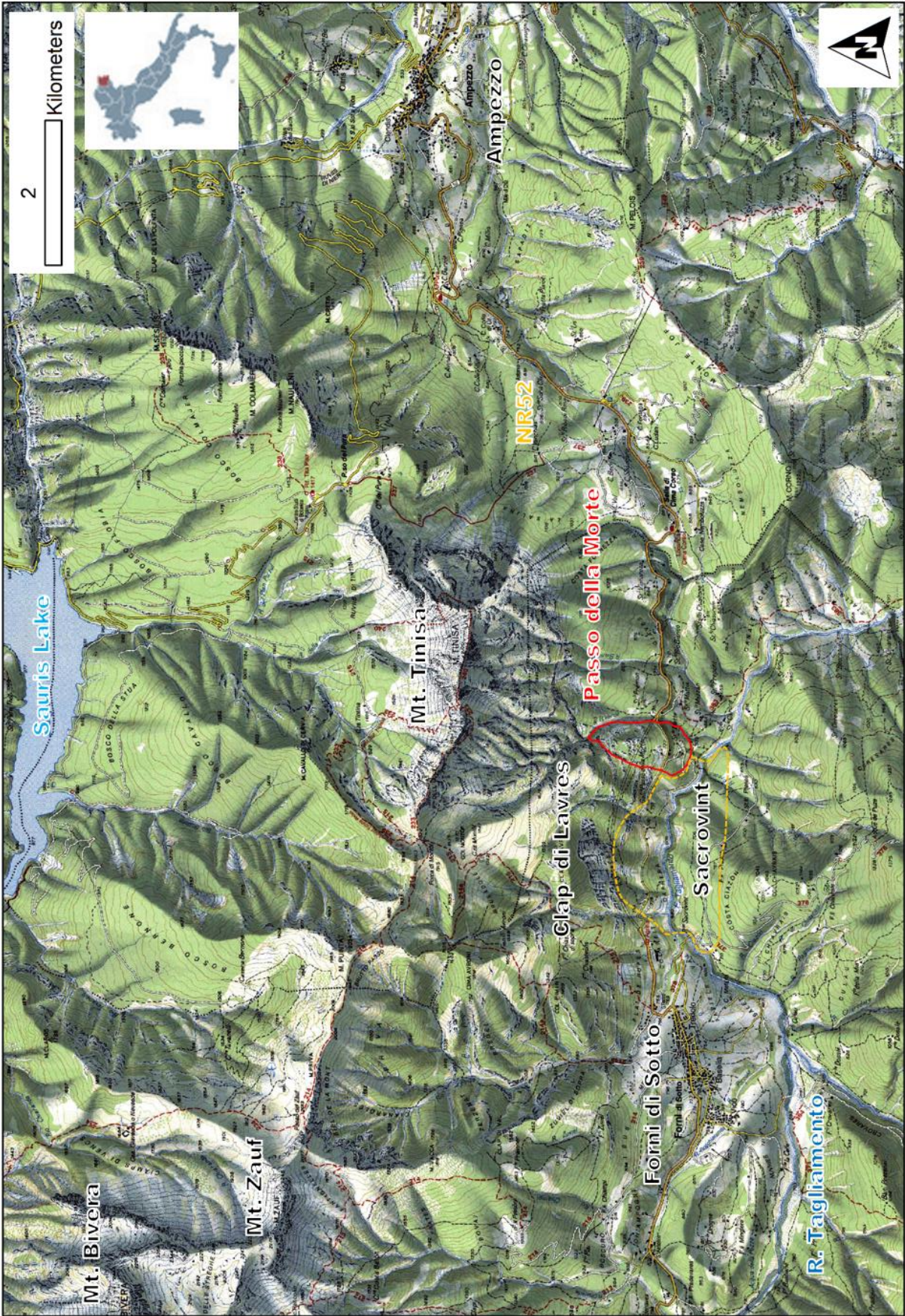


Figure 2-1 Geographical map

## 2.2 STUDY SITE

The Passo Morte slope is a well-studied landslide area. The Passo Morte – literally Death Pass - is so called referring to a death toll tribute by Austro-Hungarian soldiers during Italian Risorgimento. On 1848 May 24<sup>th</sup>, natives did an ambush breaking up with stones over a foreign soldiers column [4].



Figure 2-2 Commemorative stone of the Passo della Morte ambush at the old tunnel entrance

During the First World War, the original tunnel on the mountain side was demolished in order to slow down the Austrian advance after the Caporetto retreat on November 07<sup>th</sup>, 1917 [4].

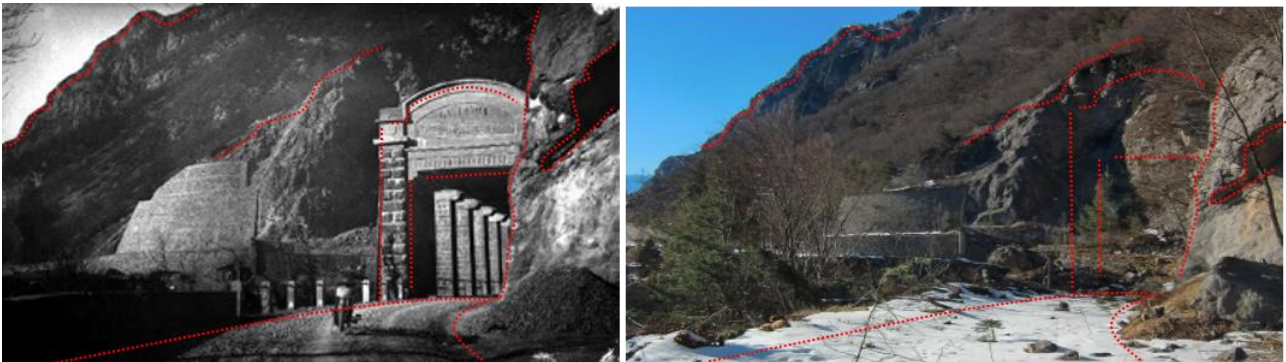


Figure 2-3 1910s and nowadays, it can be see the original NR52 route blasted as consequence of Caporetto retreat

In 1960s, Italy transferred wide powers to FVG regional administration due to the peculiar double National border with Austria and Slovenia. Considering its position, the regional infrastructures

played a strategic role in the regional and Italian security during the last century. Nowadays, that viability network is vector of economic growth both at local and international scales because of the commercial flow with the former Warsaw Pact countries.

Slope instability phenomena are reported all over the Carnic Alps valleys since many centuries ago. A famous slope failure nearby Passo della Morte site is the so-called Borta landslide, in the Tagliamento valley. According to the historical documents, during August 1692 an extremely rapid rockslide destroyed the Borta village causing more than 50 casualties [5]. An approximate definition of the pre-failure slope profile was possible thanks to a couple of paintings portraying the old settlement. Moreover, investigation on the actual deposits permitted an estimation of the rock volume involved. Studies on Borta events [6], [7], defined the geological setting as a predisposing factor, especially considering the down-slope bedding of the rock mass. A severe rainfall event after a wet season is suggested as the most probable triggering factor.

In front of Passo della Morte, on the right side of Tagliamento valley the so-called Marocca di Sacrovint is detected. This post-glacial landslide dammed the Tagliamento forming the so-called Forni Lake in the area of the present Forni di Sotto settlement. The Sacrovint deposits can be seen on scarified right flank of Tagliamento (Figure 2-1).

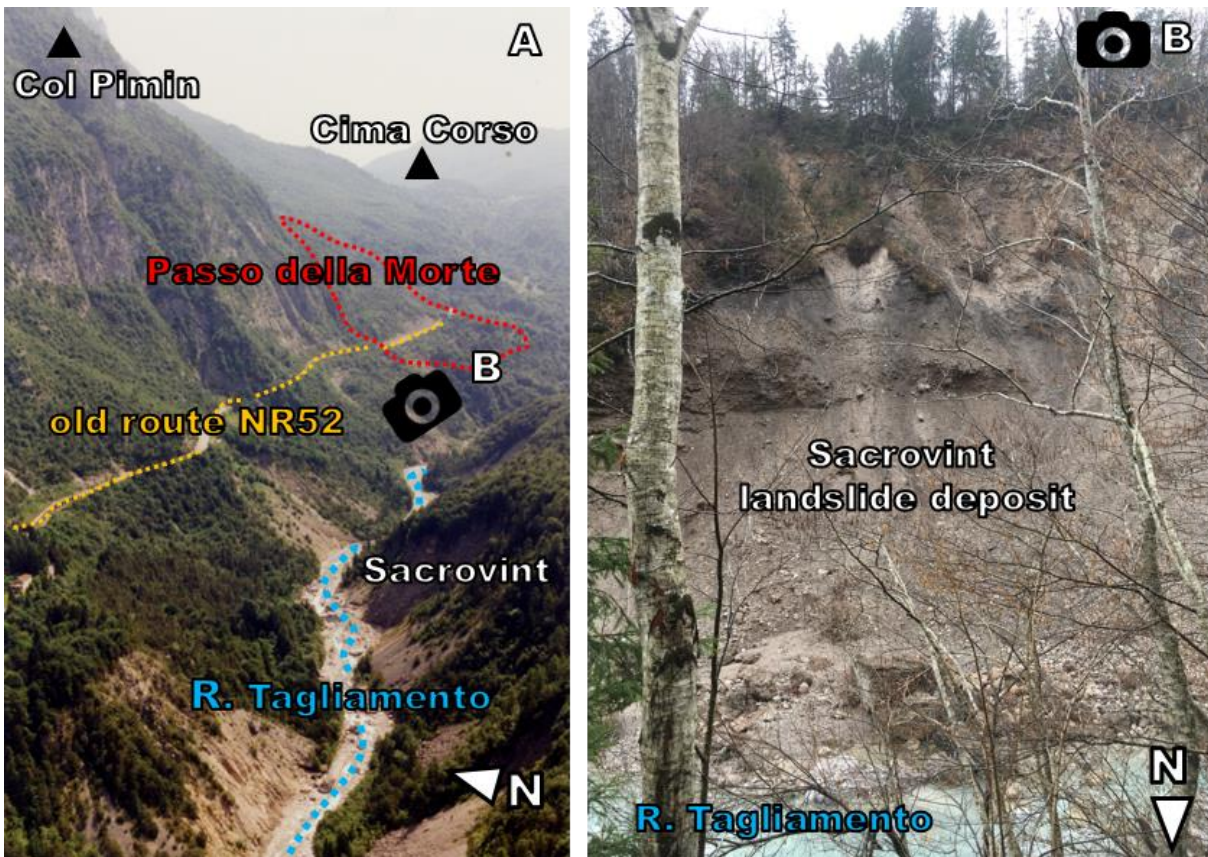


Figure 2-4 Sanacrovin post-glacial landslide in the neighborhood of Passo della Morte: on the left (A) an aerial view, on the right (B) the deposit of coarse debris delimited by the Tagliamento river bank erosion

Seismically induced landslides are recorded in Forni neighborhood. During the 1976 Friuli seismic series, a major earthquake event caused a deadly rock fall on the Bivera peak [8]. One of the fatalities was Professor Giulio Pisa, who studied the Carnian area for three decades resulting in detailed geological maps, sections and profiles [9].

## 2.3 GEOLOGICAL SETTINGS

Passo Della Morte is located in the upper Tagliamento valley in Carnian Alps. According to the International Standardized Mountain Subdivision of the Alps (ISMSA) classification [10], the study area is part of the Alpi Tolmezzine Occidentali, Bivera group.

The Carnic Alps are characterized by a North-South direction compressional thrust due to the Alpine orogenesis [11], [12]. The North-South thrust of the carbonatic units overlapped the pelitic units. A series of strike slip faults in NE-SW direction connected with the main stress are recognized in the area [13].

Locally, Quaternary deposits cover the Triassic basement. The Quaternary units result from the complex regional geomorphological process during Pleistocene and Holocene [2]. The deposits are composed of pre, sin and post-glacial debris, alluvial sediments, moraines and conglomerates.

Pisa published a series of stratigraphic sections of the Bivera area [9]. Starting from those profiles, Marcato [2] sketched the stratigraphic column representative of the Passo della Morte area. In his doctorate thesis, Marcato named the former Pisa units using the current terminology. Moreover, he modified the thickness of the Schlern dolomite bed in 300 meters.

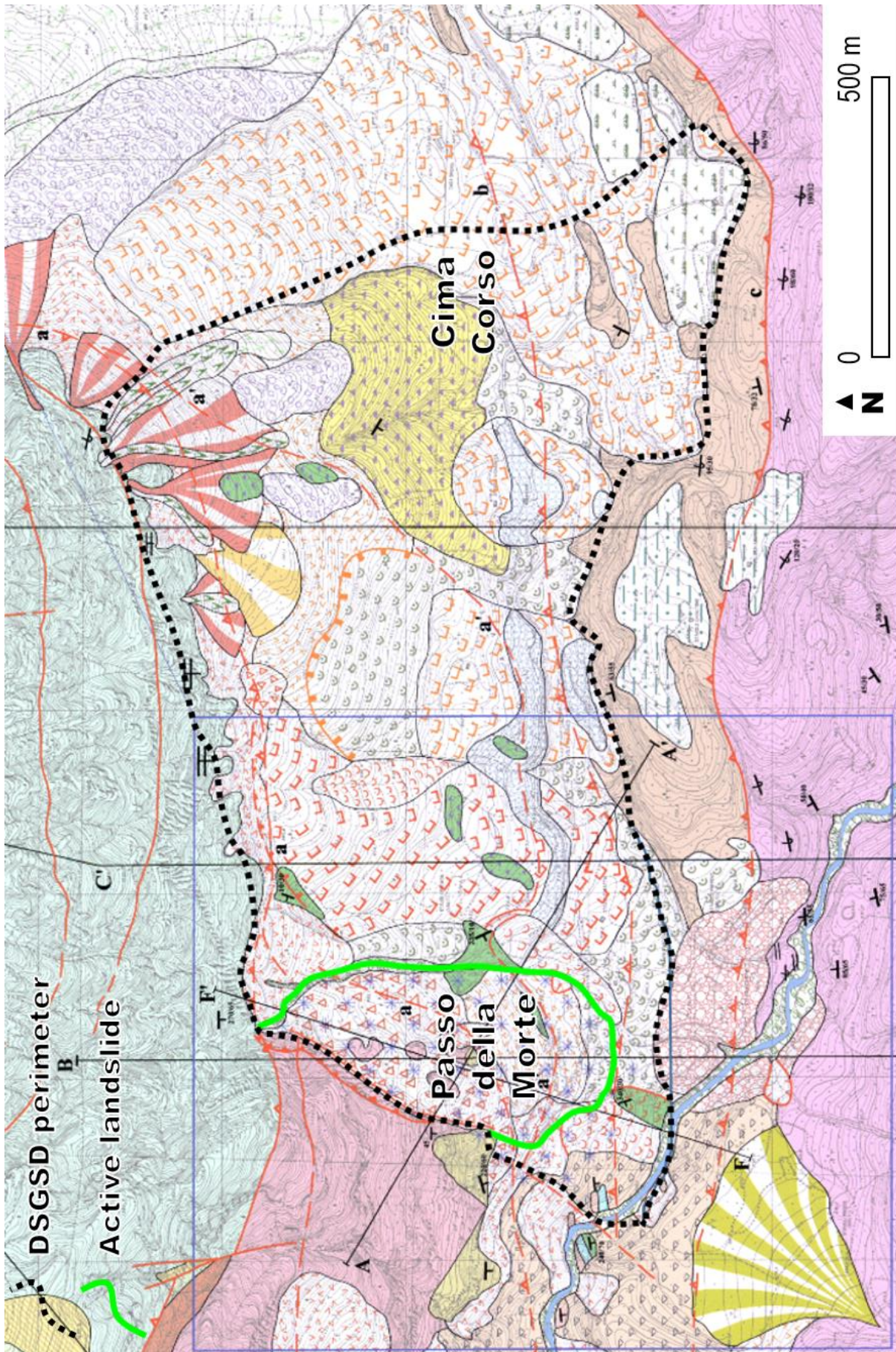


Figure 2-5 Simplified geological-geomorphological map (modified after Marcato 2007)

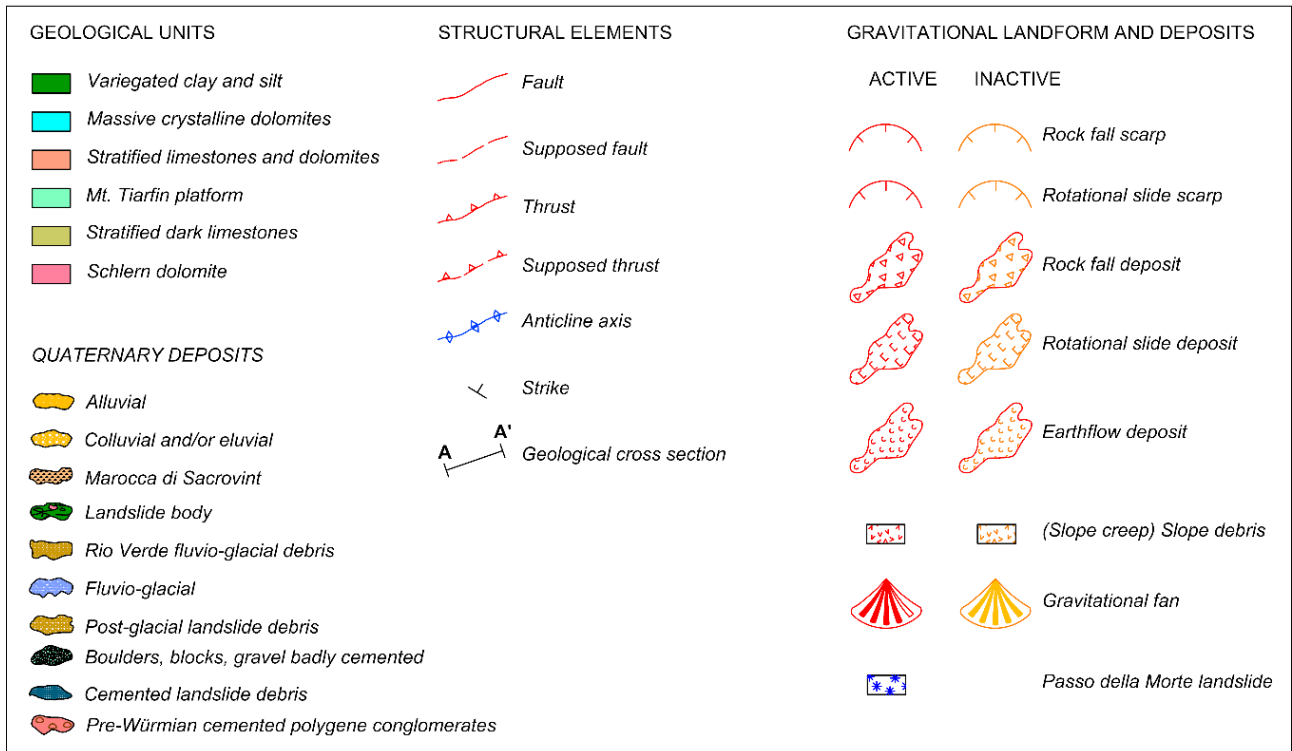


Figure 2-6 Geological-geomorphological map legend (modified after Marcato 2007)

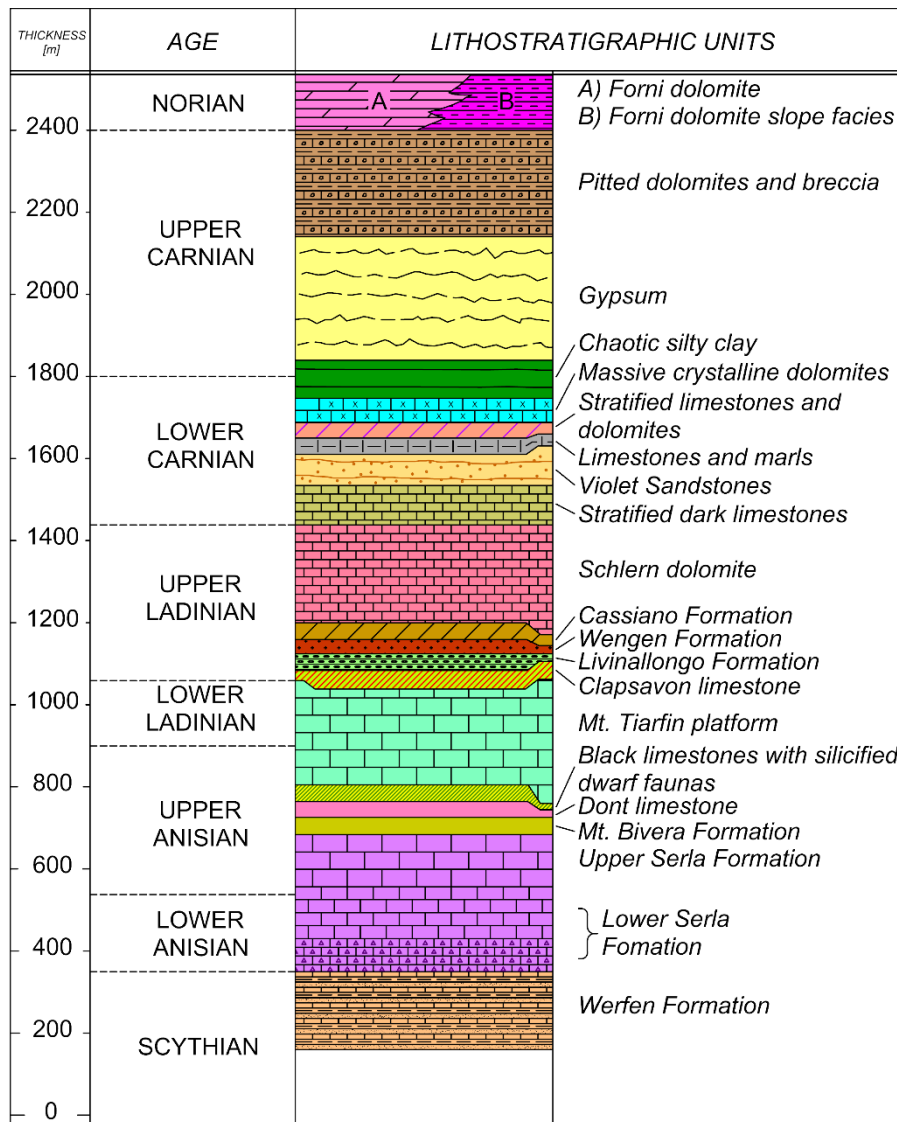


Figure 2-7 Stratigraphic column (modified after Marcato 2007)

The Schlern Dolomite is a massive rock formation of Upper Ladinian (Triassic period). This unit includes dolomite, dolomitic limestone and calcareous dolomite. The Schlern formation roof of the Sauris Line with a thickness ranging between 200 and 300 meters [2], [9], [13].

The stratified dark Limestone is an alternation of micritic limestone with levels ranging between 0.1 and 1 meter and dark marl up to 0.2 m thick. It covers the Schlern dolomitic platform as it can be seen in the Passo della Morte old tunnel. In that area, the limestone and dolomite are affected by active slope processes [14], [15]. The unit deposition occurred in Carnic epoch, reaching a thickness of 80-100 m ca.

Stratified Limestone and Dolomite were formed during the Carnian period. The units are a succession of dolomite, limestone and calcarenite with thin gray marly intercalations for a total thickness of 25 m.

The massive crystalline dolomite is a 10 m layer of compact light grey doloarenite on the top of the Stratified Limestone and dolomite units. Estimated age is Carnian.

The chaotic silty Clay is a characteristic reddish claystone with presence of arenaceous layers of thickness lower than 1 meter. The color is the distinctive element of this Carnian age unit. Some up to 10 cm intercalations of massive whitish-gray marly dolomite can be found.

The Gypsum is an Upper Carnian unit with the presence of clayey dark layers or inclusions.

Pitted Dolomite is an Upper Carnian unit made by gray marly dolomite and light-tone dolomite and dolomitic marl.

Forni Dolomite consists of dolomite and dark marly dolomite in thin layers up to a decimeter. Organic material can be detected in the marl levels characterizing the unit. Formation assumed during the Noric age.

Quaternary deposits mapped in the Passo della Morte area include: alluvial deposits, glacial moraine, polygenic conglomerates, slope debris and the chaotic deposits of late-glacial landslide, i.e. Marocca di Sacrovint, characterized by various degrees of cementation.

The main tectonic feature detected in the area is the so-called Sauris line [13]; it is classified as a tectonic dislocation due to Neogenic deformation influenced by the Triassic extension [2]. The Sauris line is also characterized by a number of extensive conjugated East-West structures.

The Sauris line is detected in the upper Tagliamento valley. This low angle overthrust is characterized by Upper Ladinian and Carnian units (Schlern Dolomite and Stratified dark limestone) overlapping the most recent Upper Carnian units (Gypsum and Chaotic silty clay).

Some Authors suggested that the direction change of the Sauris line at the Passo della Morte can be due to its intersection with a conjugated N-S directed strike fault system [2].

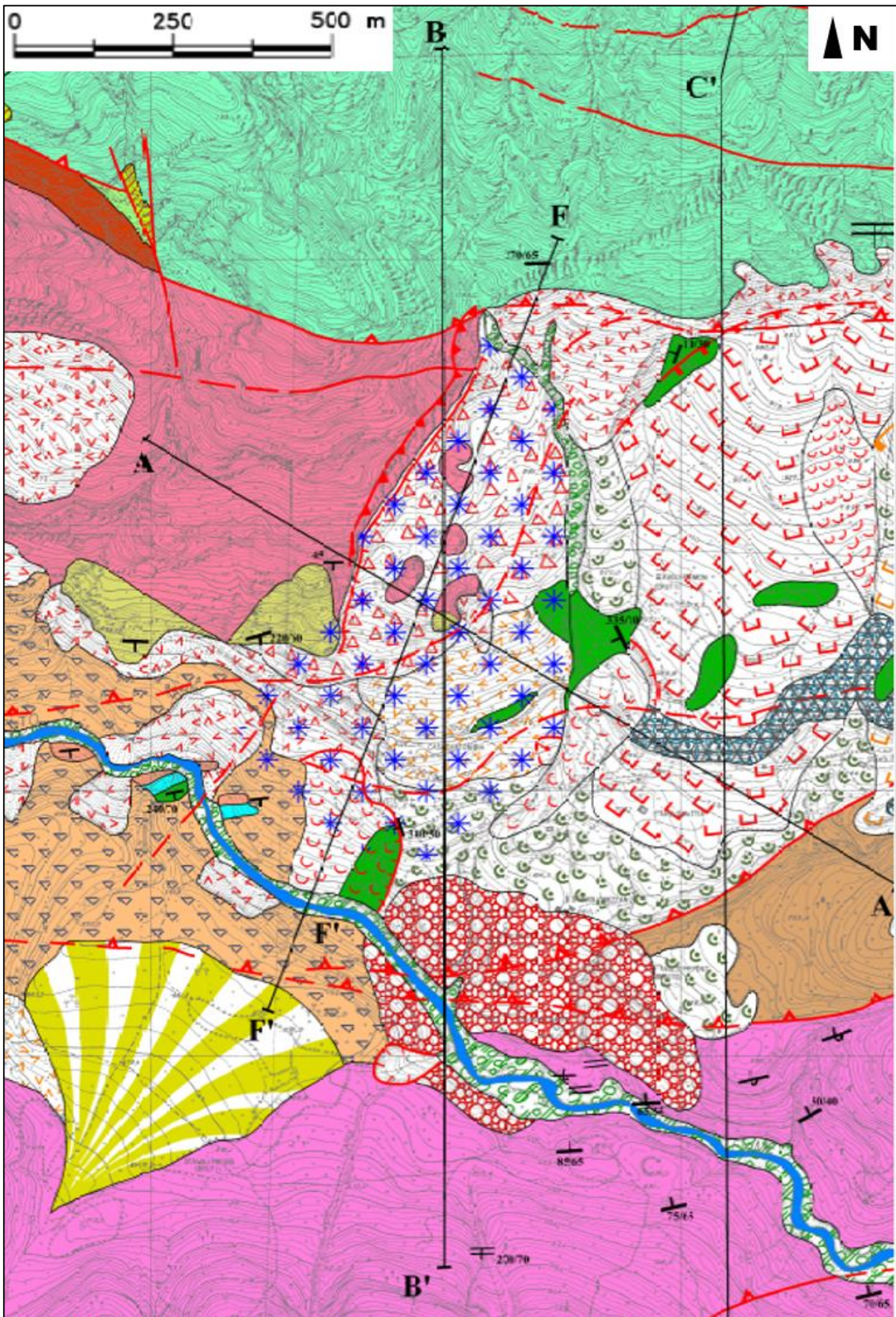


Figure 2-8 Geomorphological map legend (modified after Marcato 2007) legend in Figure 2-6

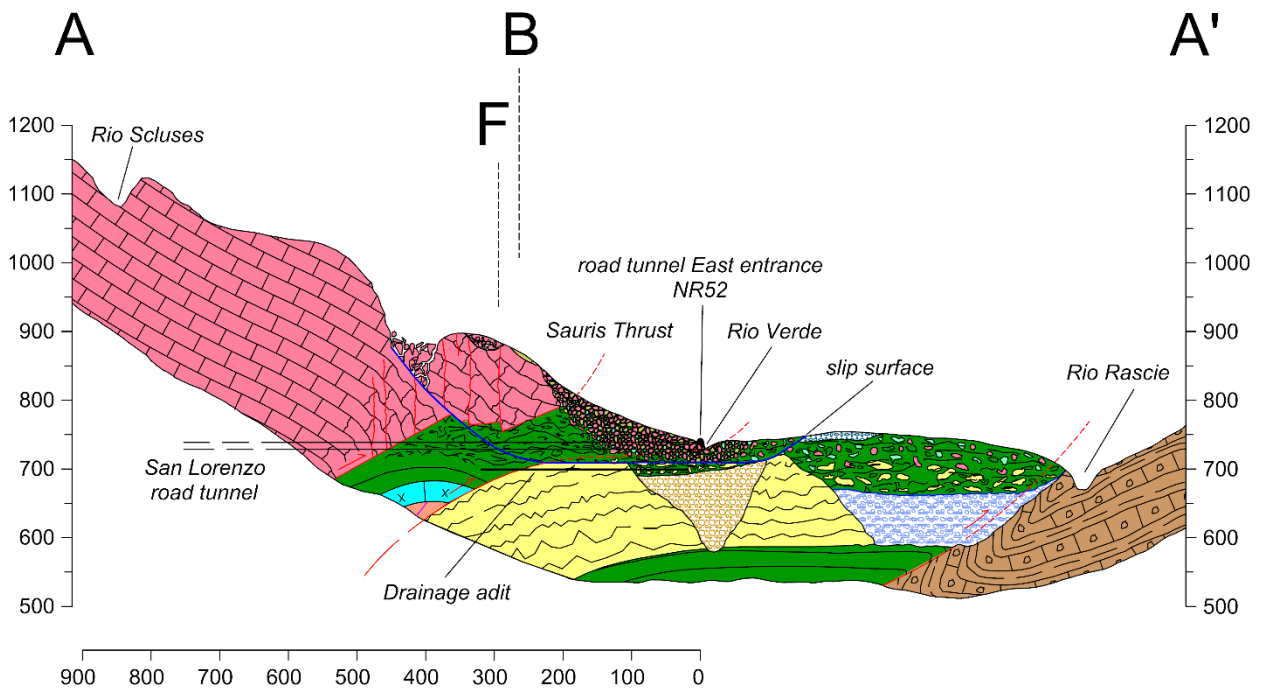


Figure 2-9 Geological section AA' (modified after Marcato 2013)

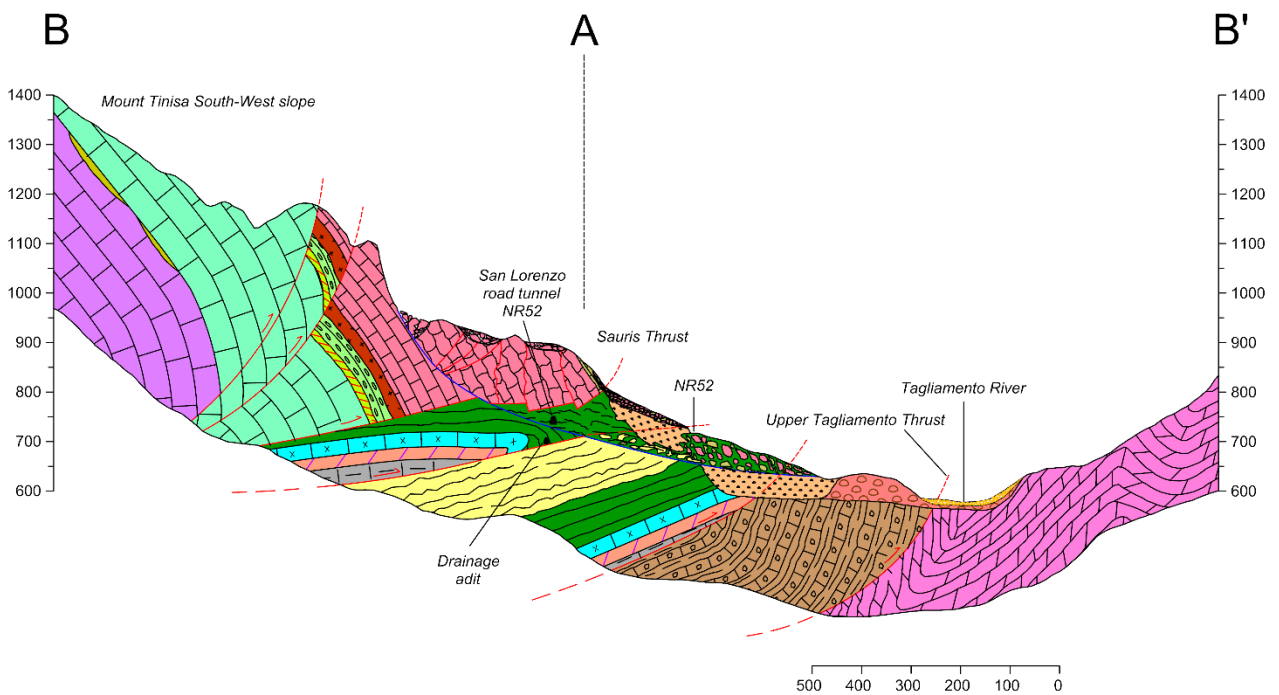


Figure 2-10 Geological section BB' (modified after Marcato 2013)

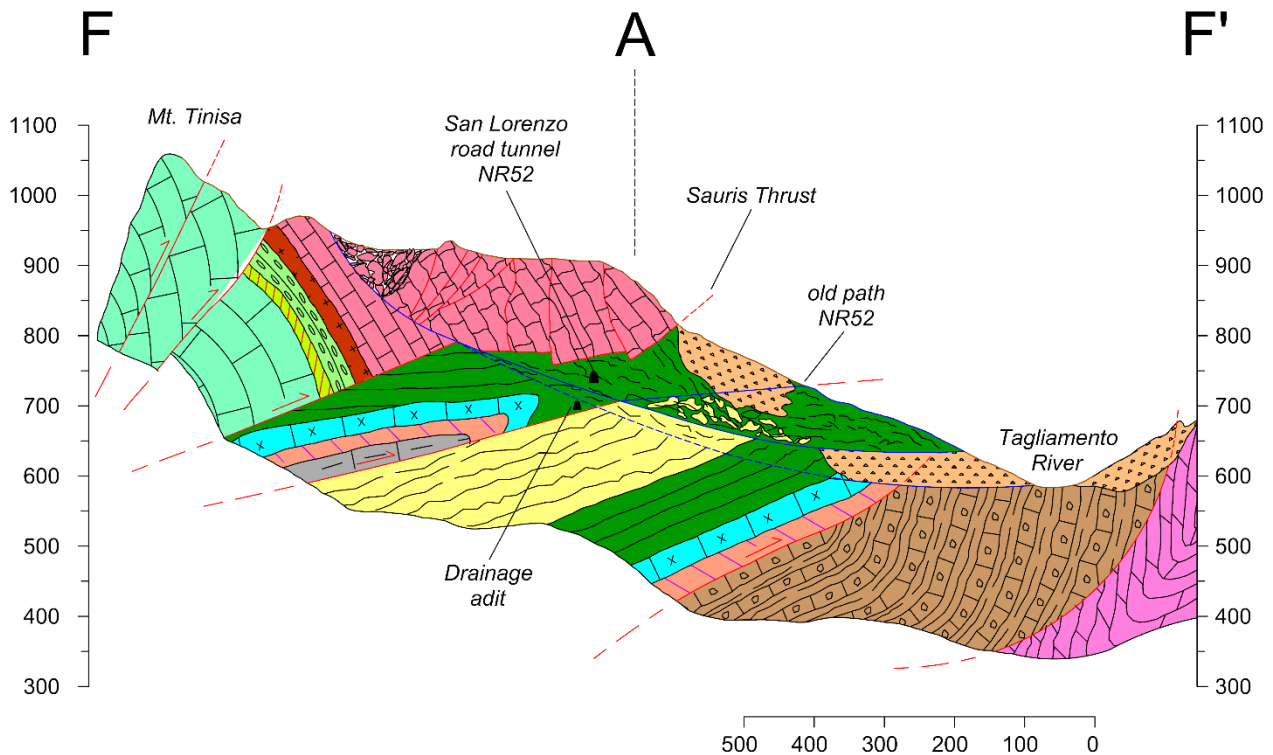


Figure 2-11 Geological section FF' (modified after Marcato 2013)

The geological section AA' (Figure 2-9) highlights another a further tectonic dislocation, which is responsible for the intermingling of gypsum and clay-rich units ([2]).

An important tectonic feature, the so-called Upper Tagliamento line, is mapped in the area. This regional South-verging structure is developed in East-West direction. At site scale, the Upper Tagliamento line brings in contact the dolomite with the most recent Forni dolomite. The Tagliamento riverbed is almost aligned with this overthrust, in the geological section AA'.

A series of minor lines is detected in the Passo della Morte area developing in approximately North-South direction [2]. Two of them are mapped in the Southern part of the Tagliamento Valley [16].

The regional Neogenic tectonic activity is considered to be on going [17]. Evidence of an evolving situation is the 1976 seismic sequence with epicenters in Gemona - Osoppo – Venzone, about 30 km South-East of the studied site, and the powerful event of Richter magnitude 6.4.

The sharp scars on the valley slopes due to streams flowing are index of a generalized uplift of the region. Generally, those tributaries have a very step and irregular path with axis perpendicular to the Tagliamento River flowing in the Valley bottom.

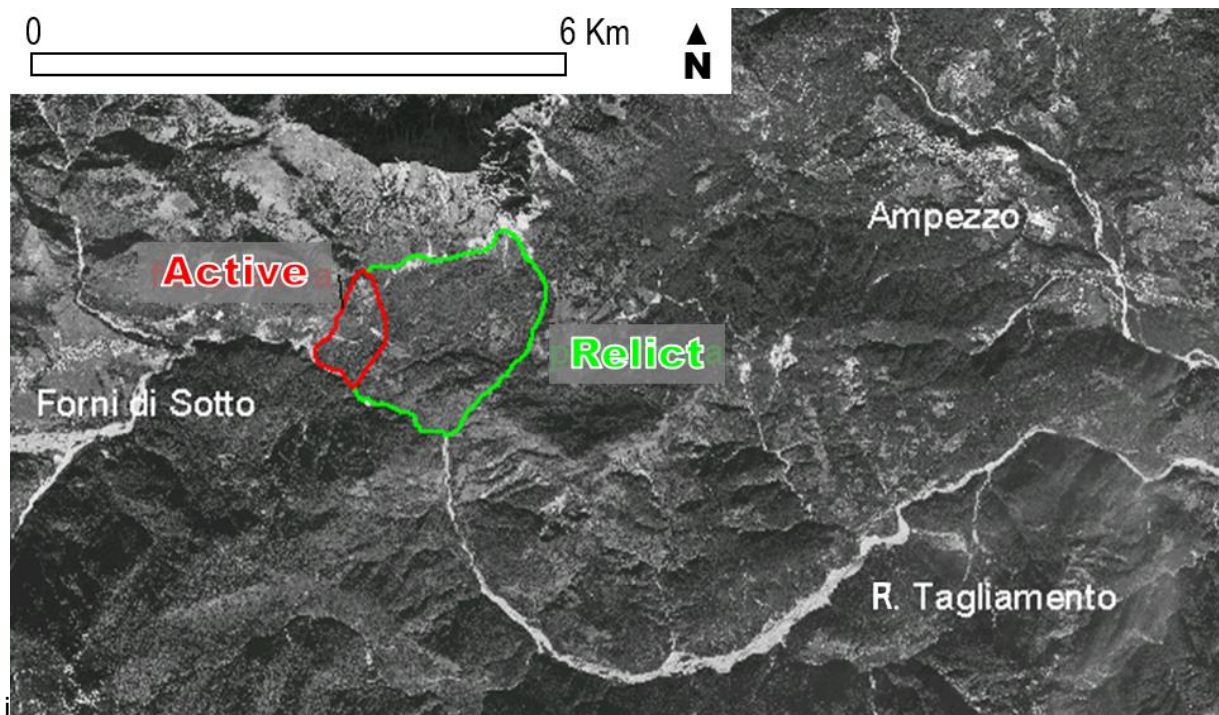


Figure 2-12 Cima Corso landslide, Passo della Morte is the nowadays active portion

The gradual balance restoration of the Upper Tagliamento valley slopes after the last glacial age represents an important geomorphological driving factor. The progressive melting of a 1000 meters thick ice mass caused a lack of lateral support for the slopes leading to several landslide and potential unstable phenomena. During the Pleistocene glacial phase, the ice reached an elevation up to 1,600 m above the sea level, which means that just few peaks were rise up the ice curtain, i.e. Mt. Tinisa and Mt. Bivera. An higher susceptibility to landslide is detected in narrowing valley sections where the glacier forked, such as in the Forni di Sotto' neighbors [3].

The support removal due to glacier regression [18] is the cause of the Marocca (Friulan dialectal word for landslide) di Sacrovint [2], extended from Passo della Morte to Cima Corso on East. As clear by aerial photo, the Marocca di Sacrovint is an impressive gravitational phenomenon detached from Clap di Lavres - Mt. Tinisa area. This event entailed the Tagliamento River resulting in the formation of the Forni di Sotto post-glacial lake [16], this temporary basin survived two-thousand years approximately. The outcropping units shows a down-slope stratification, which has been a strong predisposing factor. Passo della Morte unstable area is the nowadays active part of the Marocca di Sacrovint (Figure 2-12).

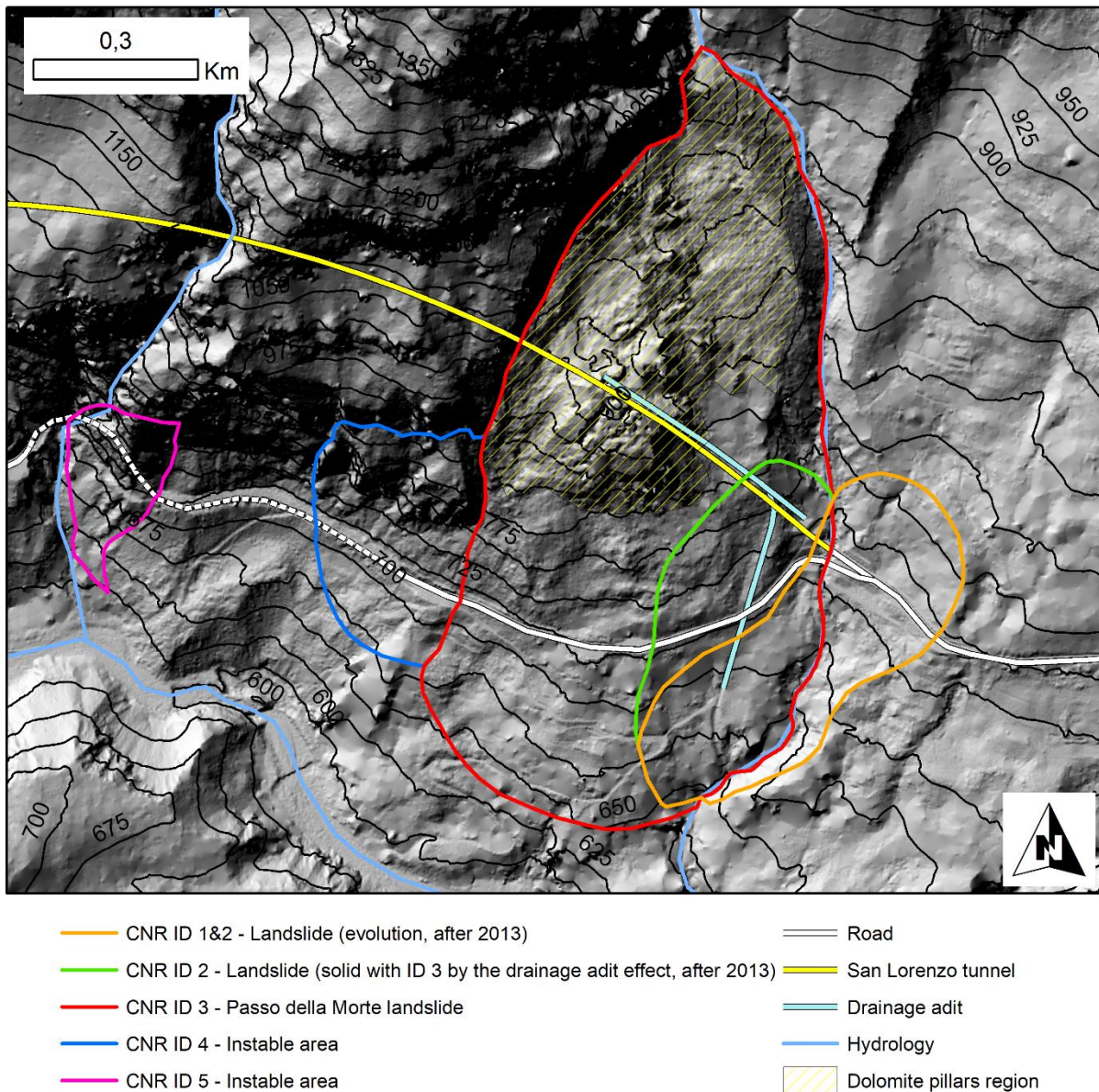


Figure 2-13 Landslides mapped at Passo della Morte area

In Figure 2-13 the landslides and potentially instable areas mapped at Passo della Morte are presented. The infrastructure is treated by landslide 1, 2 and 3 (CNR ID).

## 2.4 HYDROLOGICAL SETTINGS

The Passo della Morte area hydrological setting is governed by the geological setting, with limestone and dolomite units lying on the top Chaotic silty Clay formation.

The water network is composed by a series of tributaries of the Tagliamento, which is the main river in the area. Those mountain torrents can be perennial or ephemeral, and are all characterized by steep paths sometimes generating spectacular waterfalls and axis perpendicular to the Tagliamento Valley [2].

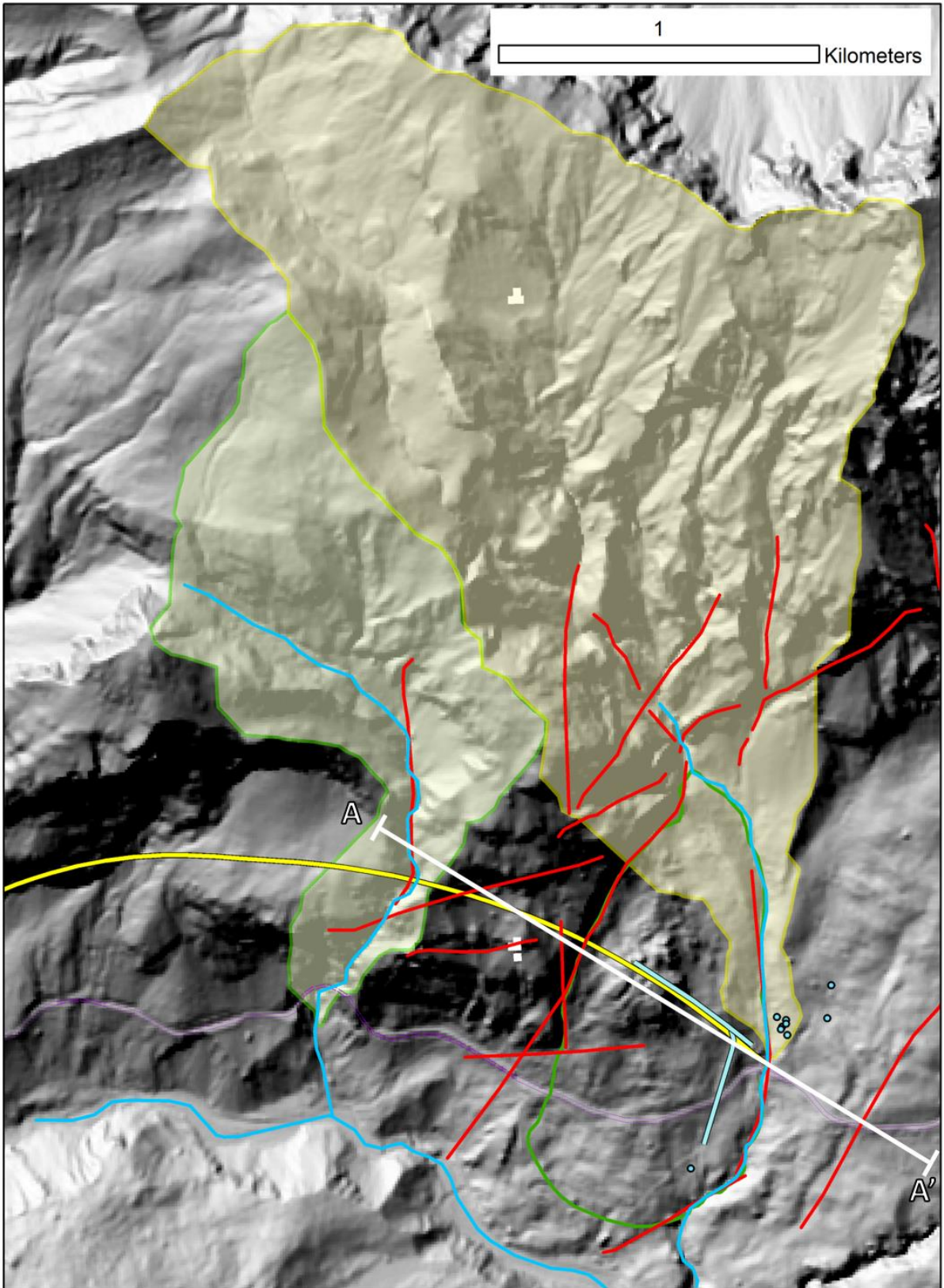
The drainage network in the Passo della Morte area includes Rio Verde and Rio Scuses streams, as well as the Tagliamento River. Those watercourses are localized at the East border of the landslide, 300 m on West and on the Valley bottom respectively. In this section of the Upper Tagliamento Valley, the river flows at an elevation of 600 m a.s.l with a 2%-slope. In this area, Tagliamento riverbed runs through limestone and dolomite drawing a quite windy path.

Rio Scluses does not have a liquid discharge for most of the year, and a similar behavior is shown by Rio Claveno flowing on the West part of the San Lorenzo tunnel [19].

In the Alpine context, streams, i.e. Rii, generally evolve matching a geological or topographic variation, like a fault zone as well as a lithology variation.

Rio Verde streambed is following the East border of the landslide. Rio Verde is the main mountain stream in Passo della Morte area. Because of the coarse material constituting the Rio Verde paleo-streambed, the water infiltration from the East flank towards the landslides is very high [16], [20].

A tectonized area is detected at 200 m from the West portal of the road tunnel, in correspondence of the Rio Scluses crossing. After the heavy rainfall event of January 6<sup>th</sup> 2018, a field survey was carried out in order to identify possible infiltration zones; no sinkholes were found but several pools in the streambed axis. Frequently, those natural pools present a draining bottom. During this event, severe seepage affected the San Lorenzo tunnel threatening its serviceability level because the water falling down from the lining crown reduces the visibility.



- |                  |                             |                    |
|------------------|-----------------------------|--------------------|
| Rio Verde basin  | Hydrology                   | Drainage adit      |
| Rio Scuses basin | Main discontinuity          | San Lorenzo tunnel |
| Spring           | Passo della Morte landslide | Road               |

Figure 2-14 Hydrological map

On the basis of the data acquired during a series of field campaigns, it has been possible to group the slope materials in five classes, which are representative of different hydraulic conductivities [21]:

Table 2-1 Permeability classes

Class ID	Rock materials	Hydraulic conductivity [m/sec]
1	Chaotic silty clay, gypsum	$10^{-7}$
2	Massive dolomite and limestone	$10^{-6}$
3	Fractured dolomite	$10^{-5}$
4	Dolomite pillars region and main faults	$10^{-5}$
5	Multigenetic debris	$10^{-5}$

In Figure 2-15 the hydro-geological section is presented (modified after Borgatti et alii [21])

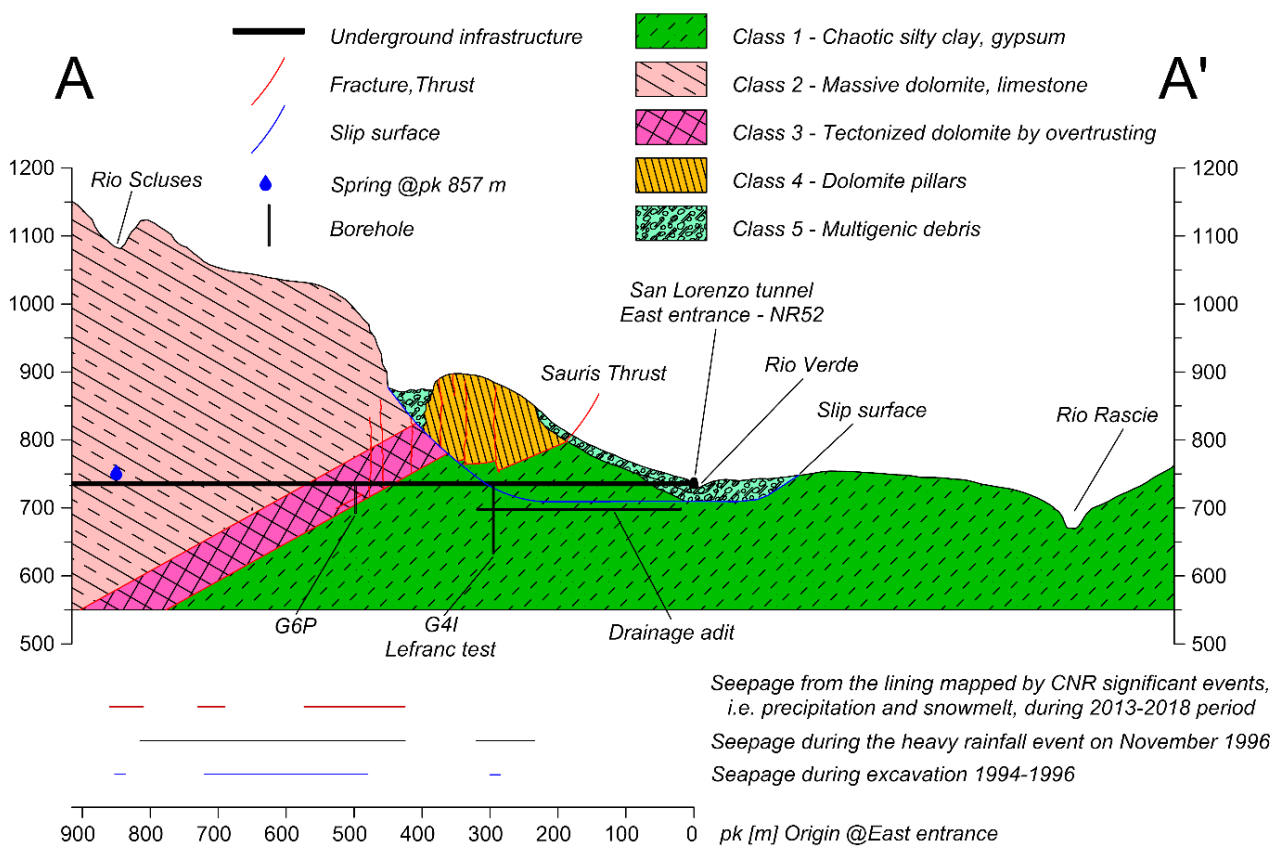


Figure 2-15 Hydro-geological section AA'

The groundwater flow in the Passo della Morte area is defined by a main flow from North to South, which means from Mount Tinisa to Tagliamento River. The regional thrust, before mentioned as Sauris line, represents the contact between the fractured limestone and dolomite units with the almost impermeable clay-rich formation. This lithological boundary outcrops on the South slope of the Mt. Tinisa around an elevation of 700 m a.s.l.

Limestone and Dolomite units host the main aquifer acting as fissured media superimposed on aquicludes in the chaotic silty clay [19]. Karst or pseudo-karst landforms such as small-scale sink holes are mapped in the Passo della Morte area [22]. This observation supports the hypothesis of the fundamental role played by the rock mass discontinuities in the groundwater circulation.

The permeability of the carbonatic rock mass is governed by the fracture network and faults [2]. Joints and discontinuities create a hydraulic connection in which the water flows downslope toward Tagliamento [2]. In this case, the groundwater movement at slope scale is ruled by the so-called secondary hydraulic permeability, i.e. representative of rock and discontinuity system together. Cervi in his study [19] reports that the washing and dissolution on the discontinuity walls can also lead to a general increase of the secondary permeability in the Mt. Tinisa rock mass.

A spring area is also detected on the left of Rio Verde. A part of this outflow has been catch in a concrete pool and connected to the aqueduct.

A minor perennial spring has been mapped few tens of meters downslope the drainage adit entrance. This outflow produces with a few square-meter humid area. The discharge is evaluated in less than a liter per second.

At 857 m from the East portal, the San Lorenzo tunnel intersects a fault zone, which corresponds to the most important spring mapped in Passo della Morte area. During the monitoring period 2014-2018, the mean annual discharge rate is 16 l/sec. There is an alignment between Rio Scluses and the San Lorenzo spring (Figure 3-4).

At the time of the restoration works on the San Lorenzo tunnel, some Lefranc tests were conducted into the San Lorenzo tunnel and in the neighborhood of the East entrance. A Lefranc test was carried out in G4I borehole (previously called I-12, Figure 3-4 and Figure 2-15) estimating a hydraulic conductivity of  $1.57 \cdot 10^{-8}$  m/sec [23]. The G4I associated value is assumed representative of the reddish chaotic silty clay rock mass.

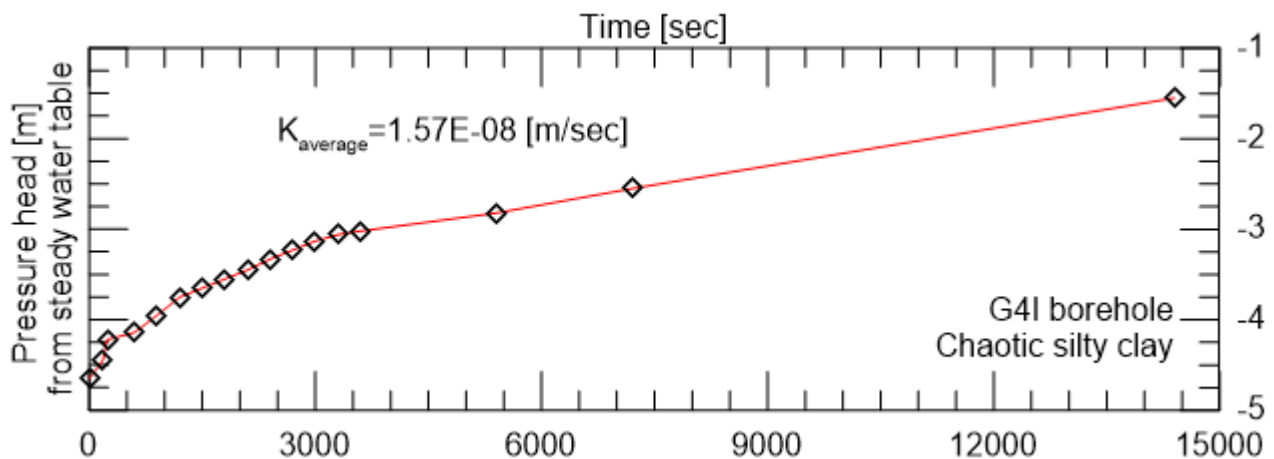


Figure 2-16 Lefranc test in G4I borehole

The hydrological response of the rocky materials at the Passo della Morte can be grouped in three main behaviors with very high, high and very low permeability. Some Authors [24], [25] estimated the carbonatic rock mass permeability in  $10^{-7}$  m/sec, resulting from joint network and localized karst phenomena, while an overall hydraulic conductivity of  $10^{-5}$  m/sec is representative of the landslide body material as well as of the fault zones. Finally, the clay-rich units are characterized by very low permeability, i.e. value in the order of  $10^{-8}$  m/sec.

The definition of the elevation of the water table in the dolomitic pillar region is a priority. For this reason, field surveys were carried out in order to find and restore the borehole I20, originally named AM14. The piezometer gauge installed in I20 allowed the delay between heavy rainfall events and water table rising to be estimated in few hours.

The minor landslide on the East of the San Lorenzo tunnel entrance [2], e.g. the so-called landslide 1, reactivates when the water table reaches the slip surface (Figure 2-13). Studies carried out in this

area on the most shallow landslides have shown that the increase of the groundwater level is the triggering factor of several reactivation events [16], [20], [26].

## **2.5 CLIMATE SETTINGS**

The Passo della Morte area is characterized by a mild climate, with short fresh summers and relatively cold winters. The annual cumulated precipitation is 1650 mm/year, almost twice the Italian mainland value. The study site is in an East – West oriented segment of the Upper Tagliamento Valley, therefore there is a high exposure to the dominant and coldest winds. The annual mean temperature is 8.2 °C. The monthly temperatures range from -0.4 °C in January to 17.9 °C in July during the period 2005-2014 [19]; those values are strictly dependent from the Valley and local exposure.

During the last 5 years, the cumulated rainfall shows a maximum of 2450 mm in 2014 due to the severe event occurred in November, while the minimum is recorded in 2015 with a value of 1300 mm.

Two weather stations are representative of the situation at Passo della Morte. In the current research, the rainfall dataset are recorded at the Forni di Sotto weather station, whereas the snow cover is taken from the Malga Cjampiuiz gauge. Those weather data stations are at a distance from the landslide of 0.5 and 11 km respectively, and both are managed by the Regional Authority.

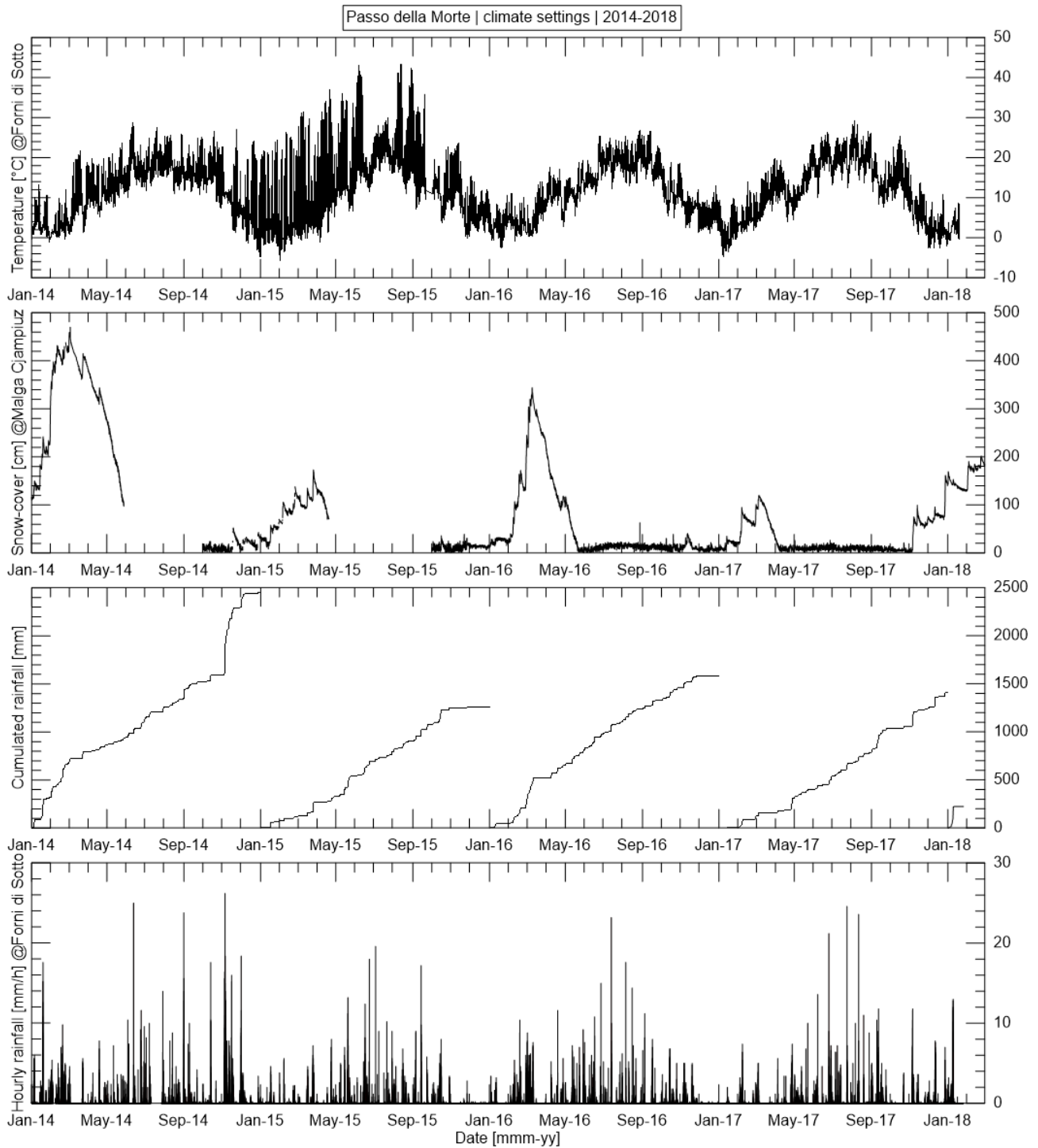


Figure 2-17 Climate setting at Passo della Morte, from the top: daily temperature, snow cover, cumulated and hourly rainfall

The snow cover is persistent during the winter season, with an alternation of melting and accumulation phases until the total snowpack melting in late March-April. For the period 2005-2014, around 215 centimeters per year is the cumulative snowfall ranging between 90 and 370-cm [19]. Obviously, the snow accumulation is locally depending on the sunlight and wind exposition, elevation and topography, this last factor has an effect on the rain precipitation too. Marcato [2] reported a higher snowiness on the right bank of the Tagliamento River.

## 2.6 PASSO DELLA MORTE LANDSLIDE

The Passo della Morte landslide covers an area of approximately 400 thousand square meters. It has a drop shape elongated in North to South direction. A North-South (crown-toe) axis will reach 900 meters, while it reaches about 400 m in East-West (flanks). The landslide is bordered by Rio Verde stream on East flank and Col Pimin on the upper West side Figure 2-18. The toe is located at the elevation of 650 m above the sea level (a.s.l), the scarp (on North) at 1000 m a.s.l. ca.

The Passo della Morte landslide is classified as a rock block slide [27]. This active landslide is the Western portion of an ancient slope instability phenomenon called Marocca di Sacrovint [2], [9], a Deep-seated Slope Deformation, extending up to Cima Corso. The Marocca di Sacrovint has been able to shift the Tagliamento riverbed as consequence of the original detachment after the Piave glacier regression at the end of the last glacial age [13].

The present study defines the landslide volume in the order of 23 million of cubic meters, with a slight reduction from previous study estimation [2]. The 10% variation is due to the availability of information about the slip surface position. Those came from the drainage adit drains cut by the slip surface movement few years after the installation. Further location data were collected thanks to the evolution of the cracks into the drainage tunnel corresponding to its entrance in the moving area.

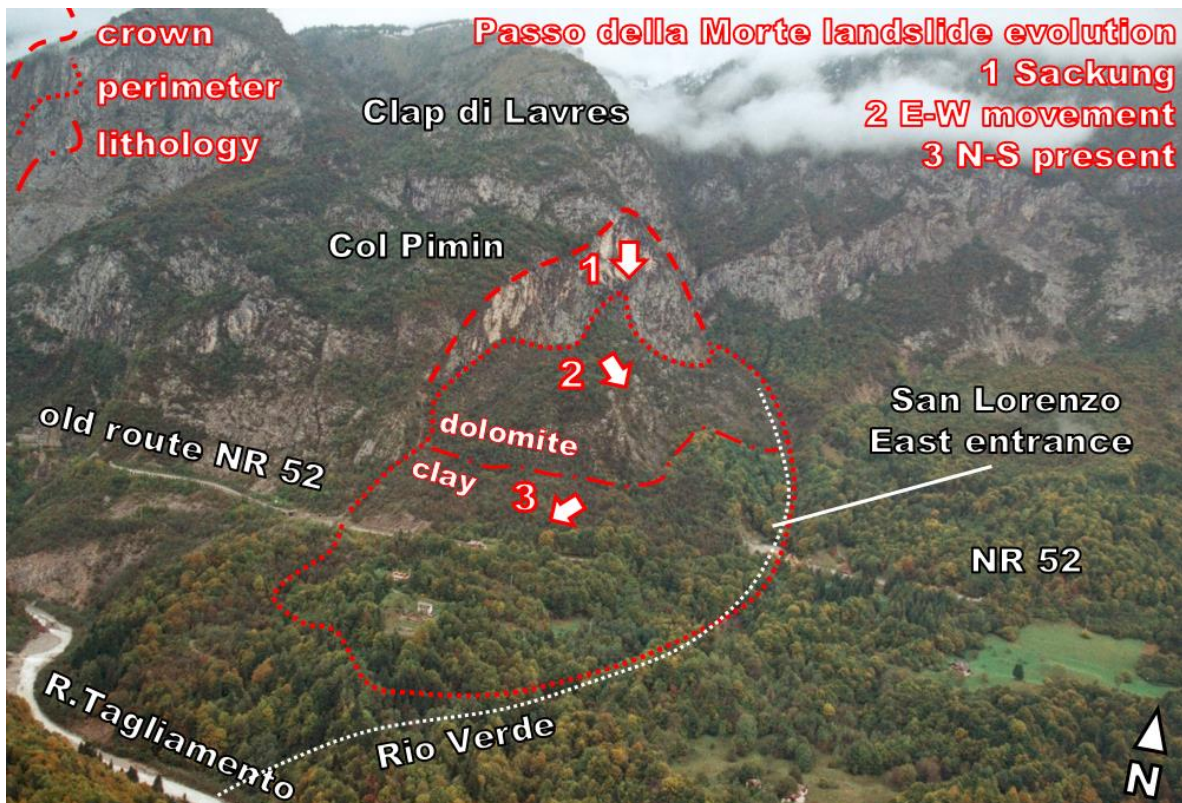


Figure 2-18 Passo della Morte landslide evolution

## 2.7 INFRASTRUCTURE

The National Road 52 (NR52) is the direct connection between the Upper Tagliamento valley and the Cadore area, in the nearby Veneto Region. In the segment pk 41 600 - 44 400 m, the NR52 old route has been abandoned as a consequence of frequent snow avalanches and rock falls. San Lorenzo is a tunnel part of the new NR52 path [28].

The San Lorenzo tunnel develops for 2212 m into Passo della Morte slope, 2119.4 m excavated in the rock mass and the remaining 92.1 meters artificial [29]. This second term is used by the National Road Authority (ANAS) when the concrete lining is built without a direct contact with the rock mass or soil. Frequently, the artificial tunnel is then buried with natural materials such as rocky debris or



the drainage capacity, and the number was increased as water seepage become more intense, i.e. where the slip surface of Passo della Morte landslide intersect the road tunnel (Figure 2-20).

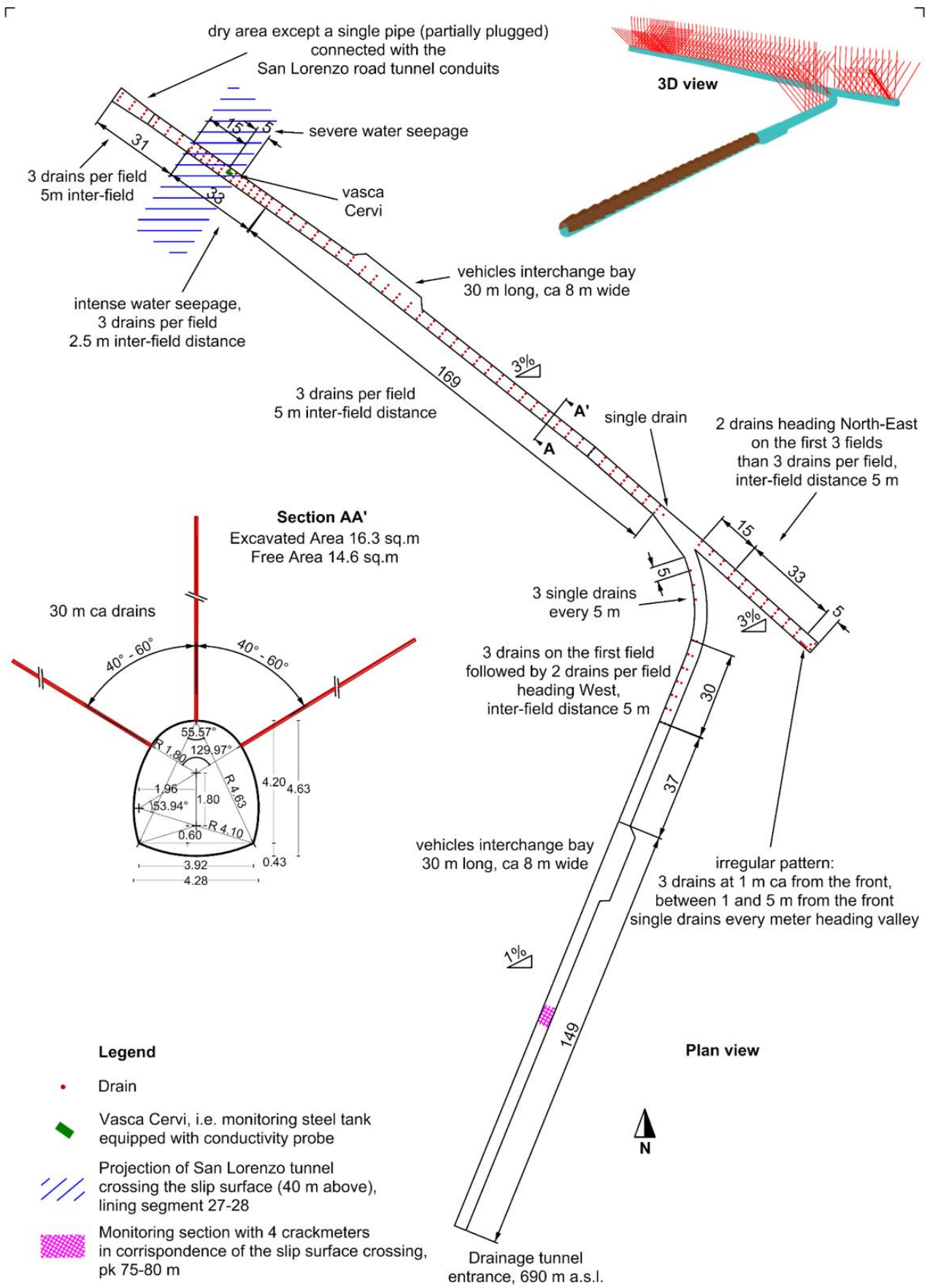
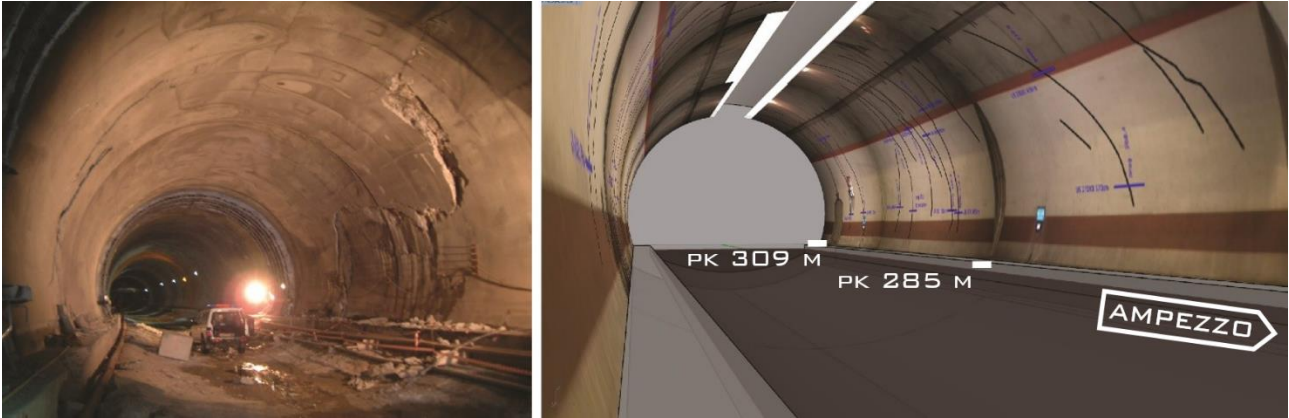


Figure 2-20 Drains pattern into the drainage tunnel



*Figure 2-21 On the left: damage on concrete lining at pk 300 (segments from 26 to 29) after the heavy rainfall event on late 1996. On the right: a 3D reconstruction of the crack in the final lining at segment 27-29 (2012 photos)*

In Figure 2-21 the tunnel-landslide intersection is shown, those pics present the damages on the tunnel lining few months after construction and the cracks in the new concrete lining.

### 3 INVESTIGATION AND MONITORING

In the Figure 3-1, the instruments installed at Passo della Morte since 1999.

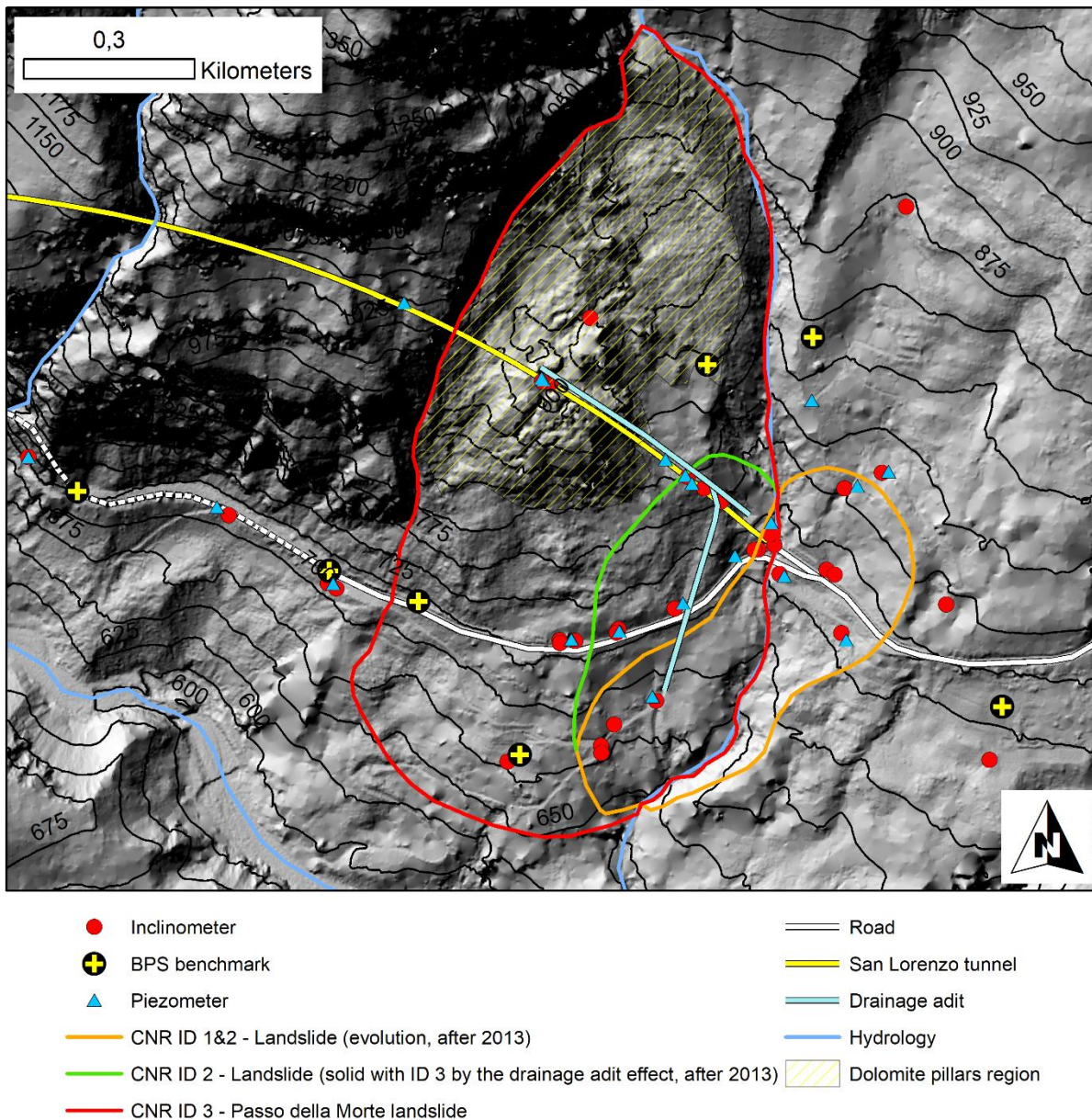


Figure 3-1 Instrumentation installed since 1999

#### 3.1 PRESENT WORK INVESTIGATIONS

The discontinuities play a key role in the definition of the rock mass behavior both from the mechanical and from the hydrogeological points of view. During fall 2016, a series of field surveys were carried out to map the fractures in the dolomite pillars area. In Figure 3-2 the stereo-net (equiangular projections) for each survey spots and two Rosette plots are shown, on the right for the central part of the landslide and close to the Col Pimin vertical wall on the left. Those datasets clearly show that the dolomite pillars area present three joint sets as well as a bedding plane. Nevertheless, each pillar or boulder is randomly tilted and rotated following the downslope movement of the Passo della Morte landslide.

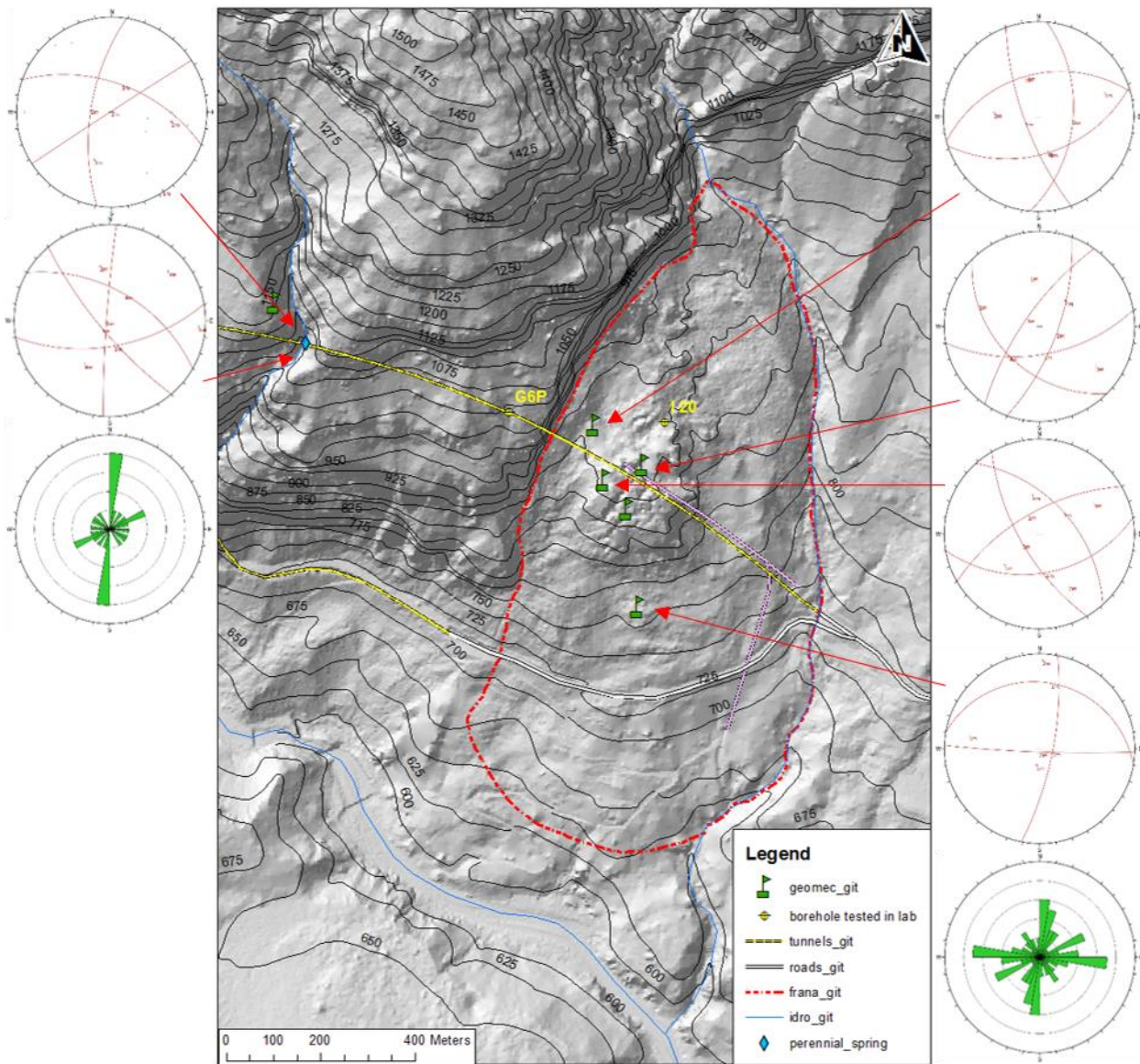


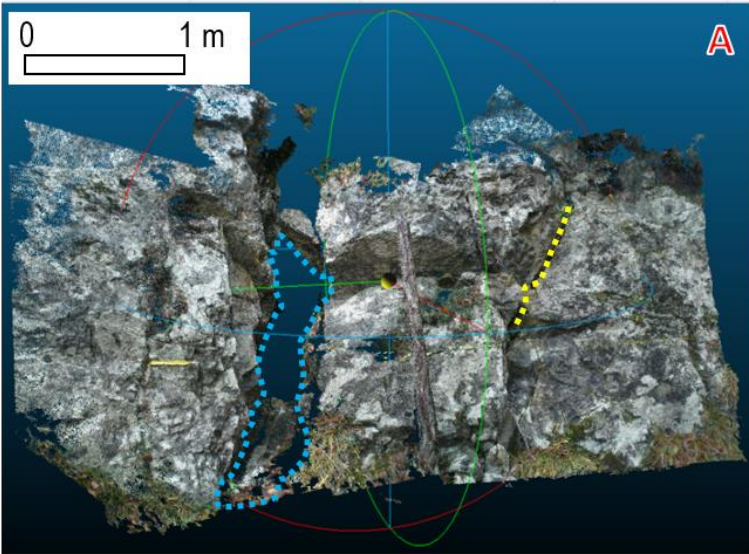
Figure 3-2 Discontinuities mapped in the landslide area (2016 field survey)

Sinkholes, discontinuities and open trenches between the pillars represent preferential water infiltration path. Following those voids, the water can rapidly pass through the dolomite reaching the lower units at depth the clay rich material composing the lower units undergoes a progressive decrease of its mechanical resistance if in contact with the infiltrated water. It is worth to mention that no water table was found in the clay-rich rock mass.

At Passo della Morte, sinkholes and open trenches create voids playing a key role in the overall slope kinematics. The diffused presence of opened discontinuities is presented in Figure 3-3.

Photogrammetric survey  
Dolomite pillar details

A  
B C D E



Open (>20 mm) fracture  
Sinkhole (> 500 mm)

Yellow dashed line  
Blue dashed line

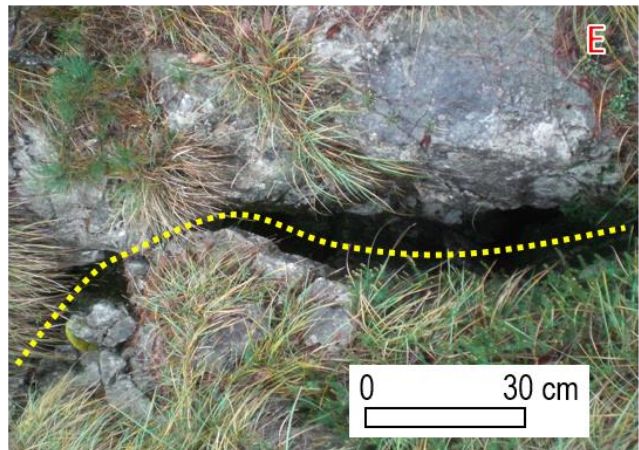
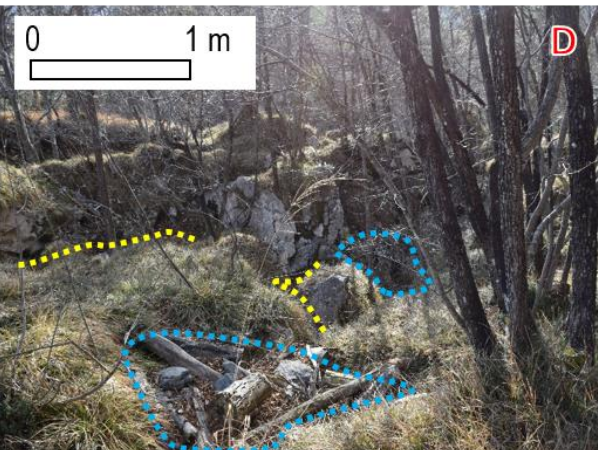
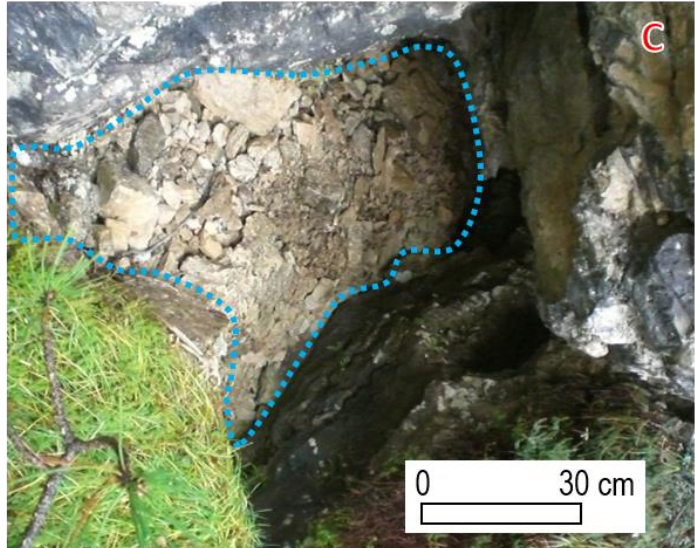
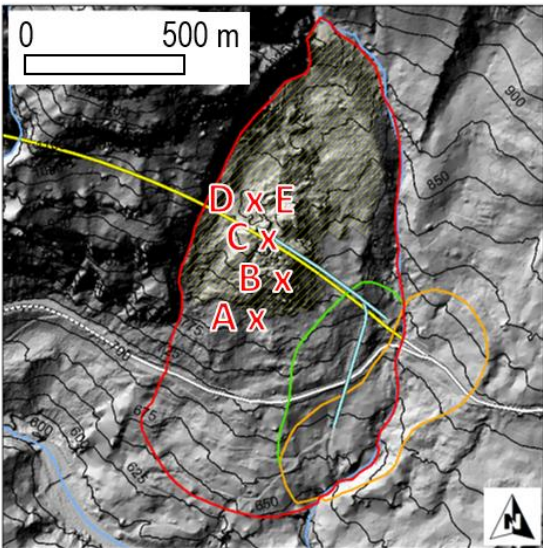
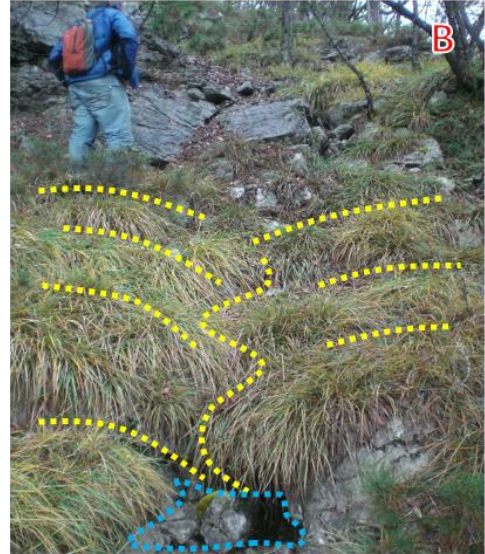


Figure 3-3 Survey of the dolomite pillars area. From the top: photogrammetric survey on left (A), open fractures on right (B), pics localization (middle-left), sinkholes (C), severely fractured area in the I20 neighborhoods (D), open fracture (E)

### 3.2 SITE MONITORING

The monitoring of Passo della Morte area become necessary in late Nineties after the fall 1996 heavy rainfall event, which led to the stop of the construction phase . Initially, in early 2000s the investigation campaign had the aim to help the design of the second tranche of countermeasure works following the building of the San Lorenzo tunnel. Those studies were focused to identify the slip surface of the landslide body threatening the East entrance of the San Lorenzo tunnel. Because of an incomplete overview due to a lack of investigation data, the conclusions reached by designers and expert reports [28], [30] were not appropriate to represent the situation. More than 15 years ago, the Italian National Research Council (CNR) started a site-costumed monitoring plan founded by the National Road Authority (ANAS) and the Regional Authority for Civil Protection (PC-FVG).

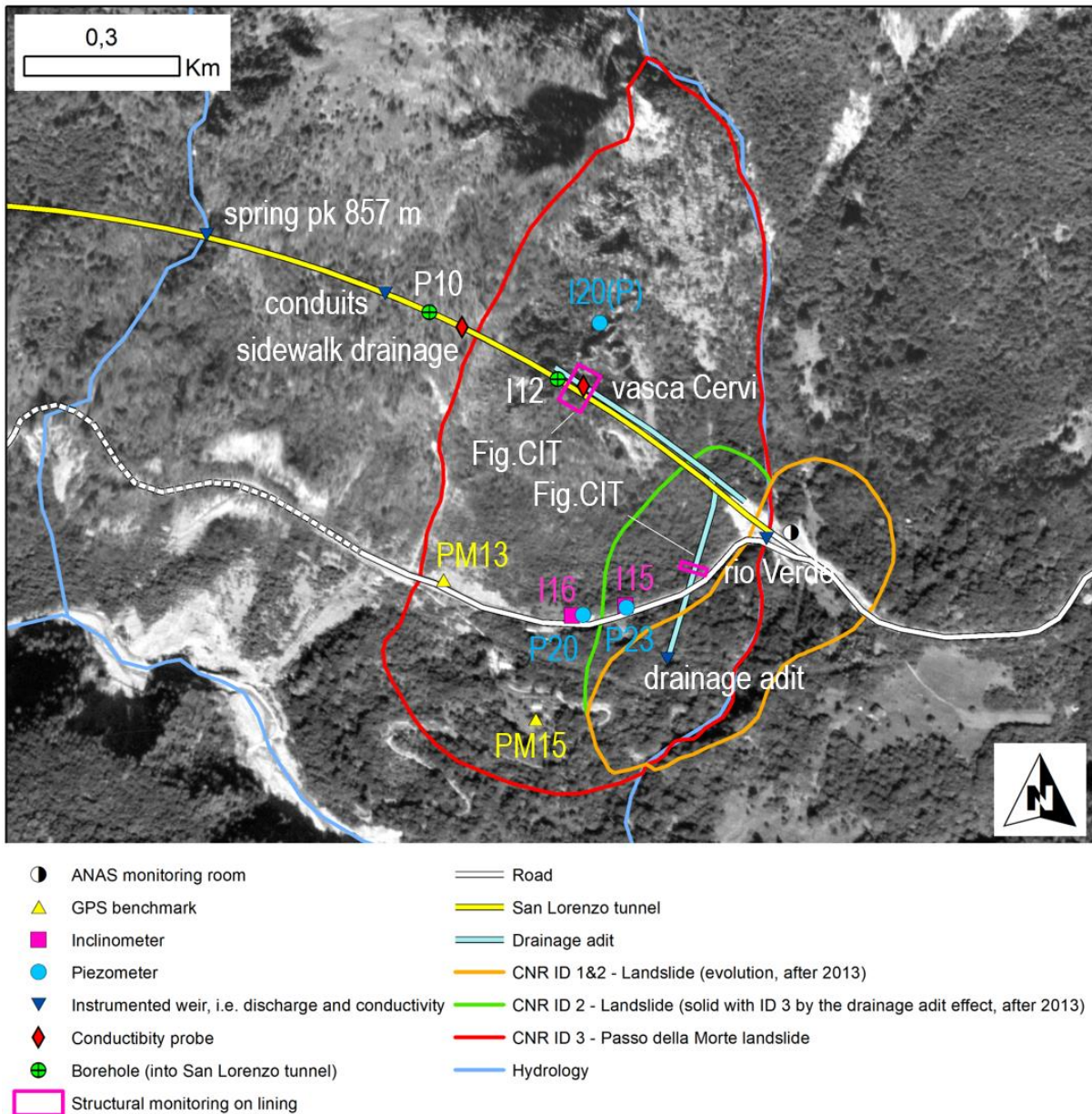


Figure 3-4 Monitoring network directly used in the current study

The Passo della Morte monitoring system was extended after the drainage adit excavation in order to evaluate the effectiveness of that countermeasures work.

It is worth to mention that the ANAS and PC-FVG Administrations are interested in different monitoring issues. ANAS aim consists in guarantying a good serviceability level for National Road

52, which means keeping the traffic into San Lorenzo road tunnel. After the drainage adit investigation and construction, direct consequence of the ANAS scope is that the monitoring has been mainly focused to evaluate the structural health [31] of the infrastructure, i.e. tunnel lining and Rio Verde bridge deck. Differently, PC-FVG monitoring has been centered on the unstable slopes themselves to evaluate risks for people and traffic. At an early stage, PC-FVG put attention on a possible Tagliamento Rover damming caused by the Passo della Morte slope failure. Authors [16], [32] demonstrated that a rock collapse took place in the past in the neighborhood of NR52 old path and that the mobilized volume run off reached the riverbed event though the Tagliamento was not dammed.

Luckily, the available monitoring dataset is almost continuous over a period of fifteen years. The long span of time covered allows to define geometry and kinematic of the unstable slopes. In the end, it makes it possible to support a customized design of the countermeasures.

Year by year, the system has been improved in order to be redundant and to guarantee a reliable data set during critical events.

### 3.2.1 GNSS

The original GNSS (Global Navigation Satellite System) monitoring network was composed by three master benchmarks (Forni di Sotto, Caprizzi, Ampezzo) and around twenty GPS (Global Position System) measuring points in the area[33].

In 2001 and 2002, the GPS acquisitions were carried out every few months, while nowadays the frequency is twice a year. In case of sudden accelerations, the GPS surveys can eventually be increased according to the research agreement between CNR and local Authorities.

To date, two GNSS benchmarks are anchored on the Passo della Morte landslide body, the so-called PM13 and PM15. Since 2013, both the topographic spot measures are regularly updated on the web portal [31]. The datasets start in the early 2000s, and the long time span covered by the GPS measurements allows estimating a mean annual rate of movement in the order of 2.5 and 2.0 cm / year, in PM13 and PM15 respectively.

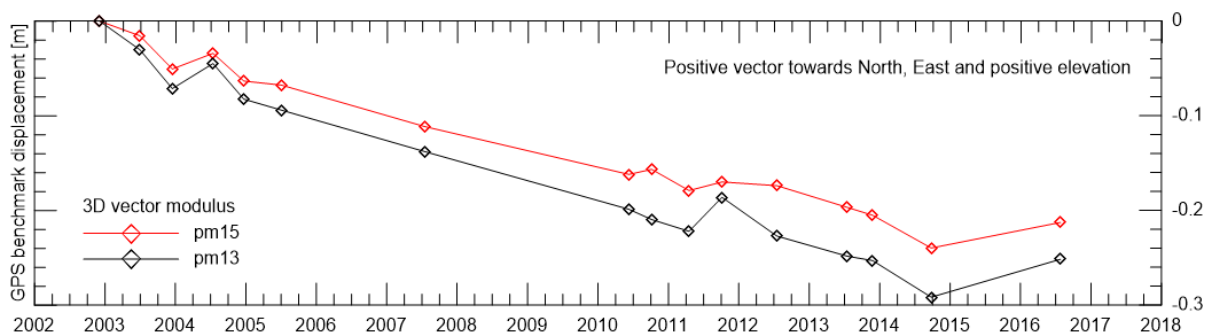


Figure 3-5 GPS benchmarks displacement (2002-2018)

On the studied site, GPS monitoring permits also to evaluate the evolution of landslide 1 and 2 through the analysis of benchmarks PM13 and PM22 displacements. Those measures permitted to confirm the effectiveness of the drainage tunnel in the neighborhood of the East portal.

### 3.2.2 SYNTHETIC APERTURE RADAR

The Passo della Morte landslide superficial displacements have been monitored by SAR both Ground and Satellite based. Ground Based radar (GBInSAR) was set up in Stavolo Mezzan. The acquisitions were done during two periods on December 2004 and July 2005. The radar was pointed on Col Cimin vertical walls and landslide 3 dolomite pillars area.

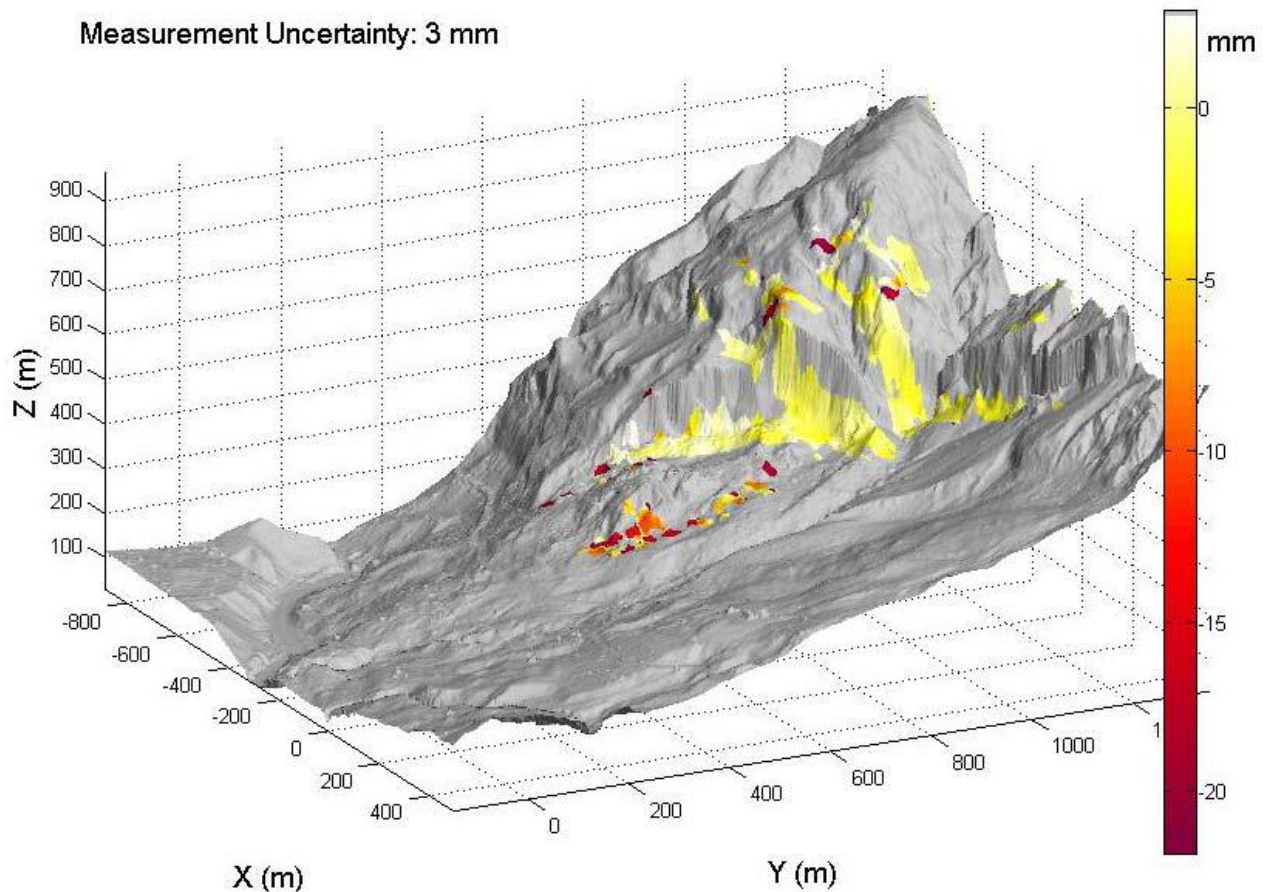


Figure 3-6 GB-InSAR displacements (campaign 2004-2005) [2]

In Figure 2-1 the recorded displacements are superimposed over a tridimensional terrain view. The results confirm the expectations, such as a predominant vertical component of displacement in the pillar region causing a predominantly horizontal component of deformation in the chaotic silty clay formation, since the highest displacement rate is concentrated in the dolomite pillars area, specifically at the bulge toe [34].

### 3.2.3 INCLINOMETERS

Inclinometer measurements lead to a proper definition of the unstable mass deformation along each borehole axis. Those instruments can be read manually or in continuous; in this latter case an in place probe is installed at the depth of the presumed sliding surface. The deformation data along the inclinometer axis permit to define if the unstable mass is moving rigidly over a distinct sliding surface or deforming throughout its body.

More than twenty-five inclinometers have been installed, mainly nearby the East portal (map in Figure 3-4). Few tubes were dug in the upper part of the slope both on the left (AM-15) and on right flank of Rio Verde (AM-14, now renamed I-20), i.e. outside the landslide perimeter and in the dolomite pillars unstable area.

Table 3-1 Pre-web portal displacement recorded by CNR in place inclinometers

ID CNR	inclinometer depth [m]	data acquisition		displacement [mm]	annual rate [cm/year]
		start	end		
i15	14	2003-12	2005-04	111	8
	30	2003-12	2005-04	35	2.5
i16	20	2003-11	2005-04	18	1.2
	57.5	2003-11	2005-04	34	2,3

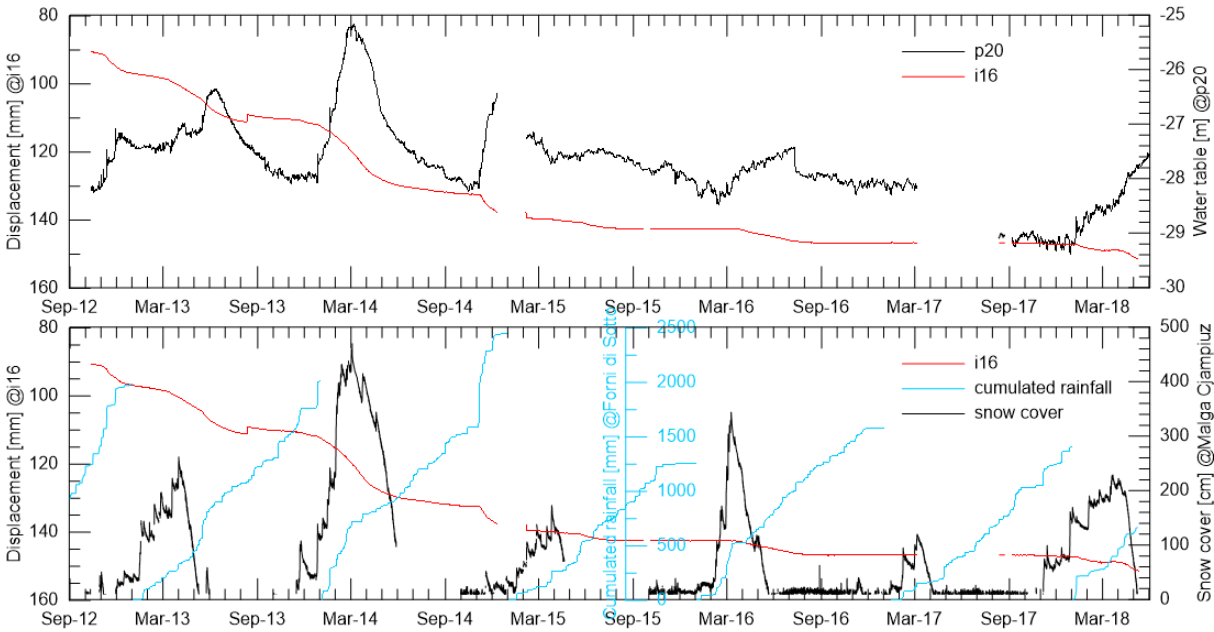


Figure 3-7 I-16 displacements and P20 groundwater table level (2012-2018)

The Passo della Morte landslide deformation at depth is monitored by an in-place inclinometer, referred to as I16. This borehole is equipped with a 1-meter long probe installed at the slip surface depth, at 60 m depth.

Thanks to the continuous data set, in-place inclinometers allow landslide movement at the slip surface to be correlated with severe precipitation events and/or seasonal snow-cover melting [31]. Matching the I16 displacement trend with the P20 (Figure 3-4) groundwater table level (Figure 3-7) and the groundwater discharge from fractured dolomite (Figure 3-8)

Inclinometer displacements are much lower than those from GPS survey because representative of a portion of the slip surface.

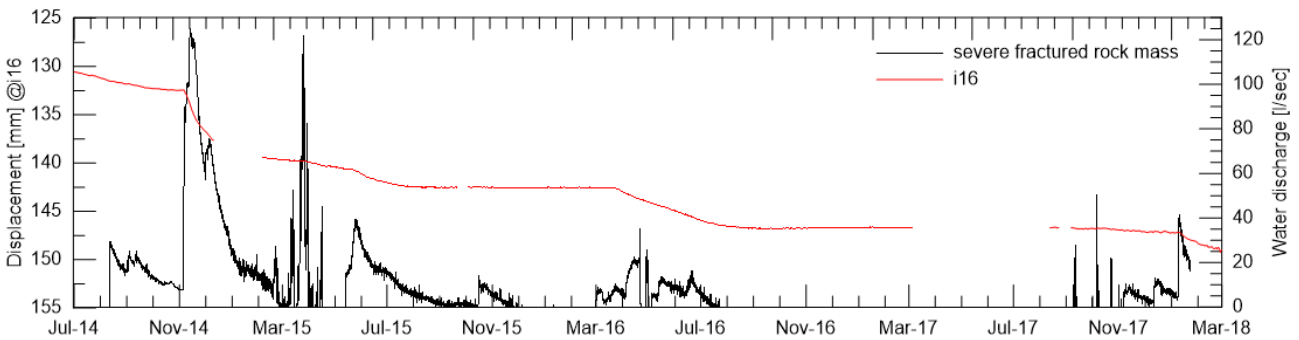


Figure 3-8 Correlation between slip surface deformation and severe fractured rock mass water discharge

### 3.2.4 PIEZOMETERS

The groundwater table in the study area has been monitored by a series of piezometers installed since late nineties (map in Figure 3-4). Nowadays, two piezometer probes are still working on landslide 3, and both P20 and P23 are standpipe piezometers. Casagrande piezometers have shown a bad performance at Passo della Morte mainly because of the clogging of the tubes in the case tip [2], as a consequence of the fine and gypsum fractions dissolved in the groundwater.

During the extreme event (650 mm in 12 days ca) on November 2014, the water table rising measured at P20 can be associated with the landslide body deformation thanks to the presence of the inclinometer I16 (Figure 3-7). In that figure, a similar behavior is shown by I15 recorded displacement.

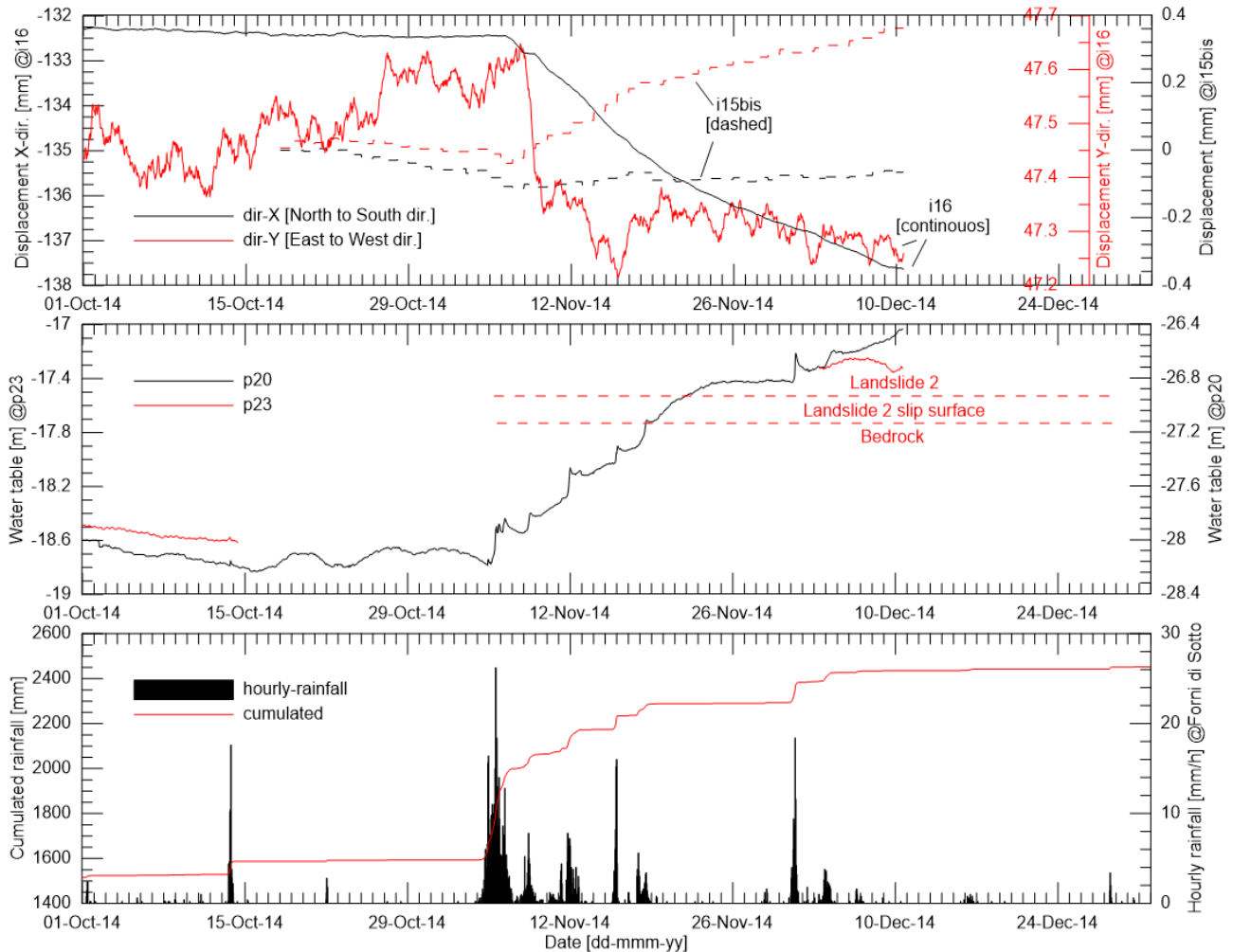


Figure 3-9 P20 and P23 water tables rising after the heavy rainfall on November 2014 and slope movement activations (I-16 on landslide 3, I-15 on landslide 2)

On January 2017, a piezometer has been installed in the I-20 borehole (previous denomination AM-14) to monitor the water table variation in the dolomite pillars region, i.e. the upper part of the landslide (Figure 3-4).

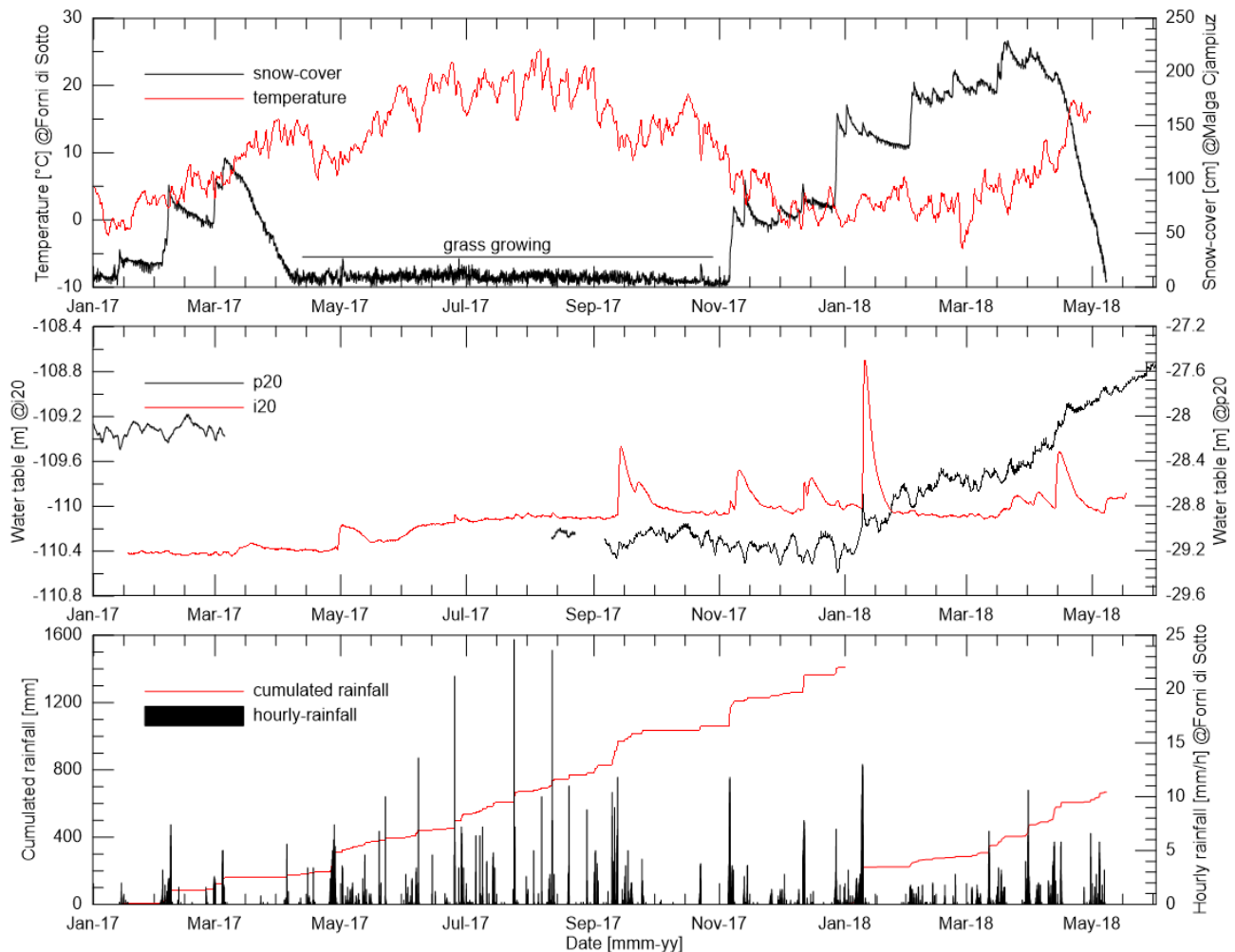


Figure 3-10 I-20 and P-20 water tables (2017-2018)

Analyzing the available 16 months dataset (Figure 3-10) it can be noticed that the water table in the dolomite pillars area is almost constant. The I20 groundwater table risings, up to 1.6 m, occurred during the most important annual infiltration events, either rainfall or snowmelt. Those peaks are generally flattened in less than 2 weeks. The I20 borehole stratigraphy report suggests that groundwater table level is localized in the coarse debris at the lower limit of the dolomite unit, around a meter above the clay-rich units. A comparison between P20 and I20 highlights the impulsive response with a higher activation threshold for the I20 signal.

### 3.2.5 INSTRUMENTED HYDRAULIC SECTIONS

Since the beginning of the CNR-Authorities plurennial agreement in 2014, five weirs have been equipped with piezo transducers, which permit a better understanding of the slope reaction to severe precipitation events and rapid snowmelt [31]. The instrumented section for the water discharge recording has been installed at (Figure 3-4):

- spring into the road tunnel (pk 857 m)
- drainage adit gate
- conduits on the road tunnel invert (left and right pipes) at pk 500 ca
- Rio Verde stream (under the NR52 old-new route bifurcation bridge).

The idea leading to the conduits discharge measurements is that the difference between this value and the spring pk 857 m value it might be a good estimation of the severely fractured dolomite discharge (Figure 3-11). That 150 m long section of the San Lorenzo tunnel (starting at pk 450 m

ca) is intercepting the groundwater circulation in the dolomite tectonized by overthrusting. Before April 2016, the spring discharge was flowing on another instrumented weir, so the conduits discharge could be reasonable assumed as completely originated by the fractured dolomite.

Discharge measures have been frequently verified by alternative methods: catching the water flow and timing the fill-time of a 75-liters pool and by analytic formulae on manual level measures on the notch section (spot measures in Figure 3-12).

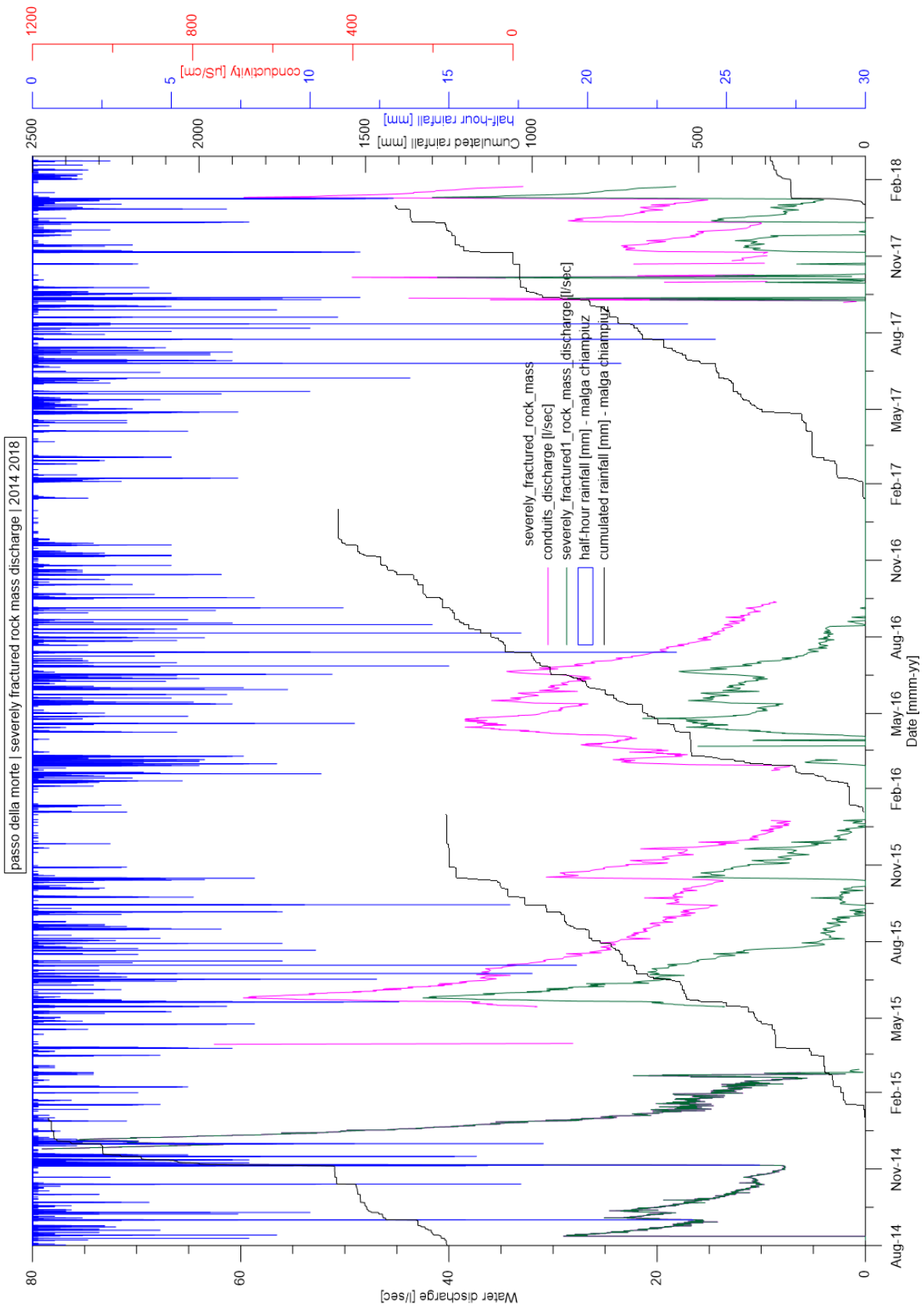


Figure 3-11 Severely fractured rock-mass and San Lorenzo conduits discharge (2014-2018)

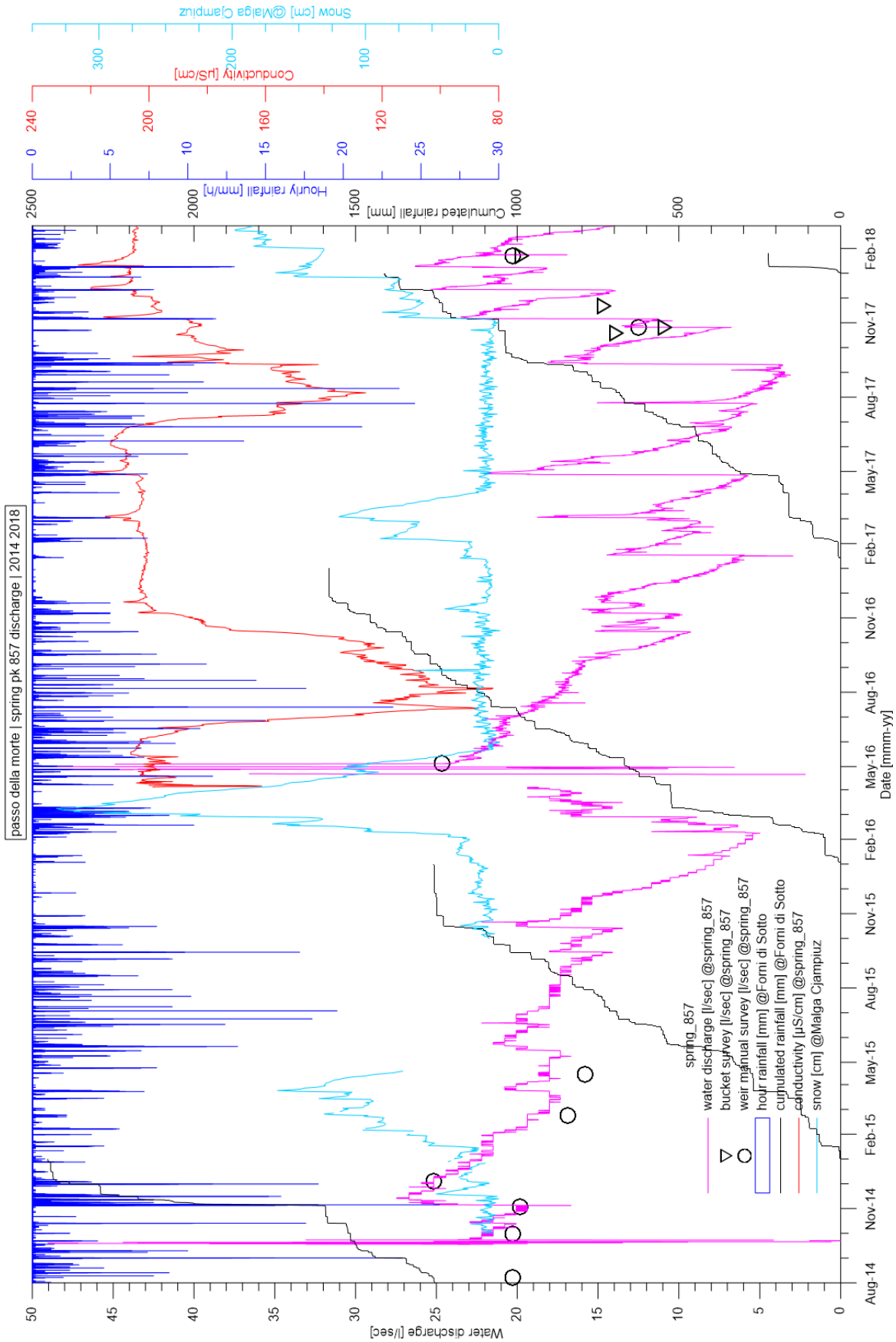


Figure 3-12 Spring pk 857 m water discharge

Conductivity measurements allow the identification of the two groundwater circulations interacting with the San Lorenzo tunnel into the Passo della Morte slope. Investigations have been conducted

in four different areas (Figure 3-4): two in continuous (spring at San Lorenzo pk 857 m and vasca Cervi into the East drainage adit branch) and two temporary (a double gauge in the sidewalks at pk 500 ca of the road tunnel, Figure 3-13).

The low conductivity of the spring at pk 857 (into the road tunnel), around 200 micro Siemens over centimeter, suggests a fast transit of groundwater into the rock mass, which means not long enough to get enriched by dissolved minerals [19], [25]. The previous observation together with the Rio Scluses-spring alignment lead to the conclusion that the spring into the San Lorenzo tunnel is directly fed by the Rio Scluses fault zone. On the other hand, the water catch by the drainage tunnel is much more conductive, around 1000 units, indicating a longer residence time into the slope materials.

The identification of the two separate groundwater systems is important for the design of the countermeasures works. The San Lorenzo water is infiltrating from the severely fractured dolomite rock mass. Once the water path at the slope scale is defined, a proper dewatering system can be studied, modelled, planned and built.

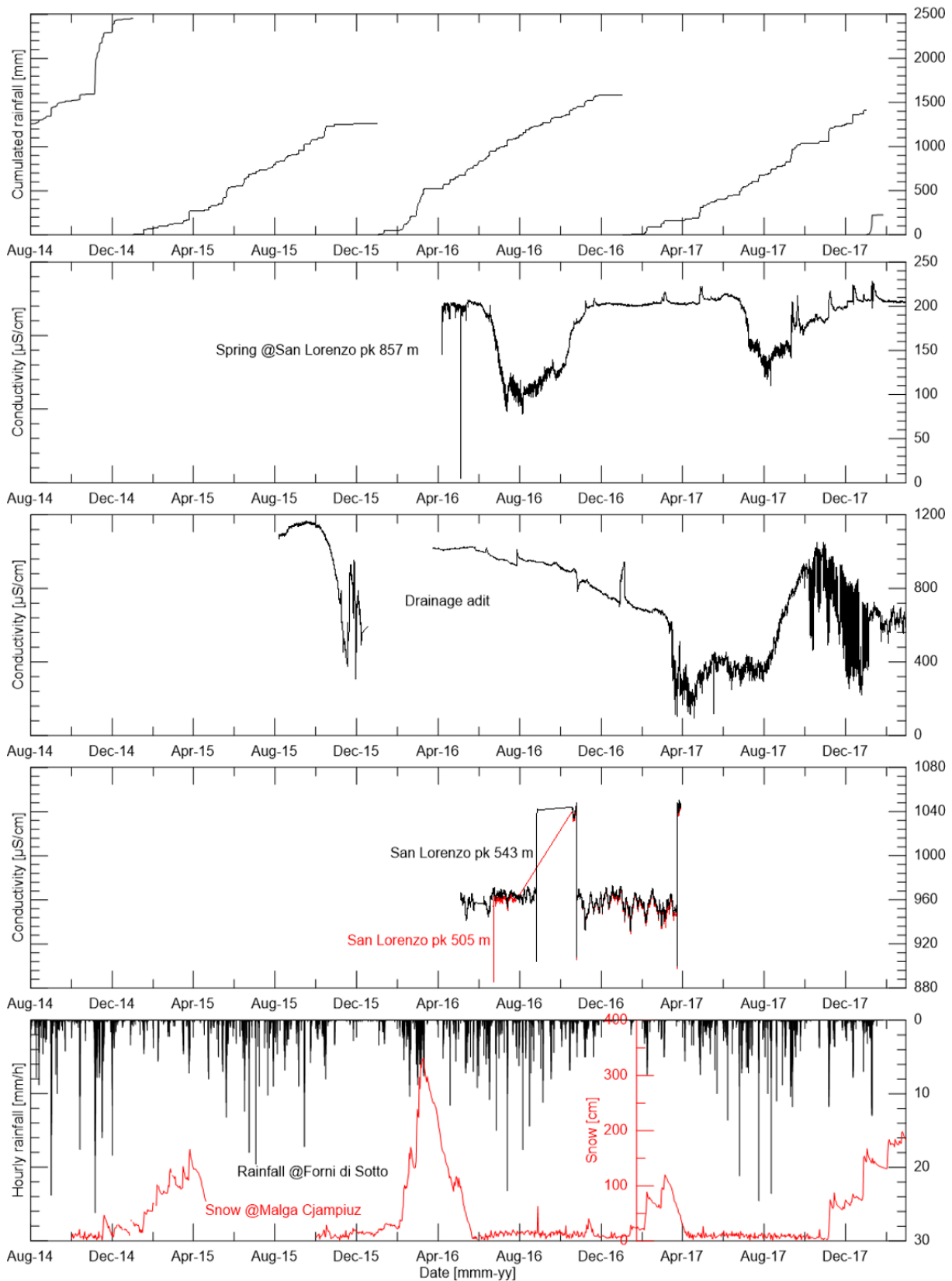


Figure 3-13 From the top: cumulated rainfall, electric conductivity at spring pk 857, at drainage adit, into San Lorenzo tunnel, hourly rainfall (black) and snow cover (red). For the location, see Figure 3-4.

Visual inspection has been carried out in order to evaluate the wetting condition of the San Lorenzo lining (Figure 3-14). The concrete status is classified in three levels: wet (also with visible water flow),



### 3.3 STRUCTURAL HEALTH MOITORING

Structural health monitoring (SHM) is fundamental in the assessment of serviceability life of a structure [31]. The instrumentations needed to catch the representative variables are depending on the complexity of the geological settings and structure.

#### 3.3.1 SAN LORENZO LINING SEGMENTS 26-29

The monitoring system is composed by 24 crackmeters, 4 bi-axial clinometers and a low cost plastic optical fiber sensor.

Since 2014, the tunnel monitoring system can be interviewed by an online-based platform [31].

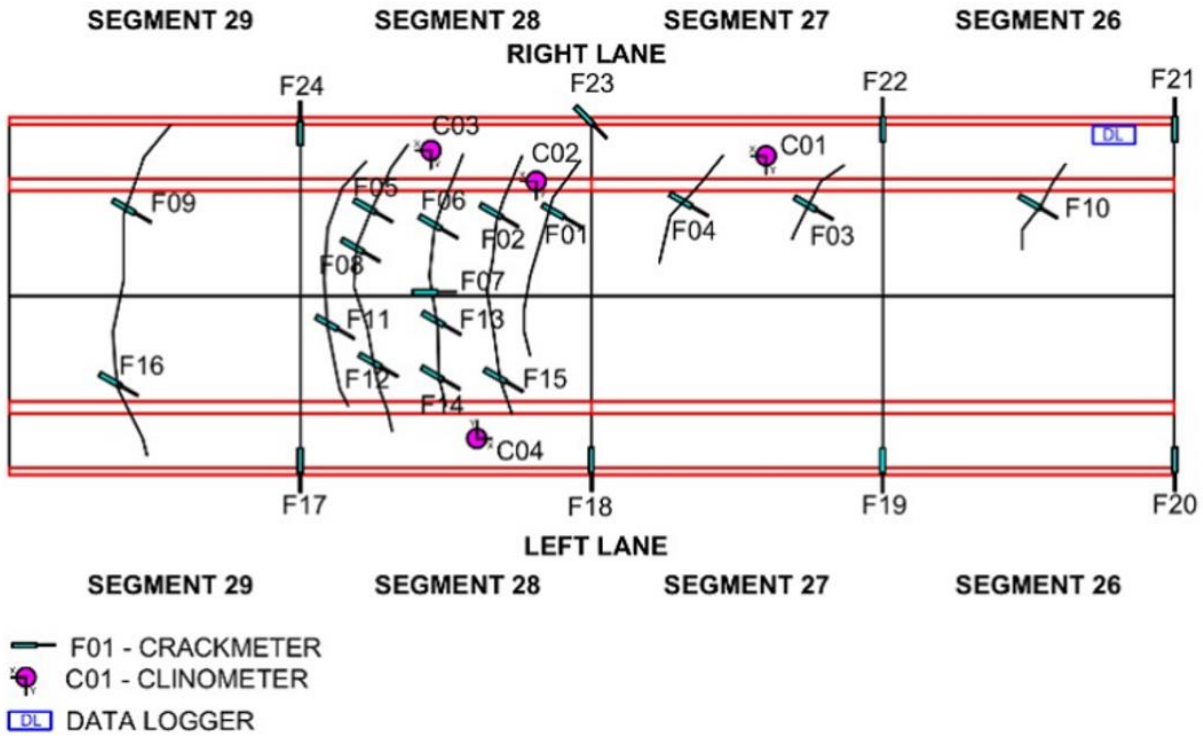


Figure 3-15 Structural monitoring on lining segments 26-29 of the San Lorenzo tunnel

Active instrumentation is shown in Figure 3-16. In the concrete lining, the crackmeter were installed inclined of 45° with the main crack direction.

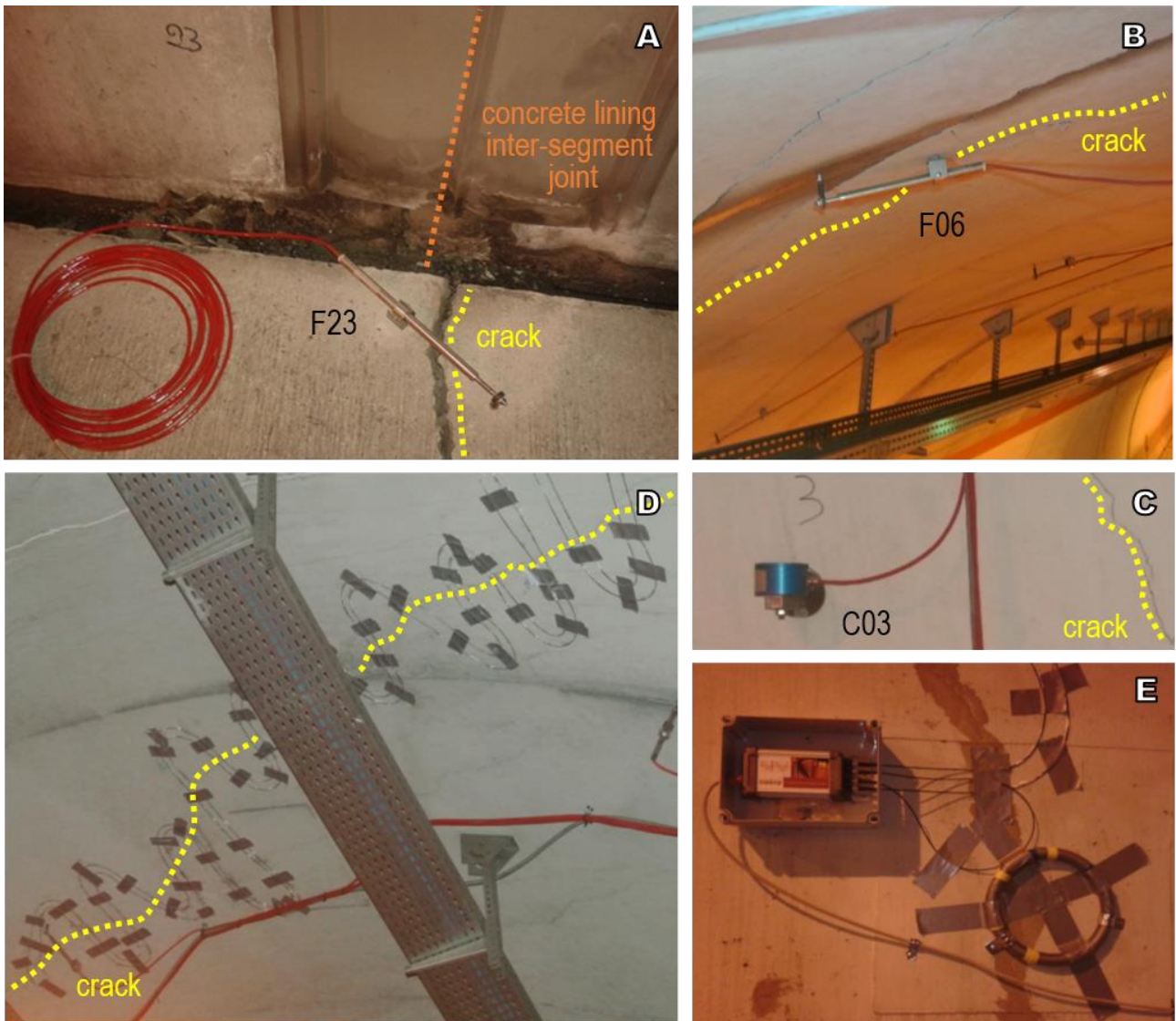


Figure 3-16 Monitoring instruments at tunnel lining segment 26-29. Clockwise: crackmeter F23 on lining joint, (B) crackmeter F06 on the roof, (C) clinometer C03 on the roof, optical fiber on the roof (D), reference fiber loop installation loop (E)

In Figure 3-17 the bar extensometers displacements is presented, instruments trends are grouped based on the vector magnitude, relatively up to 0.2, 0.6 and 8 mm. Generally, cracks show an opening trend. Extensometers can be gathered together by those installed on the lining cracks and in inters-segments lining joints.

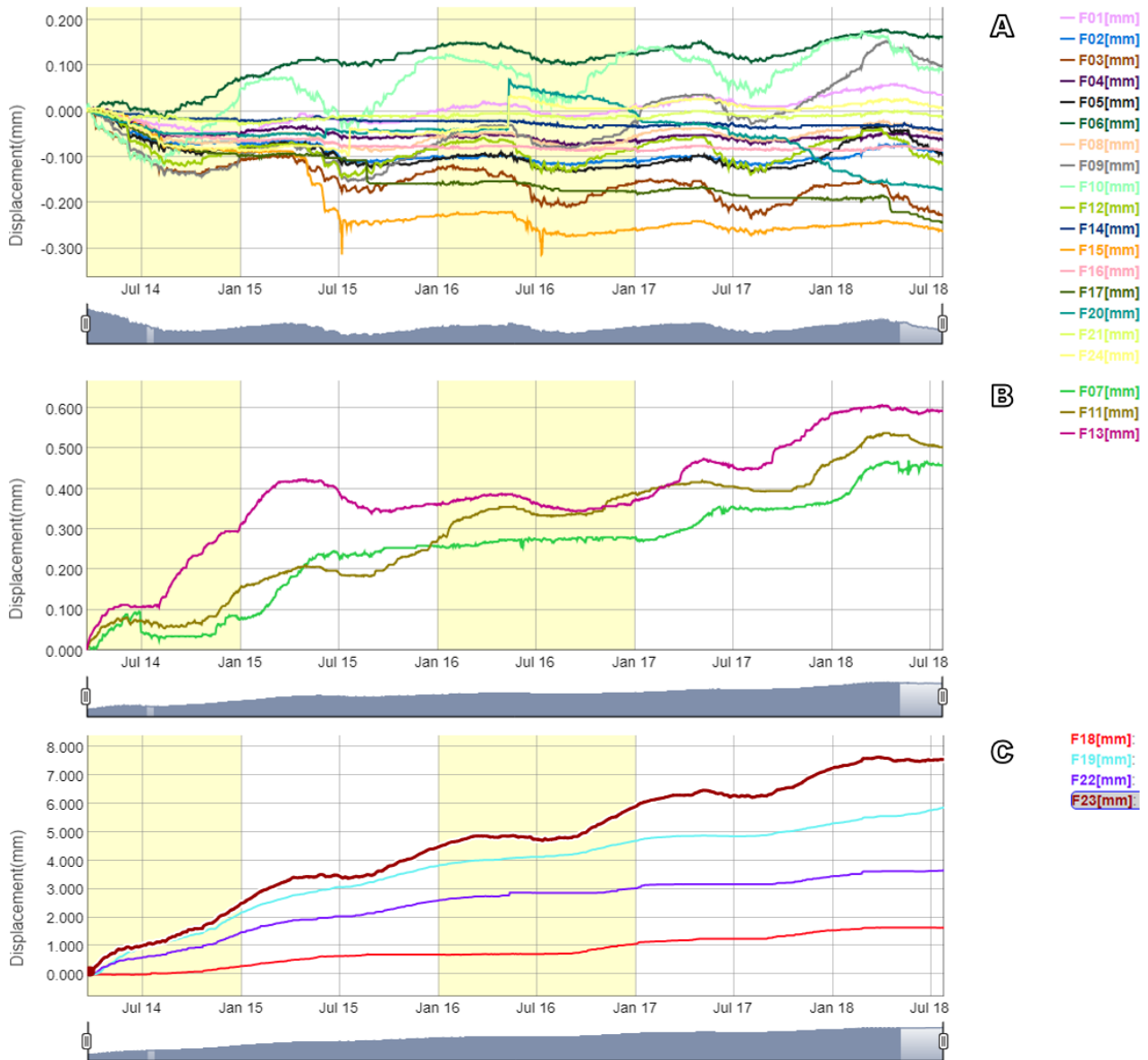


Figure 3-17 Deformations in the road tunnel lining. Instruments are grouped by the displacements magnitude, up to 0.2 mm (A), 0.6 mm (B) and 8 mm (C, 2014-2018. Screenshot of the online monitoring portal).

The cumulated tilt angles measured by four clinometers is graphed in Figure 3-18 divided between perpendicular (A) and parallel (B) to the tunnel axis. In 2015, clinometer C04 change his rotation pattern, which might suggest a kind of plastic hinge in the concrete lining [31]. This observation can anticipate a loosening of stiffness of the tunnel section.

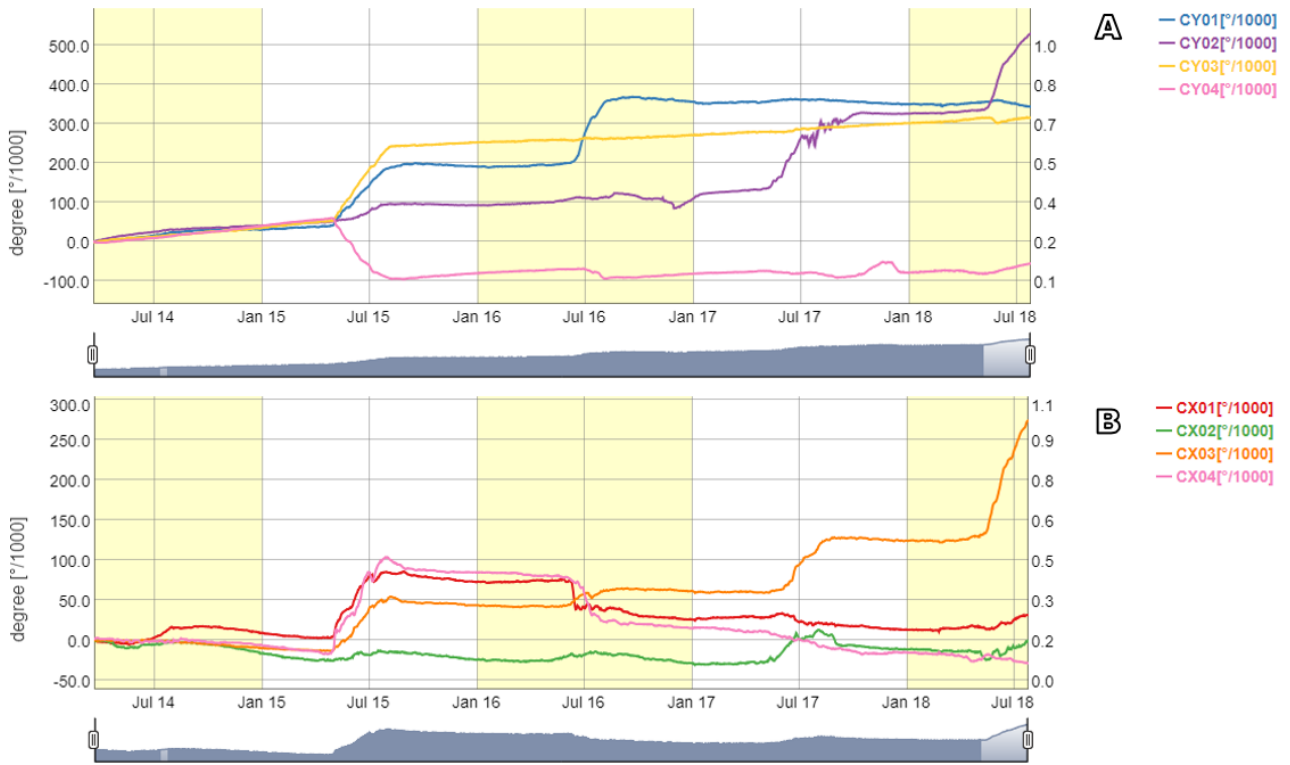


Figure 3-18 Rotations in the road tunnel lining. Top-down: (A) rotations perpendicular to the tunnel axis, (B) rotations parallel to the tunnel axis (2014-2018. Screenshot of the online monitoring portal).

A simplified scheme of the concrete lining crossing the slip surface at pk 300 m ca is proposed in Figure 3-19.

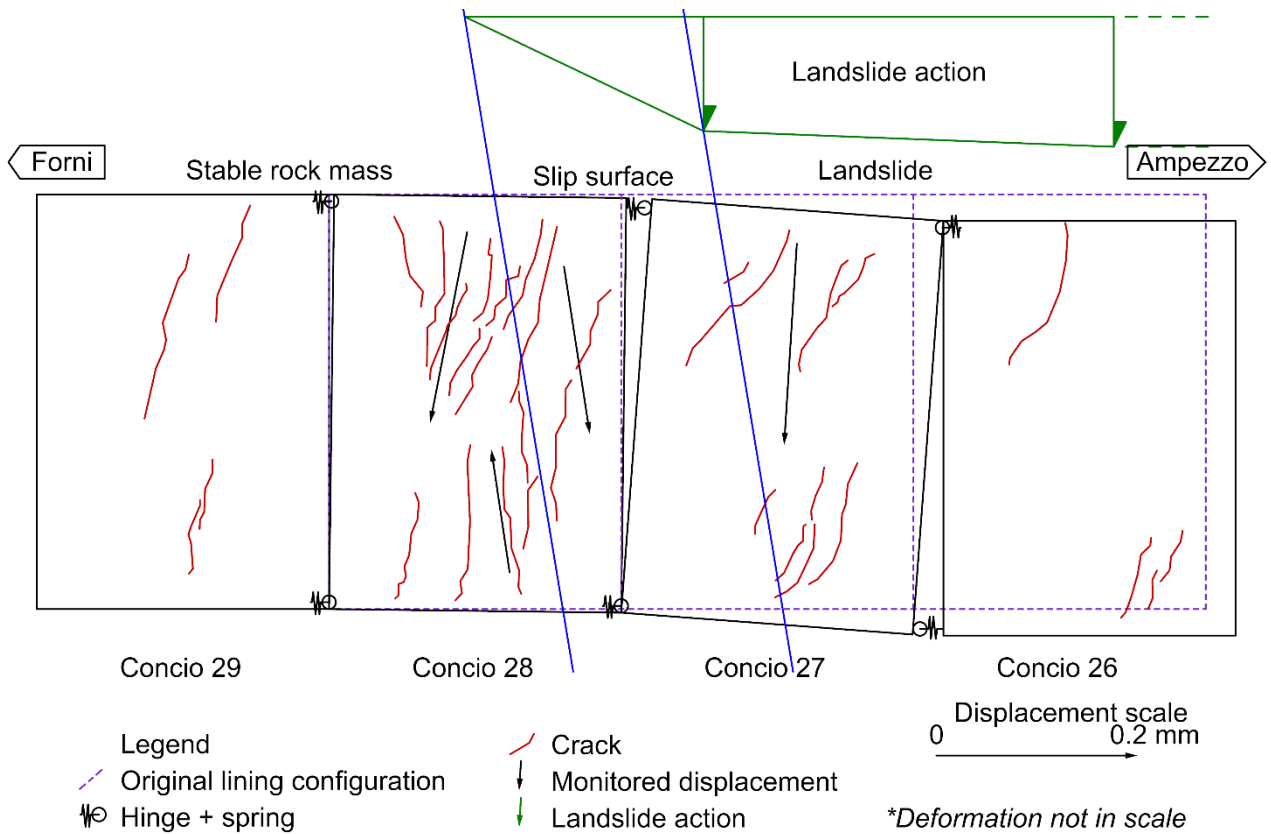


Figure 3-19 Proposed static scheme of the tunnel lining at the landslide crossing (segments 26-29)

### 3.3.2 DRAINAGE TUNNEL LINING

On the first week of August 2017, four crackmeters were installed in the drainage tunnel lining where the tunnel left the landslide body entering in the sound rock mass. This new monitoring section become necessary in order to establish a correlation between rainfalls, i.e. landslide activity, and damaging the concrete lining. In Figure 3-20, the instrumented tunnel sections are shown.

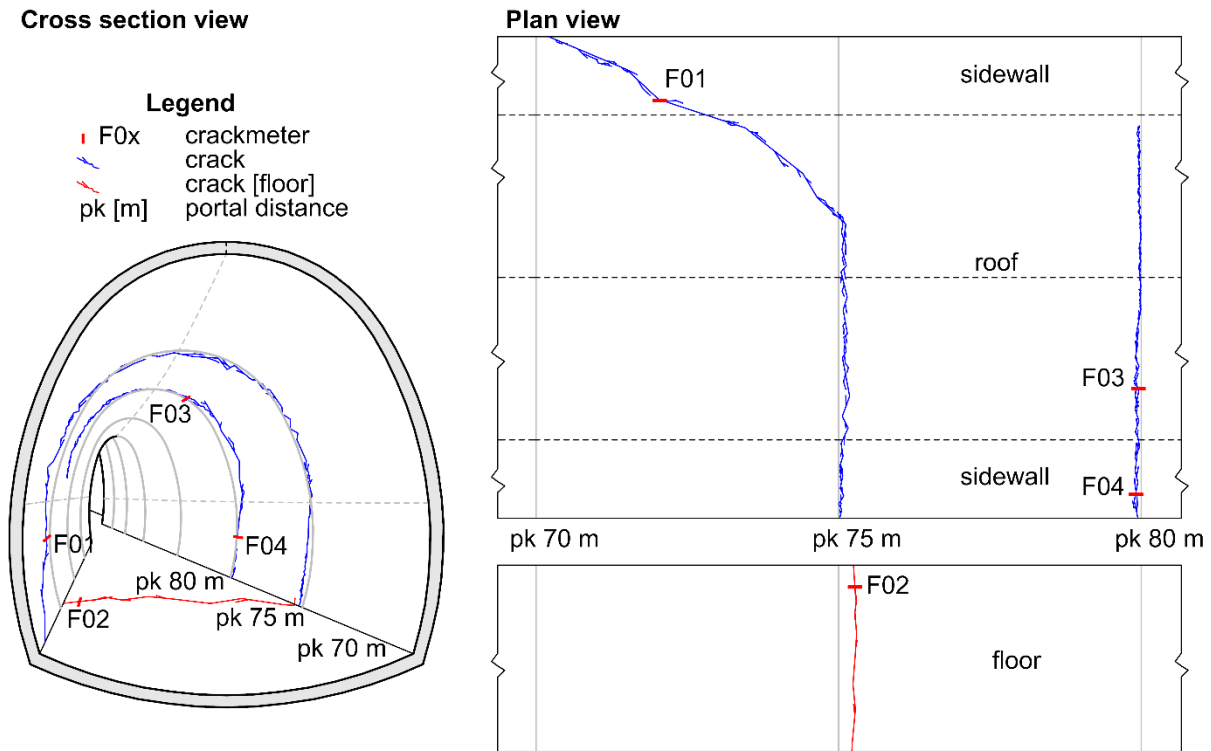


Figure 3-20 Structural monitoring in the drainage tunnel lining

In Figure 3-21, the lining deformations of the drainage adit are shown for the monitored time span. Irregularity on crackmeter F01 signal is probably related to a bad quality data transmission due to a too long cable path between data logger and transmission device, i.e. the distance entrance-monitored section is around 80 meters.

Crackmeters F01 and F02 shown an opening tendency, the displacements are in the order of magnitude of few millimeters. On the contrary, crackmeters F03 and F04 present negligible records.

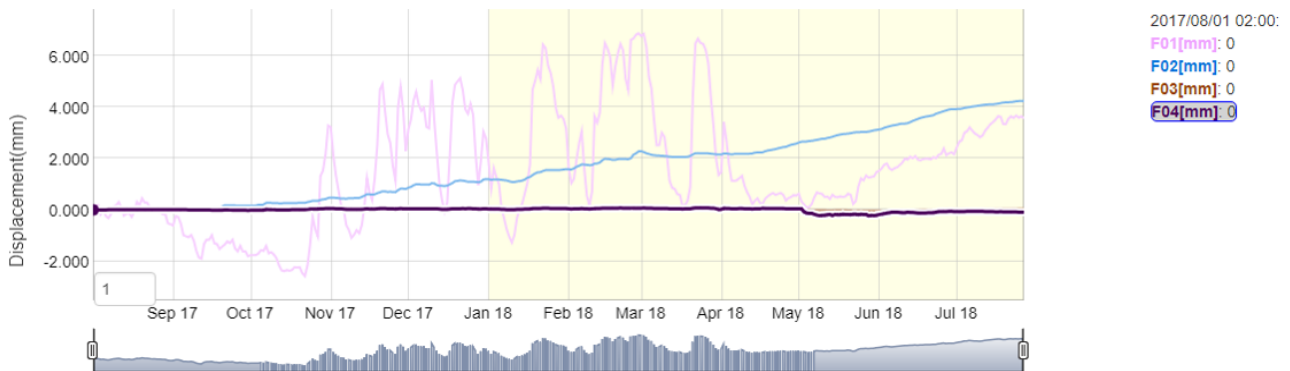


Figure 3-21 Deformations in the drainage tunnel lining (2017-2018. Screenshot of the online monitoring portal)

## 4 MATERIAL CHARACTERIZATION

In the following section, the results of rock lab testing are presented. The tested G6P borehole is crossing the overthrust contact at 36.20 m depth, and it was chosen because representative of the rock mass that would be excavated if the existing drainage tunnel would be extended.

The strength of rock masses depends on the intact rock properties and on the discontinuities. Primary and secondary discontinuities represent a weakness for the rock mass. Hence, even in the same geological unit with equal intact rock properties the discontinuity network plays a key role in the rock mass behavior. A severely fractured rock volume will not be able to fail according to its intact rock strength but according to a scaled value linked to the joint system. Normally, the rock mass geo-mechanical properties are scaled from the intact one considering some parameters, which are representative of the discontinuities such as rock bridges percentage, geological strength index (GSI) [35] or other semi-empirical methods. In the PRESENT WORK INVESTIGATIONS section, the results of engineering geology surveys has been presented. As before stated, in the region where the dolomitic pillars are found, i.e. in the head of the Passo della Morte landslide, given the large amount of open and persistent discontinuities, whose evolution is presently largely driven by active slope movements, a mere description of the discontinuity network definition gives only a partial description.

The present lab work has been carried out to evaluate the mechanical properties of the intact bedrock materials in the Passo della Morte landside area, with reference to the dolomite and the claystone.

The mineralogy of the material in the surrounding of the road tunnel has been characterized by X ray diffraction analysis. This investigation permitted the identification of minerals fraction responsible of the high water sensitivity of the rock mass. Xrd is presented in the last sub-section of this chapter. During this study several hypothesis concerning the impulsive activation of the landslide have been analyzed as it will be explained in the modelling section, but only a severe degradation of the properties can explain the observed deformation rates and trends.

### 4.1 LAB TESTING

A complete geo-mechanical characterization has been carried out at the Laboratory of Geoenvironment and Natural Resources (LAGIRN) of the Bologna University, under the careful supervision of Dr Fausto Peddis.

The specimens were taken from G6P borehole (Figure 3-4), where the dolomite-clay transition was detected at 36.20 m depth. In the boxes well-maintained 15-years old core logs, with a diameter of 100 mm can be found.

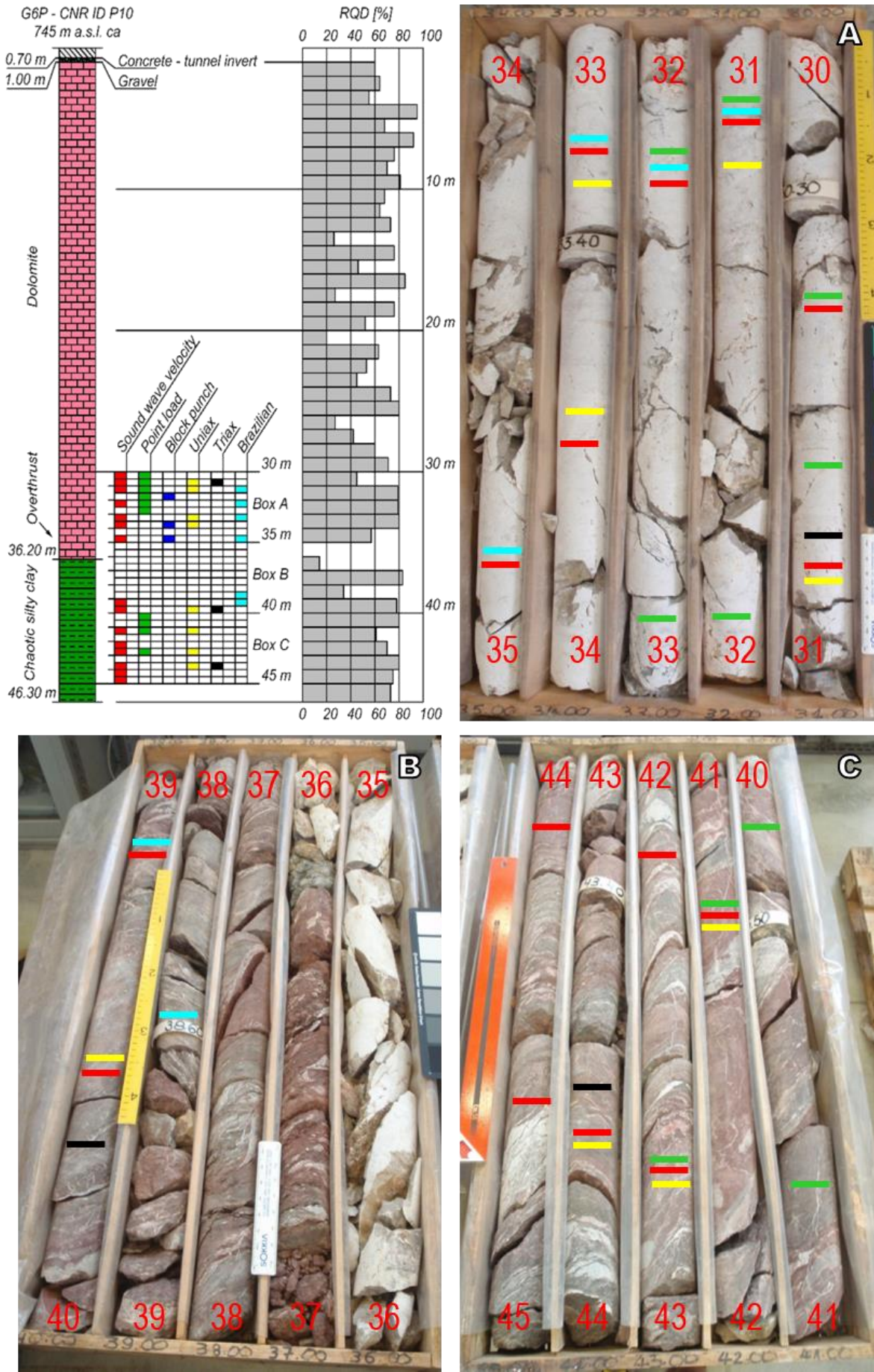


Figure 4-1 G6P (P10) core log boxes and testing localizations

In Figure 4-2 the unit weight for dolomite and chaotic silty clay.

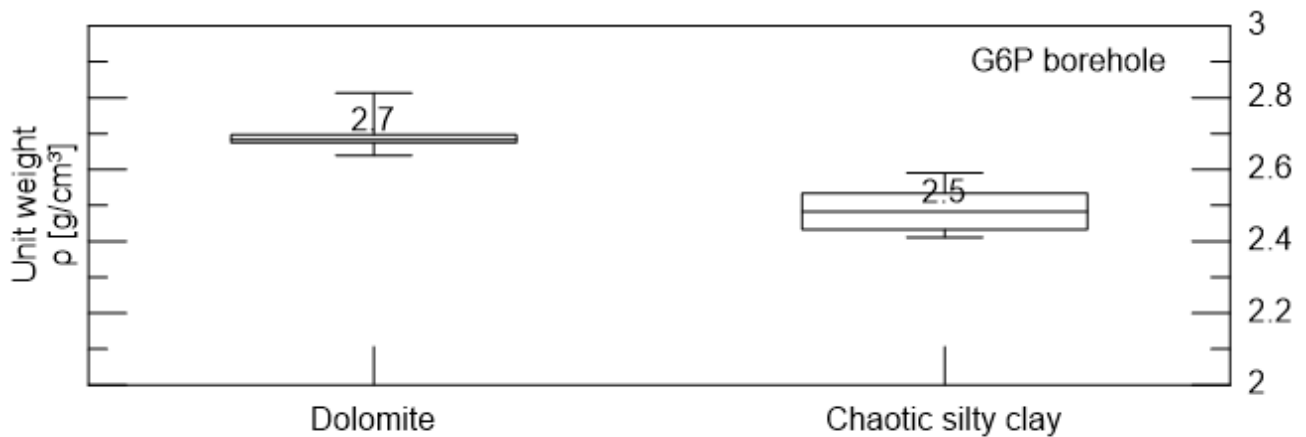


Figure 4-2 Unit weight

Destructive tests were carried out on specimens with suitable aspect and sound wave velocities. Preliminary identification of the sample quality is described in section SOUND WAVE VELOCITY of the present chapter.

#### 4.1.1 SAMPLES CORING

The specimen preparation process can severely disturb the rock samples. In rock mechanics practice, the disturbance related to coring is due to both stress release and contact with the drilling fluid. In few cases, this rheology variation of a rock sample must be considered. Holt et alii [36] reported a downscaling of the 20% for the UCS and 2% for the sample porosity compared to the field measurements. In the available literature, the Authors are mainly focusing on properties degradation related to coring of good quality rocks from oil and gas reservoirs.

The lab coring of G6P chaotic silty clay logs of clay shale led to poor quality samples. Frequently, the drilling fluid, i.e. water, washed the thin hematite lens (Figure 4-15) causing the loss of material. This could be recognized by the murky red tone took by the drilling fluid.

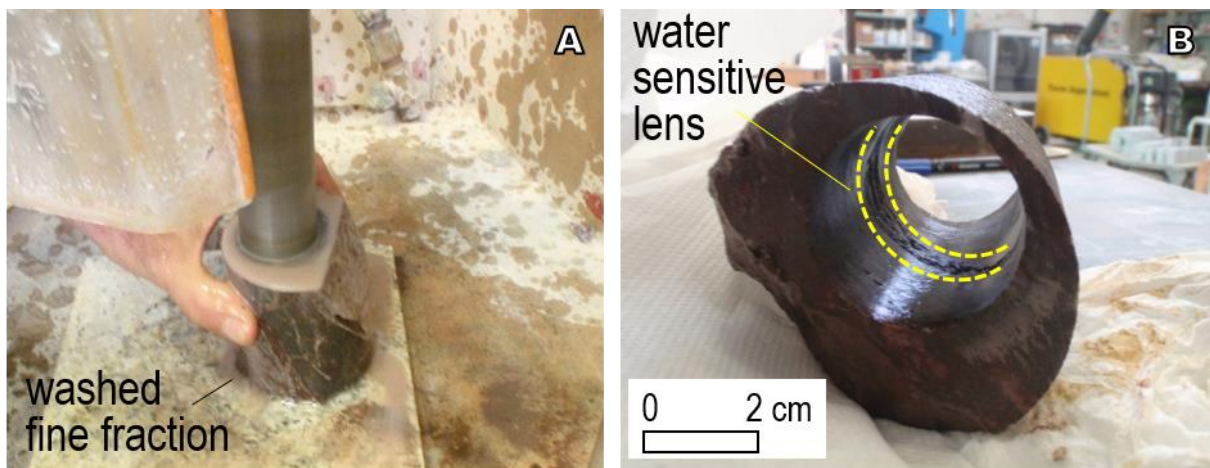


Figure 4-3 Sample coring: a visible lens of water sensitive material (left), muddy drilling fluid, i.e. water (right)

The coring of the dolomite material was generally more effective, with the exception of the logs nearby the overthrust surface. Frequently, those samples broke up along pre-existing open fractures (Figure 4-4)

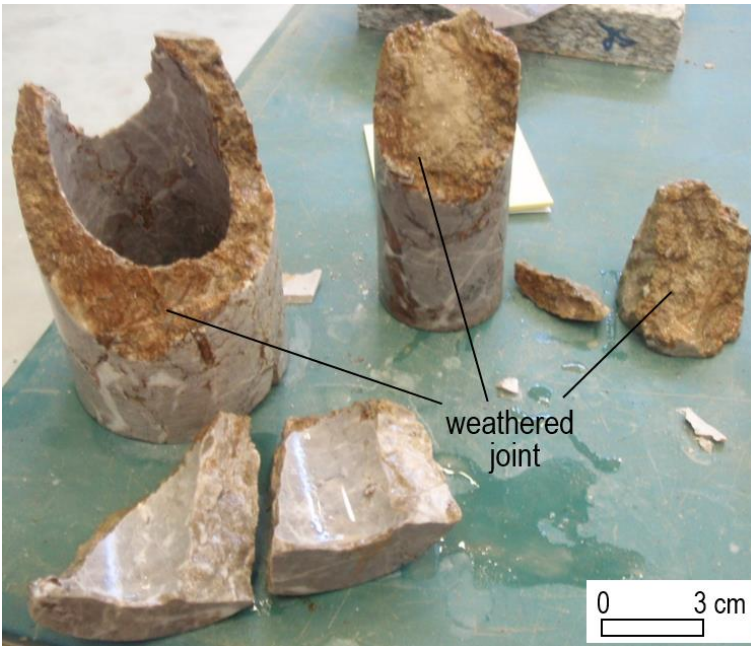


Figure 4-4 Open fracture in a dolomite specimen intercepted during coring stage

#### 4.1.2 SOUND WAVE VELOCITY

A preliminary characterization was done by measuring the sound wave velocity of the materials. This non-destructive technique was used to define the sample quality in order to reduce testing on poor specimens leading to useless results during the subsequent destructive procedures. Compression and shear wave velocities are presented in Figure 4-5.

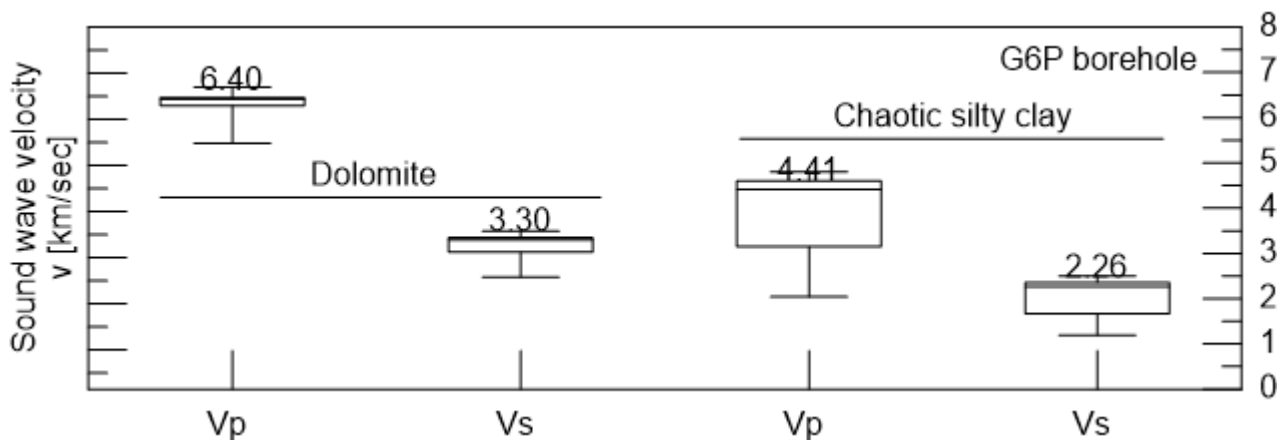


Figure 4-5 Sound wave velocity

Authors define several formulations to derive the elastic parameters, i.e. Young modulus and Poisson ratio, from the compression and shear wave velocity of a rocky material. Elastic parameters calculated from sound wave velocities are called dynamic [37]. The diffusion of this non-destructive technique led to the study of the link between dynamic and static characteristics [38], [39]. In Figure 4-6 the Young moduli through formulas proposed by different Authors [40] are shown, the static value from lab destructive tests is reported too.

The distinction between good quality and poor samples was done by observation by considering core attitude and visual aspect. Dolomite specimens with several cemented fractures or slightly chipped were classified as bad quality samples. Chaotic silty clay samples chipped, with a rough or striped on the lateral surface during coring were identified as bad quality too.

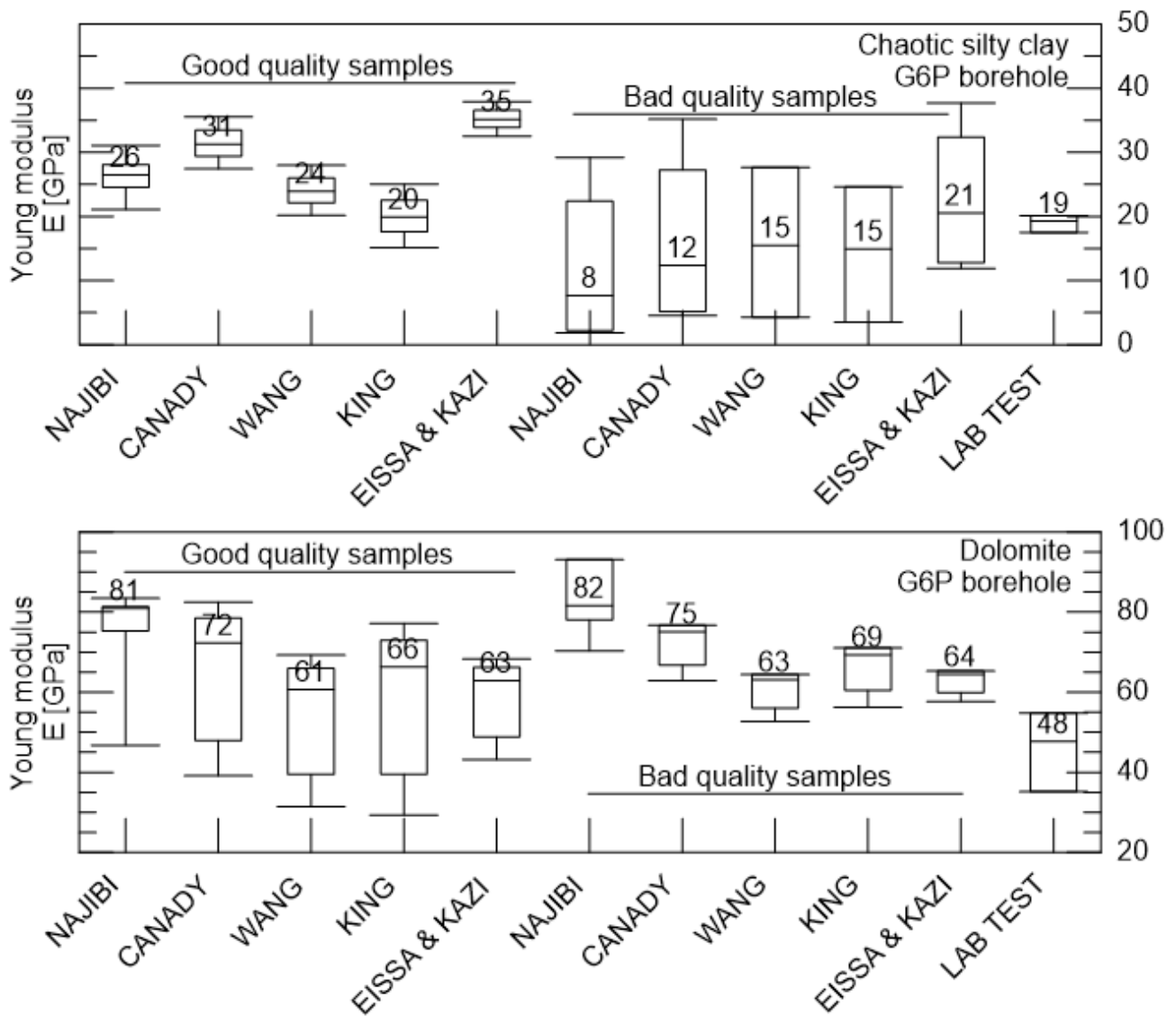


Figure 4-6 Young modulus calculated with different formulae and derived from lab testing

The results on the dolomite samples reported in Figure 4-6 allow supposing that the material cementing the fractures is stronger than the rocky matrix. On the contrary, the clayey material categorized as bad showed lower moduli values than the good quality specimens and from lab testing.

Velocities on chaotic silty clay specimen were measured on the borehole axis and perpendicularly to the bedding plans. A strong anisotropy was revealed. Unfortunately, it was not possible to core enough samples perpendicularly to the bedding planes, i.e. tested population might be not significant.

### 4.1.3 UNIAXIAL COMPRESSIVE STRENGTH AND ELASTIC PARAMETERS

The Uniaxial Compressive Strength (UCS) represents the most diffused parameter in rock engineering design [41]. GSI-based strength of a rock mass is based on field observation and UCS [42], [43]. Six samples of dolomite and claystone have been tested in uniaxial compression. The standard recommendations were followed [44], i.e. sample geometry, loading rate and testing procedure. A high-diameter ratio has been kept around two for every 38 mm-diameter specimen.

In Figure 4-7 the UCS from different testing procedures are shown, as found in literature [45]. More than 40 20-mm specimens were tested at the point load machine following the regular procedure [46]. Furthermore, ten specimens were tested on the block punch machine [47].

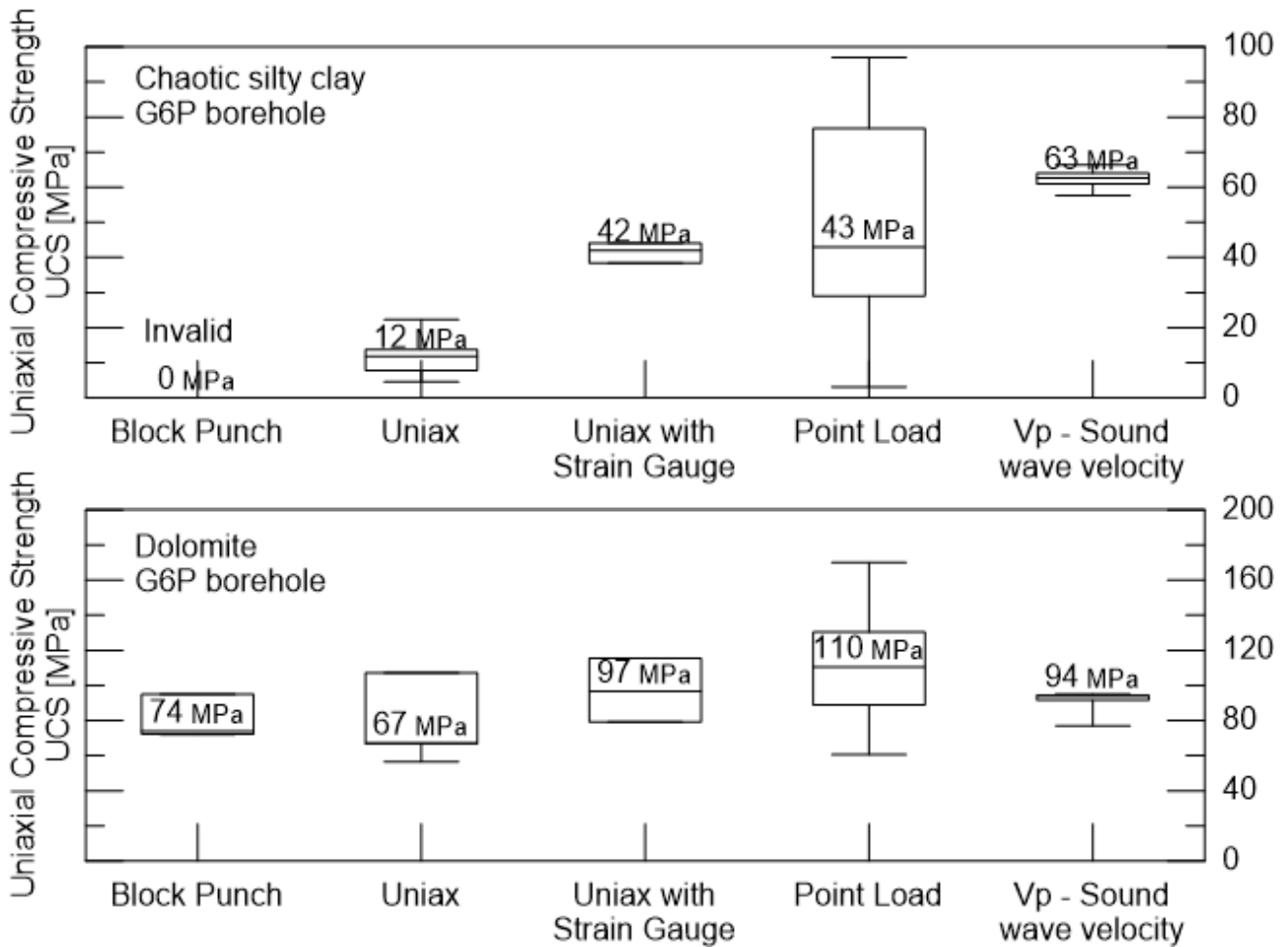
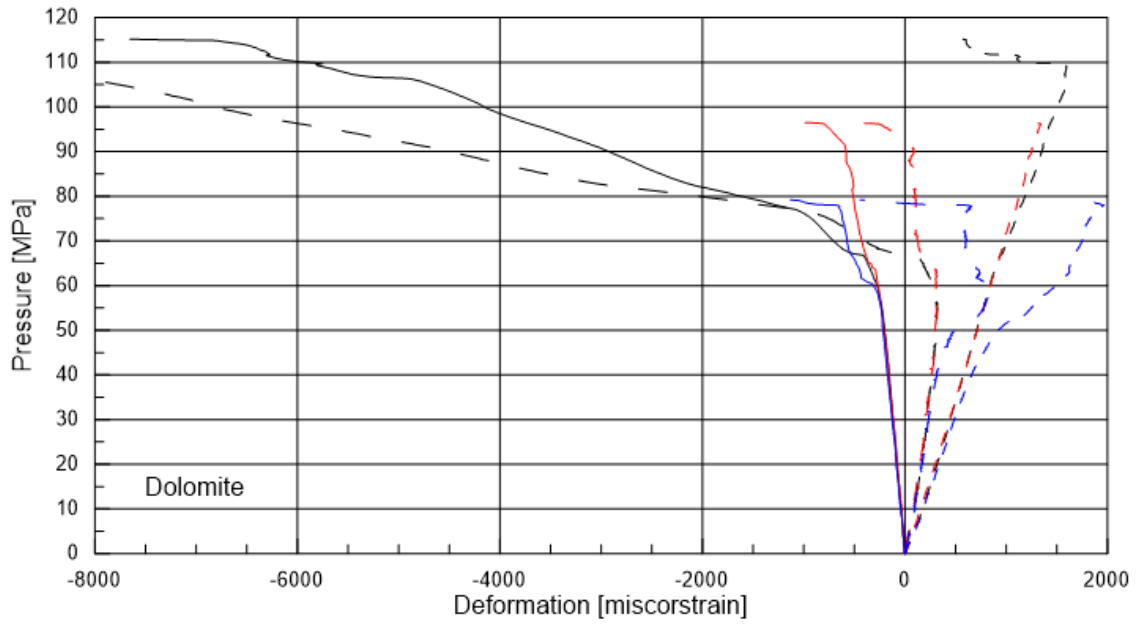


Figure 4-7 Uniaxial Compressive Strength

Additionally, three specimens for each lithology have been equipped with strain gauges and tested. Those tests record the circumferential and axial strains together with the load increments, which allow determining elastic moduli and Poisson ratios.

— S10 - Volumetric strain      - - - S9 - Volumetric strain      - - - S7 - Volumetric strain  
 — S10 - Circunferential strain      — S9 - Circunferential strain      — S7 - Circunferential strain  
 - - - S10 - Axial strain      - - - S9 - Axial strain      - - - S7 - Axial strain



— S13 - Volumetric strain      - - - S12 - Volumetric strain      - - - S11 - Volumetric strain  
 — S13 - Circunferential strain      — S12 - Circunferential strain      — S11 - Circunferential strain  
 - - - S13 - Axial strain      - - - S12 - Axial strain      - - - S11 - Axial strain

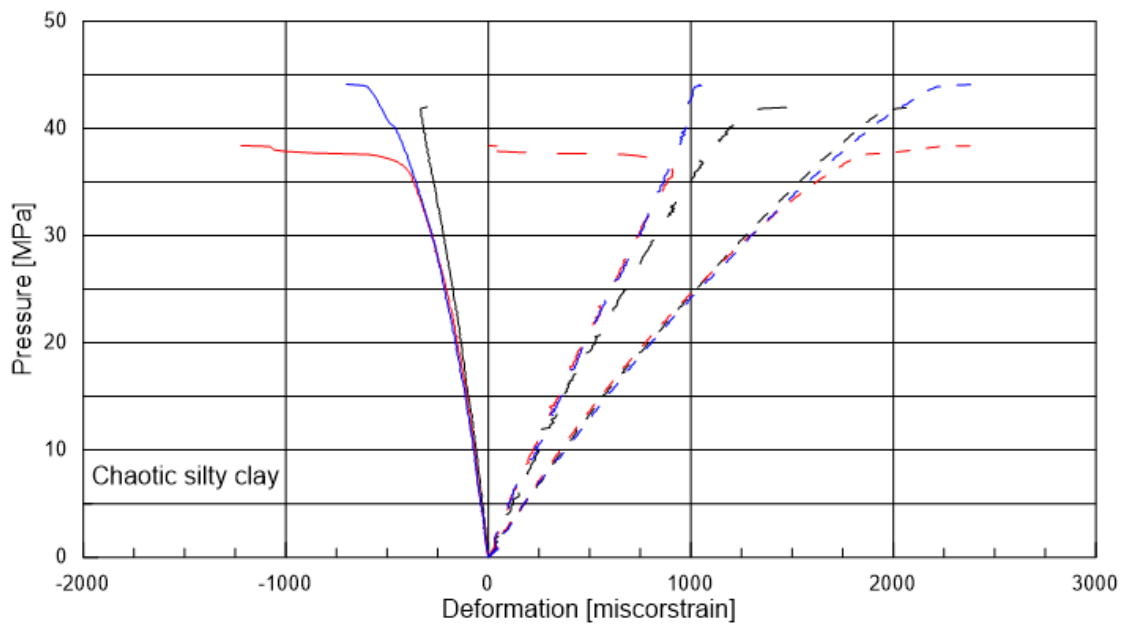


Figure 4-8 Uniaxial compression tests equipped with strain gauges

In Figure 4-9 it can be seen that the dolomite samples have instant “explosive” rupture once the failure load is reached, while the flat curves part (Figure 4-8) can be representative of the role played by the fractures. Apparently, the glue used to attach the strain gauges have partially modified the rupture of the claystone.

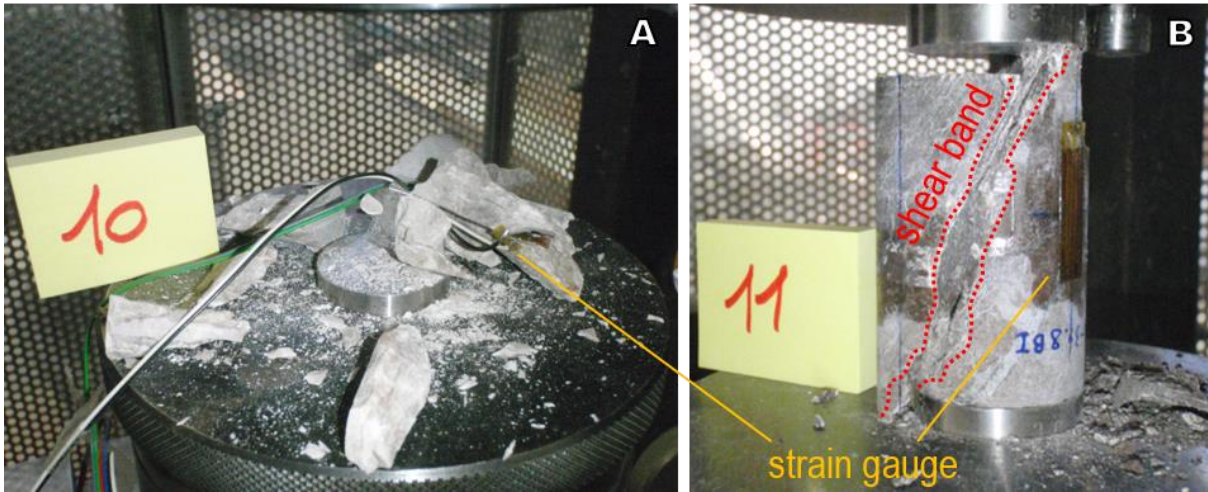


Figure 4-9 Uniaxial test on dolomite (A) and chaotic silty clay (B)

Through the classic continuum mechanic formulation, it has been possible to determine the Poisson ratio of the tested rocks.

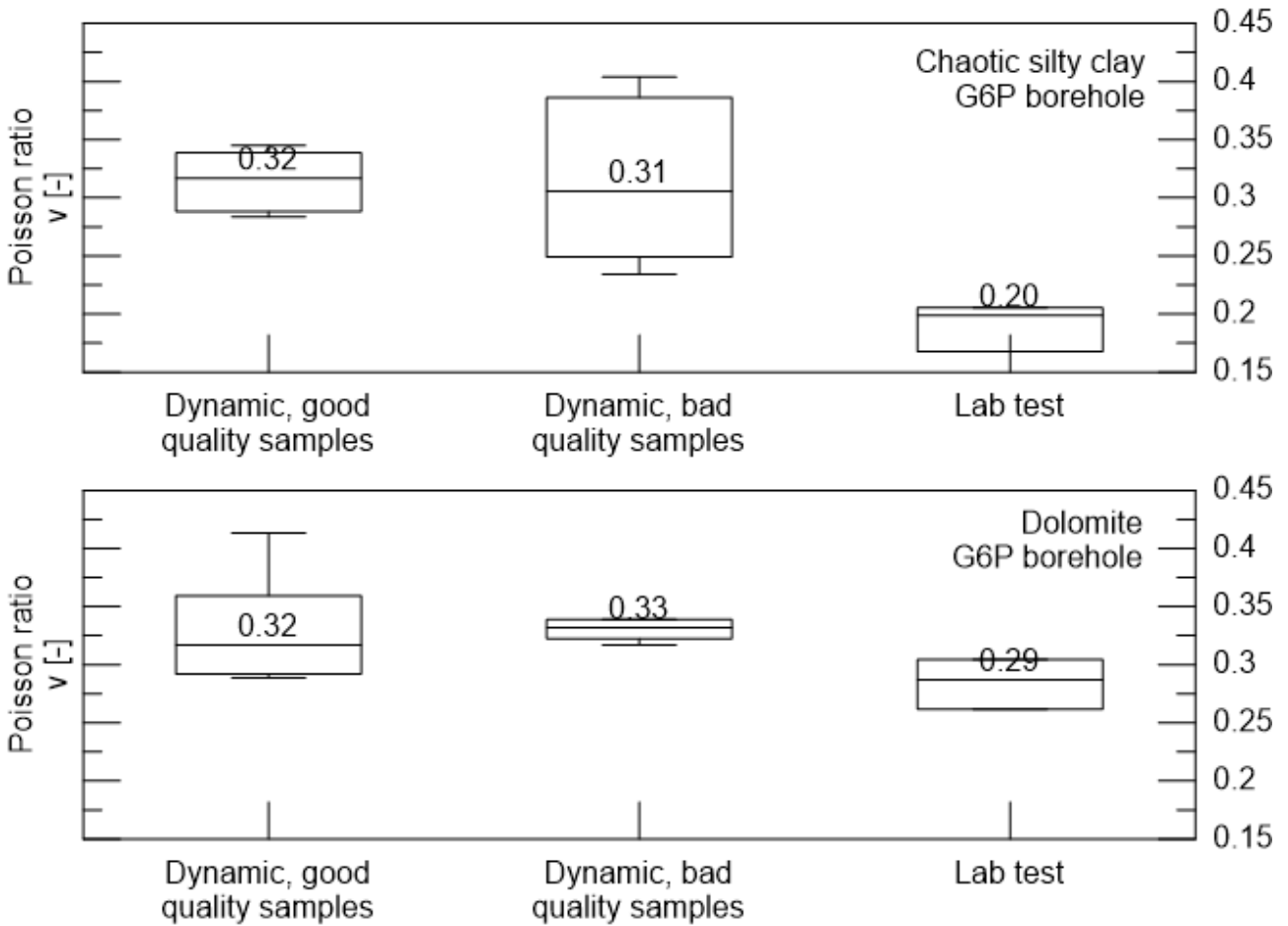


Figure 4-10 Poisson ratio

In Figure 4-10 the Poisson ratio for both the tested lithology. The experimental values fall in the range defined in literature [48].

#### 4.1.4 TRIAXIAL TEST

Triaxial tests were carried out on three samples per lithology. The confining stresses were defined as the assumed lithostatic in situ stress at the specimen depth  $\pm 50\%$  [49].

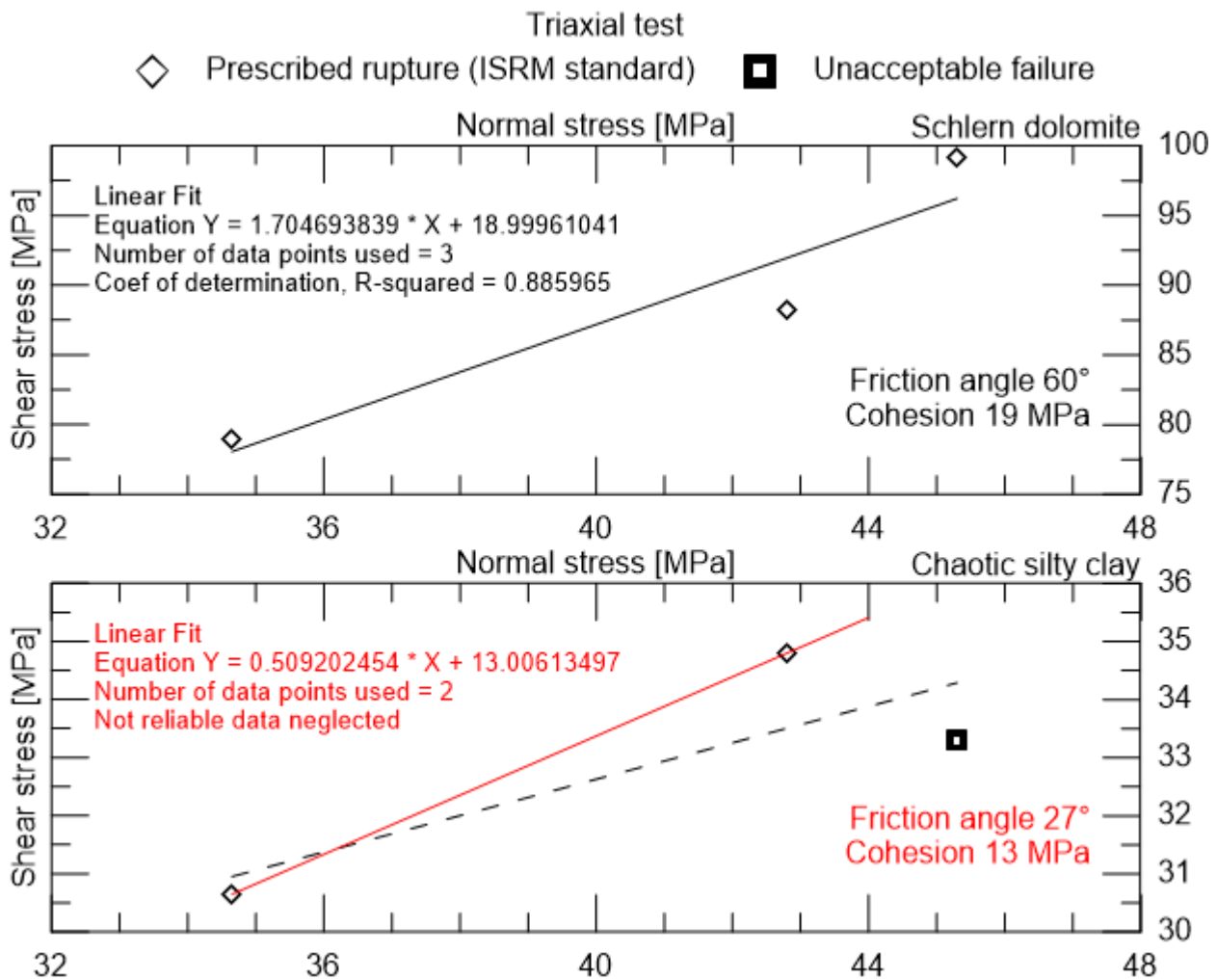


Figure 4-11 Triaxial test

The triaxial test results has been elaborated in order to obtain the Mohr-Coulomb failure criterion parameters, i.e. friction angle and cohesion. Those mechanical parameters have been estimated by linear regression and curvilinear envelope fitting through the rocData code [50].

Table 4-1 Calculated friction angle and cohesion from triaxial test data interpretation

	dolomite		chaotic silty clay	
	friction angle [°]	cohesion [MPa]	friction angle [°]	cohesion [MPa]
rocData [50], i.e. non-linear envelope	46	35	25	12
linear regression	60	19	27 *	13 *

Star/\*: Regression over two remaining samples having a ISRM standard acceptable failure [44]

Results from different data regression are shown in Table 4-1.

#### 4.1.5 TENSILE STRENGTH

The tensile strength is a fundamental parameter of a rocky material, which governs the general slope behavior and eventually failure [51]. The most diffuse method to determine the tensile strength is the indirect test, also called Brazilian test. Twelve dolomite and six clayey samples were tested up to failure through the application of a constant load rate of 0.1 kN/second [52]. Resulting values are presented in Figure 4-12.

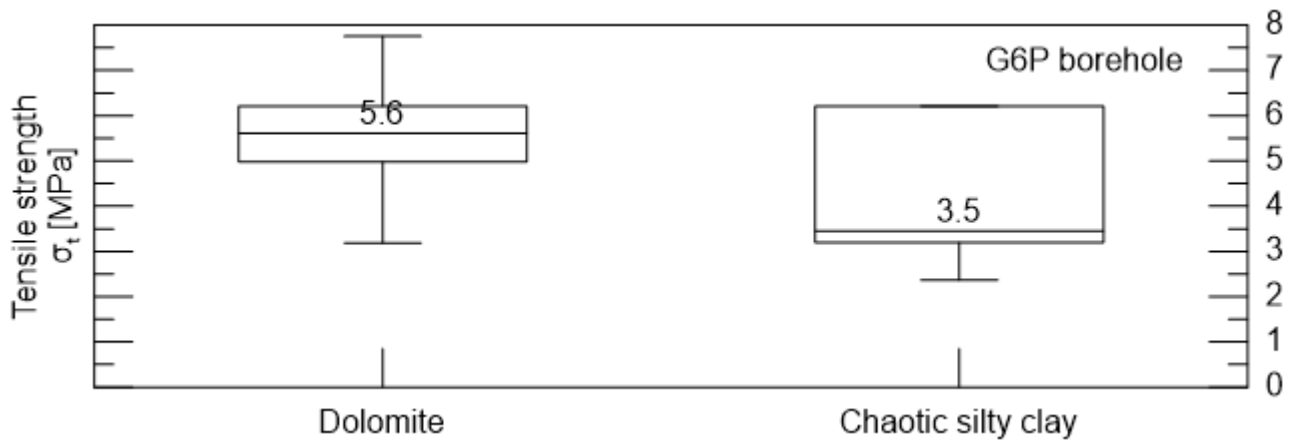


Figure 4-12 Tensile strength from indirect (Brazilian) test

In Figure 4-13 in can be seen that the cemented rock joints do not represent preferential rupture planes for the specimens. This fact proves the relatively high strength of the cemented discontinuities in the dolomite, which has been already observed in the herein reported lab investigations i.e. during uniaxial and sound wave velocity testing.

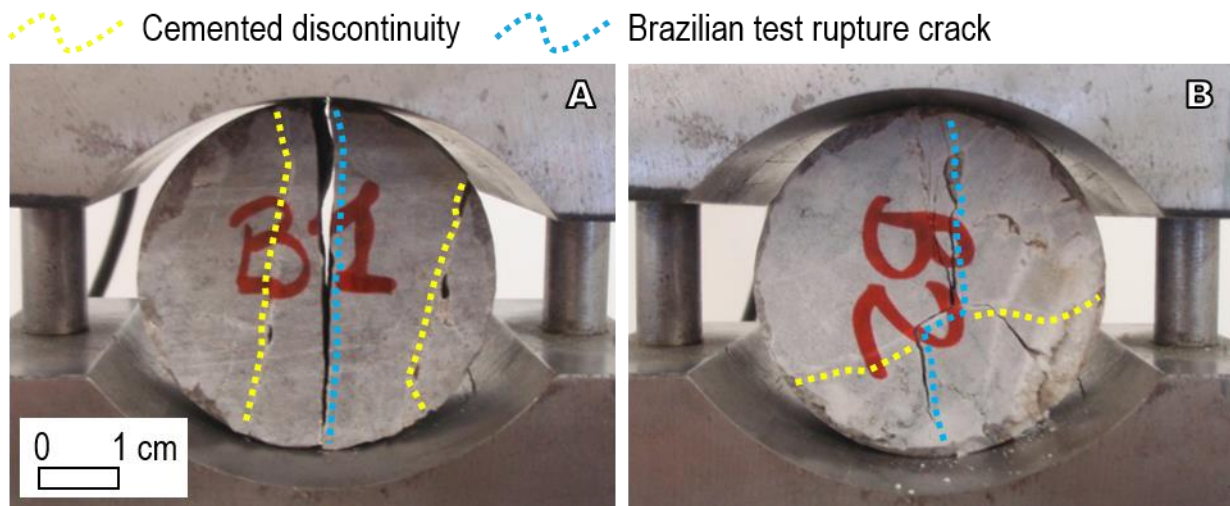
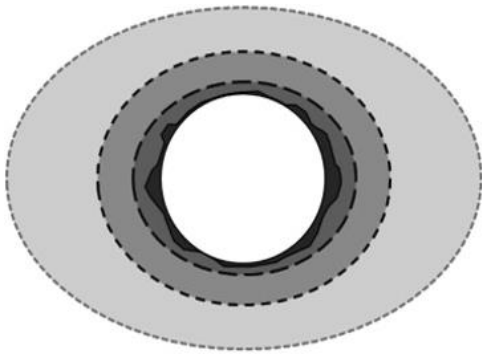


Figure 4-13 Indirect tensile test (Brazilian) sample failures. Developed ruptures look completely (A) or partially (B) not dependent from the cemented cracks.

#### 4.1.6 X-RAY DIFFRACTION

Mineralogy analysis by X ray diffraction has been carried out on the chaotic silty clay from G4I borehole (CNR ID I12, Figure 3-4) This material has been selected because it appears to be weathered as the rock on the sliding surface is supposed to be. The change of the properties alteration is related to the tunnel presence and is caused by enhanced groundwater circulation because the tunnel works as a pipe conveying water from the fractured dolomite. Furthermore, the high percentage of gypsum drives the water sensitivity of the weak rock mass. The tested sample was took about four meters below the tunnel invert, i.e. into the Excavation Influence Zone (EIZ) propose by Perras & Diederichs [53] (Figure 4-14).



- EIZ – Excavation Influence Zone
- EDZ – Excavation Damage Zone
- HDZ – Highly Damaged Zone
- CDZ – Construction Damage Zone

Figure 4-14 Disturbance zones around an underground opening (by Perras & Diederichs [53])

Preliminary results are shown in Figure 4-15. The presence of iron oxides gives the typical reddish color to the chaotic silty clay.

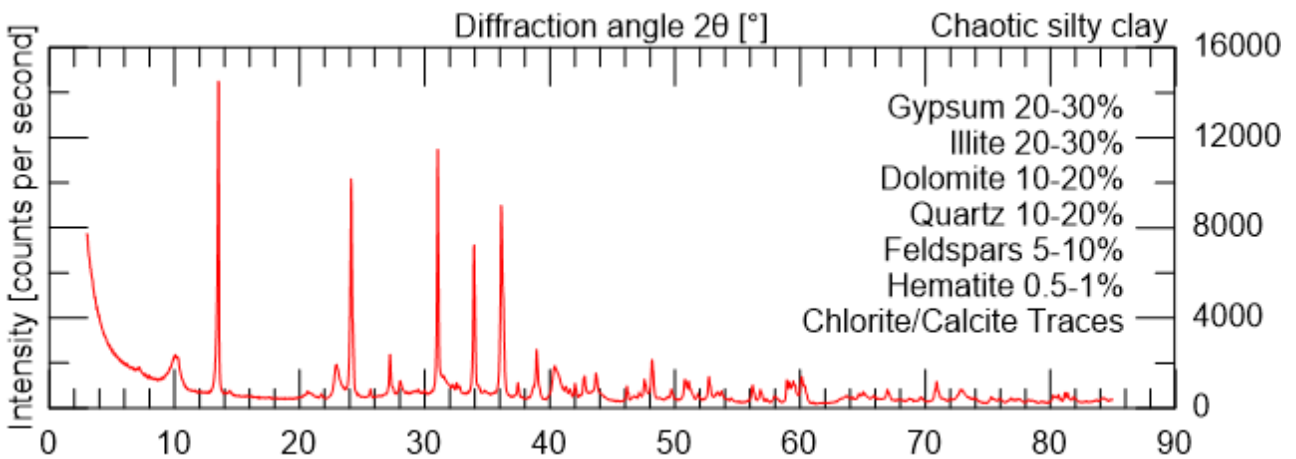


Figure 4-15 Mineralogy by X ray diffraction analysis of sample from G4I borehole (depth 4 m)

The mineralogical analysis by X ray diffraction has been possible thanks to Professor Simonetta Cola (Padua University), my colleague PhD Giulia Bossi (CNR IRPI) and performed by Dr Fabio Tateo (CNR Geosciences and Earth Resources-IGG).

## 5 SLOPE MODEL

Flac3D is an explicit finite difference code largely used in geotechnical engineering. Ranging between commercial and open source codes, Flac3D has been selected because extremely flexible and accurate in large strain deformation.

Flac3D is the acronym of Fast Lagrangian Analysis of Continua and it is specifically implemented for tridimensional problems. A discrete number of zones forming the grid is representative of the real geometry of the object. Each zone is defined by a series of nodes at the edges, the number of nodes is depending from the zone shape adopted and the discretization. When the simulation starts, the code calculates the discrete derivative in the set of the governing equations directly through an algebraic expression. At each node, those equations are wrote in terms of field variables, such as stress and displacement. Every single zone behaves following its assigned stress-strain law. The boundary conditions and the applied loads represent the known variables for the iterative solving process.

First, the code adaptability allows the user to upload grid, water seepage or load condition and any kind of spatial information in a text file. This feature becomes fundamental considering the grid construction workflow adopted and explained below. The built-in programming language called FISH, representative of FlacSH, was used to customize simulation. It permits the definition of specific functions representative of any kind of soil rheology, i.e. user-defined mechanical models, hardening laws or flow laws.

Secondly, the lagrangian framework adopted leads to accurate and relatively fast results in large strain deformation, this computational advantage is fundamental in simulating landslide phenomena. In large strain mode, the code can simulate plastic flows of soils and rocks when the yielding status is reached, consequently the original grid deforms and follows the displacements.

### 5.1 SLIP SURFACE SIMULATION STRATEGY

The landslide body and the slip surface geometry have been drawn through geomorphological evidence mapped in the field and interpreting a large number of boreholes drilled in the past twenty years. The geological sections proposed and later modified by Marcato [2], [33] have been very helpful in this stage. In a 3D drawing suit, the detected slip surface elevation points (Table 5-1) were added to the existing 2D geological section. The resulting slip surface was then imported in a GIS environment, resampled and finally uploaded in a Flac3D [54] compatible format through a Matlab script (.txt extension).

Table 5-1 Slip surface reference points at Passo della Morte (Figure 3-1 and Figure 3-4)

ID CNR	depth [m]	slip surface depth [m]	borehole head elevation [m] a.s.l.
I1	72.2	13 / 35*	730
I2	76	20	690
I3	92	40 / 10	730
I4	84	53* / 36 / 24	757
I5	46	23* / 5*	737
I6	50	32*	737
I7	58	45 / 8	729
I8	75.5	32	734
I9	20	floating	736
I10	41	31* / 16	735
I11	100	35, / 70	735
I12	70	5 / 23 / 50*	735

I13	80	60 /	793
I14	65	10* / 17 / 49	745
I15	39.7	24 / 32*	729
I16	65	59 / 23*	728
I17	54	25, / 50*	710
I18	80	floating	715
I19	150	80	880
I20	200	floating	900
PC1	60	23	685
PC2	97	33 / 65*	679
PC3	97	13	770
PC4	60	not recognized	721
PC5	80	not recognized	660
<b>Star/* marks case of uncertainty</b>			

During the drainage tunnel construction, the slip surface was crossed at pk 75 m ca. The thin sliding surface founded is shown in Figure 5-1.



Figure 5-1 Slip surface intercepted during the drainage tunnel excavation, note the thickness of 2 m ca

## 5.2 MODEL DEFINITION

The sliding surface was modeled using interface elements. Interface acts as a 0-thickness layer connecting the nodes at the surfaces contact. Furthermore, the link can be free to slide or a mechanical model can be assigned [54]. This simplification of the slip surface geometry permits to overcome several mesh issues like element penetration and bumping, which are frequent in large

models accounting for relatively small geometry features. Several Authors [54], [55] have highlighted the importance of reliable simplified mesh.

As a reference for the interface strategy adoption the displacement profile of inclinometer I16 (Figure 5-2) has been used. This confirmed other evidence detected at Passo della Morte such as the visive inspection of the slip surface thickness intercepted during the drainage tunnel excavation (Figure 5-1).

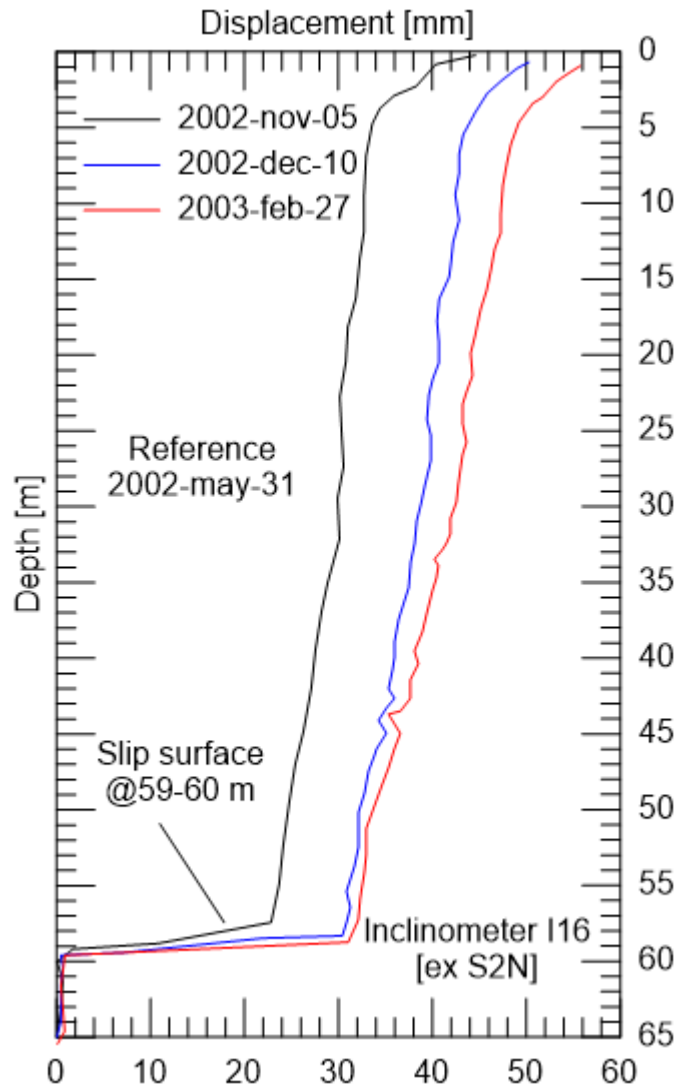


Figure 5-2 Inclinometer S2N (same location I-16)

The grid construction followed a specific procedure, which guarantees a perfect match between the nodes on the stable and unstable areas border. As shown in Figure 5-4 the mesh was built by triangular and brick elements in order to have no nodes attached on the side of a neighborhood element.

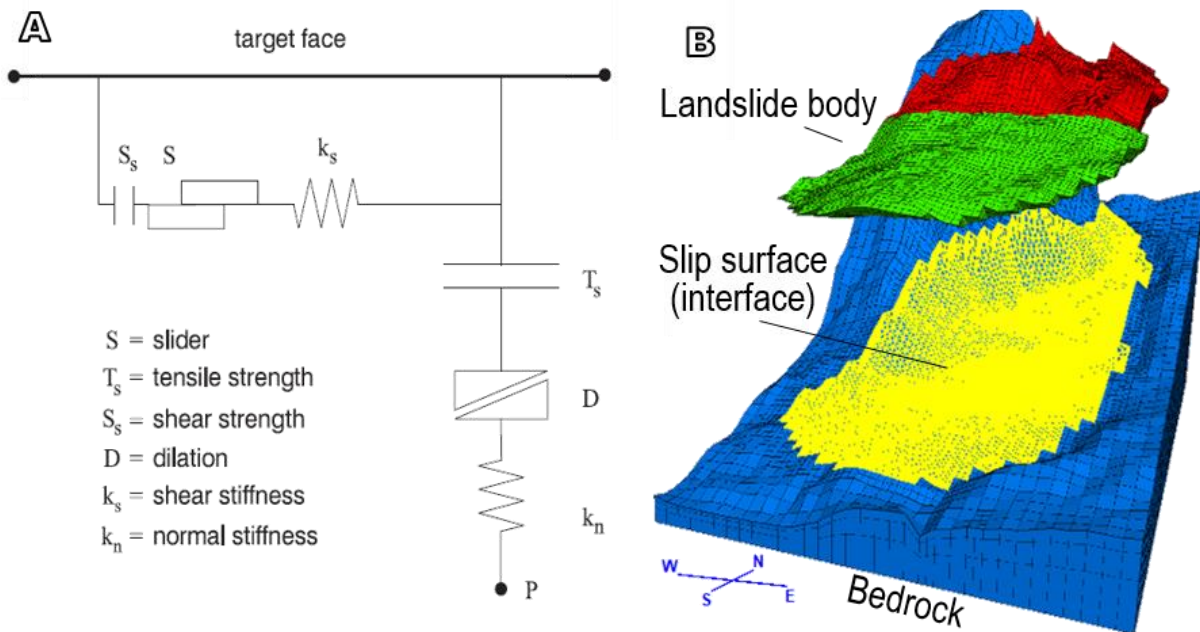


Figure 5-3 Interface elements in Flac3D: rheological scheme (after Flac3D manual [54], A) and present model application (B)

The geometrical details adopted to build a reliable mesh are reported in Table 5-2.

Table 5-2 Mesh (grid) regions settings

group name	element shape	X,Y-dir. size [m]	n. Z-dir. subdivision [-]	Z ratio [-]	material model [-]	fig. [-]
<b>stable regions not bordering with the landslide region</b>						
stable	brick	20 x 20	3	0.5	Linear elastic	
<b>unstable-stable bordering regions</b>						
stable	brick	10 x 10	3	0.5	Linear elastic	
landslide	uniform wedge	10 x 10	2	1	Mohr-Coulomb	
<b>unstable-stable bordering regions</b>						
stable	brick	10 x 10	3	0.5	Linear elastic	
landslide	brick	10 x 10	10	1	Mohr-Coulomb	
<b>In a further step, the landslide region is going to be further subdivided by lithology</b>						

The transition between dolomite and chaotic silty clay in the dolomite pillars area was defined by the section AA' Figure 2-9), BB' (Figure 2-10) and FF' (Figure 2-11) and I20 borehole (Figure 3-4). The resulting average plan is almost horizontal (15°), dipping 300° North ca.

The overthrust contact between dolomite and chaotic silty clay has been assumed as a planar surface. This strong hypothesis was adopted in order to simplify the model geometry but also because of the lack of data required for defining a more detailed 3D surface. A regression procedure over the mapped contact points allows estimating the dip direction of the contact surface in 238° North, dipping 30°. Those reference points are located at the Rio Verde fall area, San Lorenzo pk 450 m and 36.20 m depth into the G6P borehole (Figure 3-4).

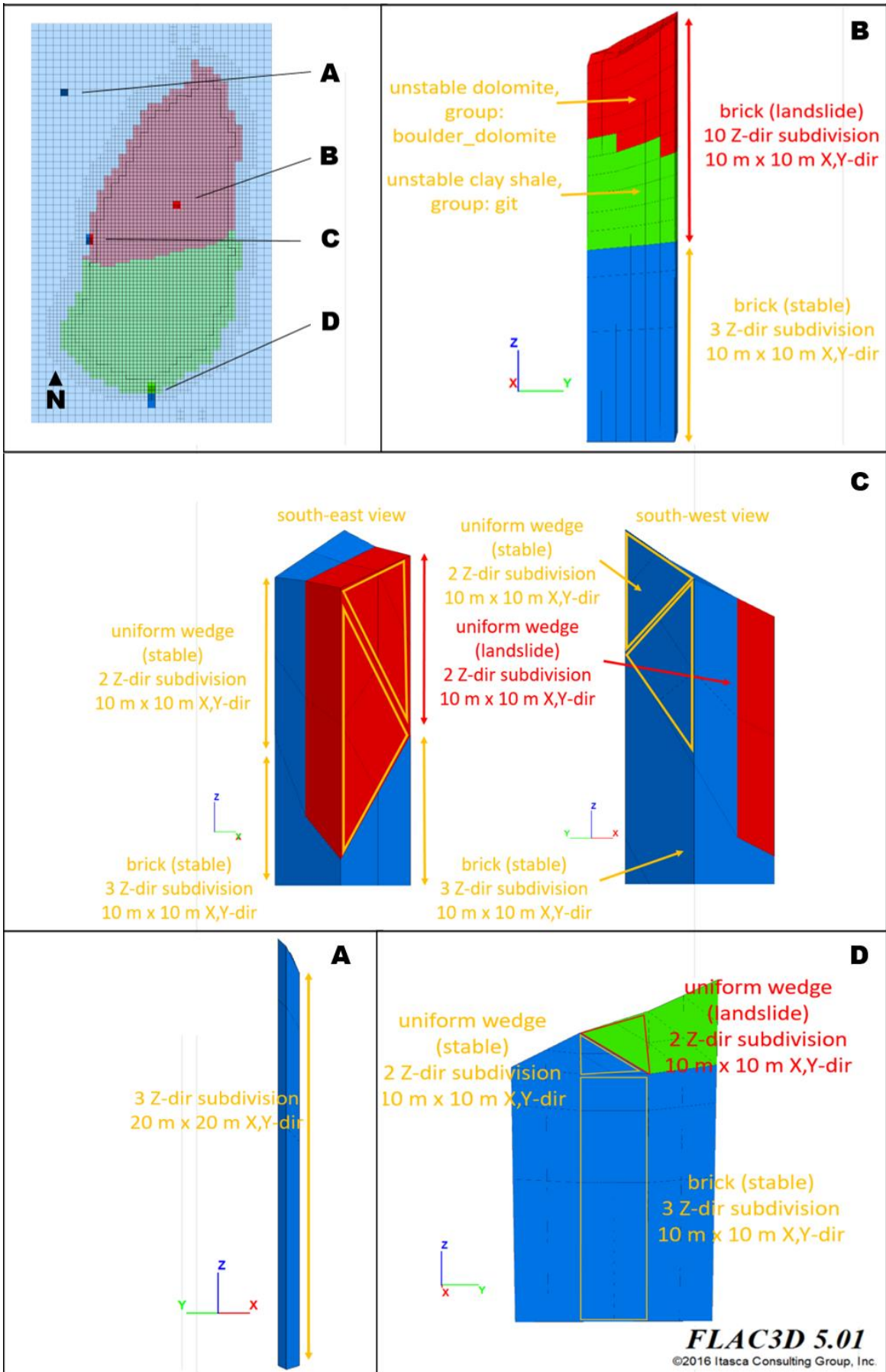


Figure 5-4 Flac3D grid (mesh) construction details

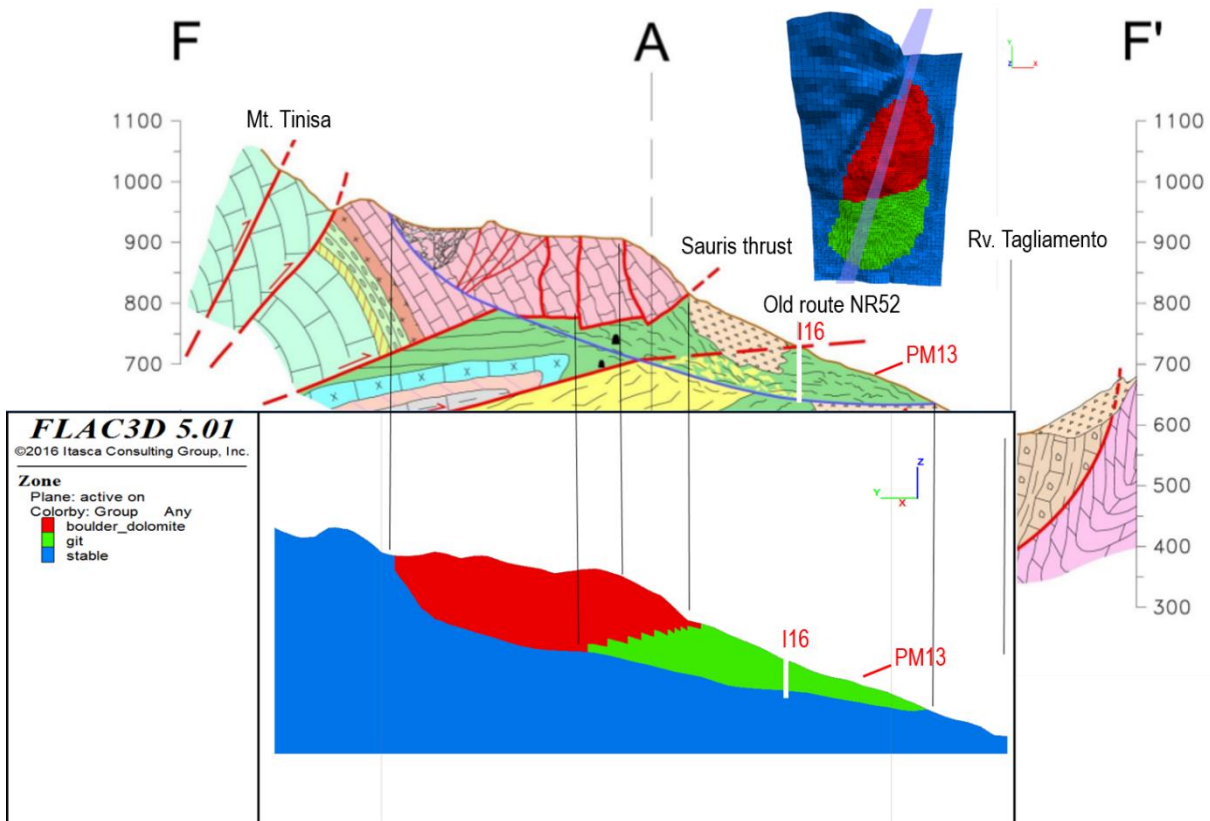


Figure 5-5 Comparison between geological and modeled sections

### 5.3 SENSITIVITY ANALISYS

A wide range of model settings was tested in order to define the model results sensitivity to the properties variation. The results are grouped by landslide body, slip surface and model setting parameters.

Three reference points were used as displacement benchmarks, i.e. pm13, i16 head and peak of the dolomite pillars region. Superficial deformation in the models has been checked against satellite interferometry data available in the web-GIS of the Italian Ministry of Environment [56].

Firstly, in Figure 5-6, it can be seen that the model displays a high sensitivity to variation of the slip surface friction angle and stiffness. In numerical modelling, normal and shear stiffness cannot be univocally defined at slope scale [41].

Secondly, the results of the elastic moduli, tensile strength, friction angle and cohesion variation in the landslide body are presented in Figure 5-7. It can be observed that the model displays a low variation if the material tensile strength and friction angle are decreased. On the contrary, the bulk and shear moduli influence severely the simulation output.

Finally, Figure 5-8 reports the simulation in which a model setting was modified. The general configuration having the major influence on the results is the elastic moduli used during the stress activation-gravity phase. Moreover, the adoption of the modified Hoek & Brown failure criterion lead to a sensible variation in the displacements magnitude ( $\pm 20\%$  ca). Similar difference can be seen selecting a horizontal-vertical stress ration ranging between 1 and 3, the benchmark value was set as 2 [13].

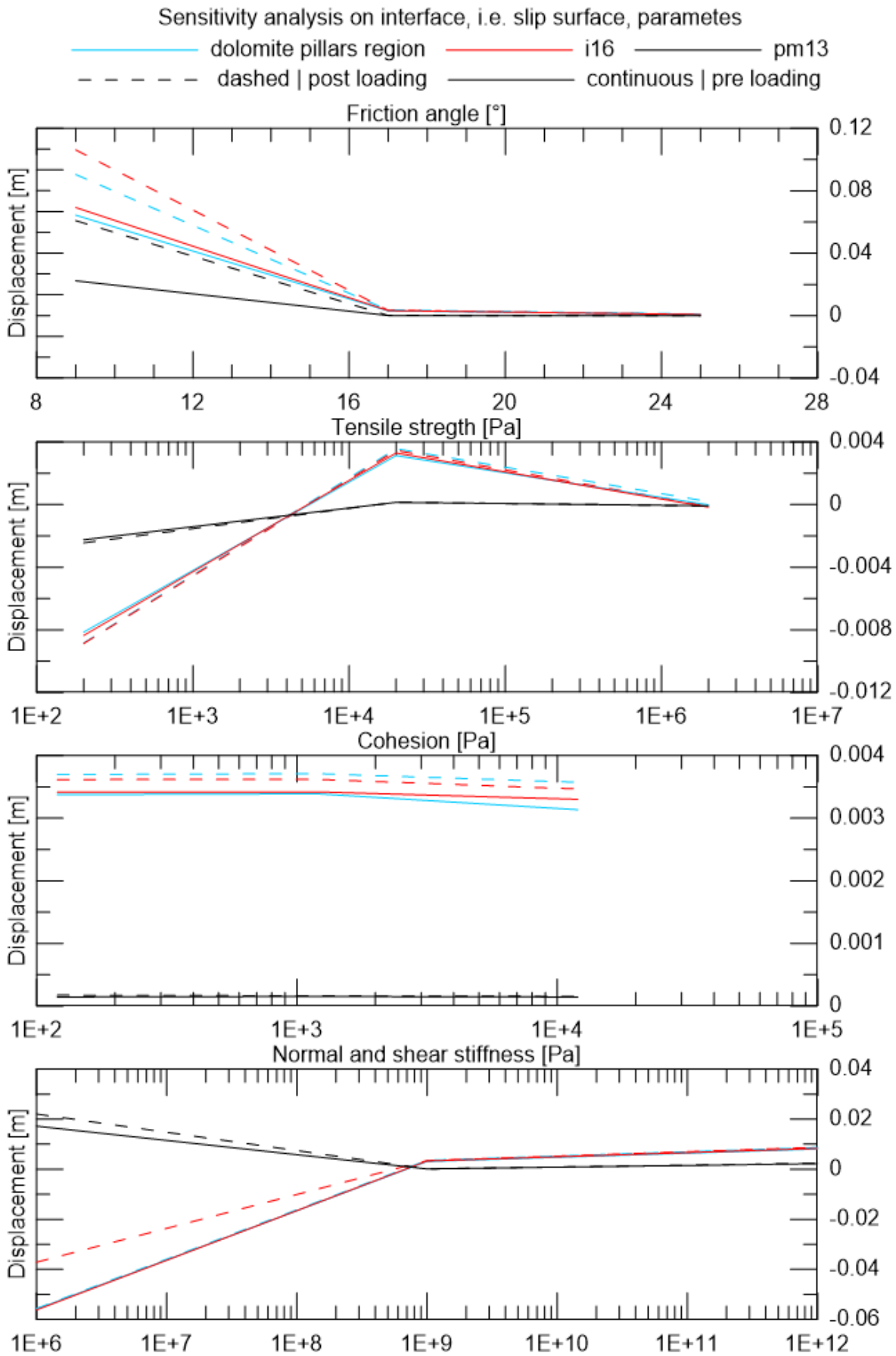


Figure 5-6 Sensitivity analysis on the landslide slip surface, i.e. interface elements

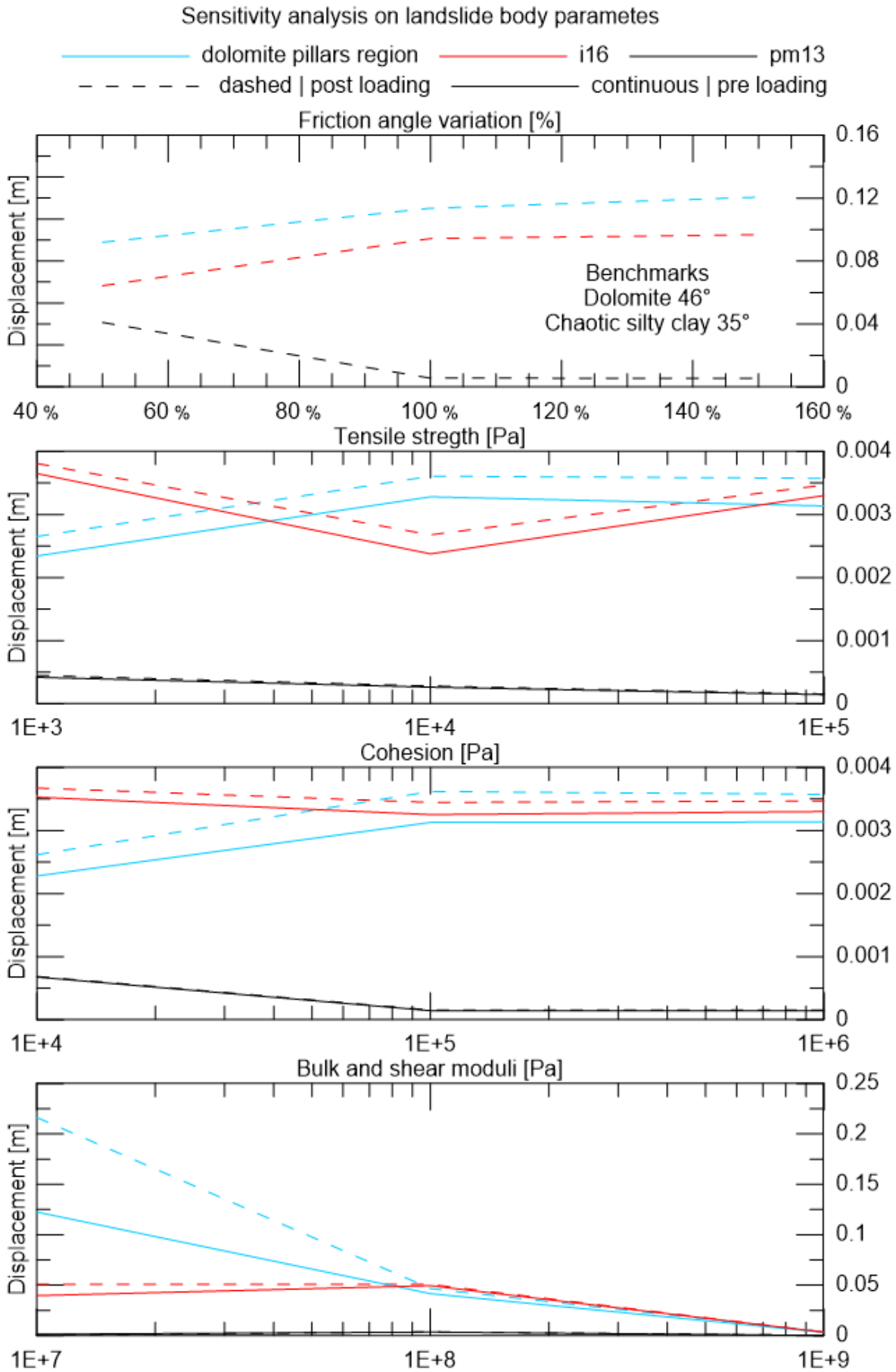


Figure 5-7 Sensitivity analysis on the landslide body materials

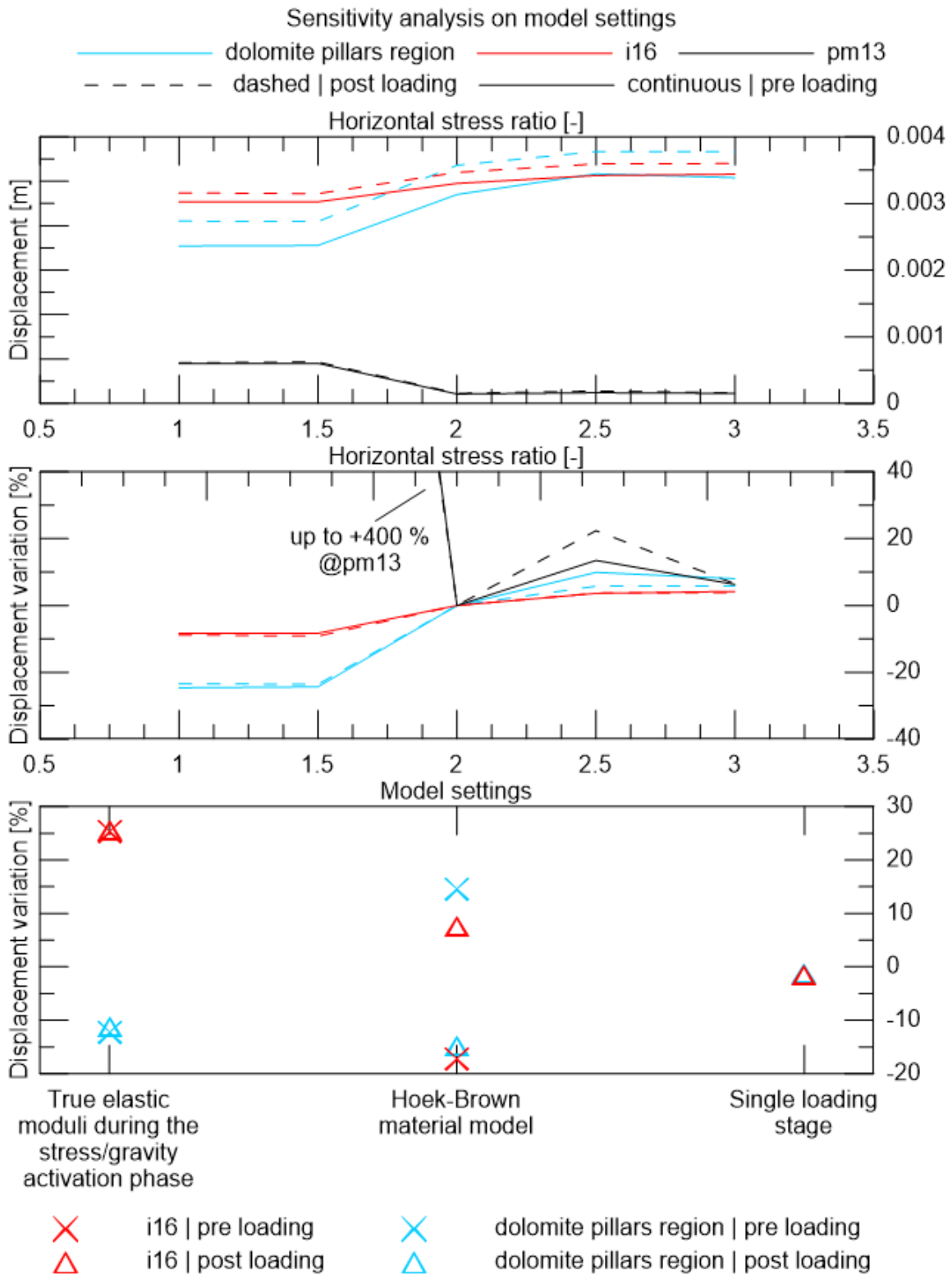


Figure 5-8 Sensitivity analysis on general model settings

The material properties used in modelling are listed in Table 5-3 compared to those obtained by lab testing used as a starting point.

Table 5-3 Material properties used in Flac3D modeling

GEOLOGY						
Material	Elastic moduli		Failure criterion [Mohr-Coulomb]			Unit weight $\rho$ [kg/m <sup>3</sup> ]
	Bulk K [GPa]	Shear G [GPa]	Friction angle $\phi$ [°]	Cohesion c [MPa]	Tensile strength $\sigma_t$ [MPa]	
<b>Lab</b>						
Dolomite	40.0	18.5	60	19	5.6	2690
Chaotic silty clay	10.6	7.9	27	13	3.5	2450
<b>Flac3D model</b>						
Dolomite pillars area	8.0	3.7	60	19	0.56	2690
Chaotic silty clay	2.1	1.6	27	13	0.35	2450
Stable bedrock	1800	930	linear elastic			2690
INTERFACE						
Material	Stiffness		Mesh	Failure criterion		
	Normal K <sub>n</sub> [GPa]	Shear K <sub>s</sub> [GPa]	Minimum width $\Delta z_{min}$ [m]	Friction angle $\phi$ [°]	Cohesion c [MPa]	Tensile strength $\sigma_t$ [MPa]
<b>Calculated from intact material properties (lab)</b>						
Dolomite	6.5	0.65	10	60	19	5.6
Chaotic silty clay	2.1	0.21	10	27	13	3.5
<b>Flac3D model</b>						
Dry slip surface	1.3	0.13	10	20	0.26	0.04
Wet slip surface	1.3	0.13	10	14	0.07	0.04

Normal and shear stiffness were calculated using the Alzo'ubi et alii formulation [57]. This relation was developed for numerical modelling. It correlates the elastic moduli of the materials in contact, i.e. bulk and shear, with the minimum width of the element in normal direction to the faces in contact.

The friction angle for the wet condition of the slip surface is set equal to 14° as found in literature [20] referred to a rotational-sliding slope movement on the East flank of the Passo della Morte landslide.

In Figure 5-9 the weathered material by water contact is shown, it has been assumed representative of the slip surface material.



*Figure 5-9 Weathered chaotic silty clay material at the Passo della Morte slip surface daylighting at the landslide toe*

As demonstrated in section 2.6, the landslide activation is triggered by severe rainfall events or rapid snowmelt [31]. Thanks to the availability of groundwater table monitoring data in piezometer I20 in the dolomite pillars area, it has been possible to discard the hypothesis of a large water storage capacity of the dolomite pillars area itself.

Based on the comparison between the monitored slope movements, groundwater levels and precipitation, it is reasonable to assume that a large amount of water infiltrates in the dolomite pillars zone reaching the chaotic silty clay at depth. The rough and irregular basal surfaces of the pillars embedded in the clayey substratum enhance the water infiltration, which flows through the slip surface reducing its shear strength. At the same time, a large amount of water flows in the Passo della Morte landslide through the dolomites severely fractured by overthrusting. The degradation of the mechanical properties of the slip surface in wet conditions can be assumed, given also the mineralogy analysis presented in subsection 4.1.6.

## **5.4 FINAL MODEL**

As far as the other slope materials are concerned, the disturbed rocks composing slip surface at Passo della Morte can be described as weak rocks, lying in between rock and soil. For this reason, their mechanical properties are obtained by back-analysis in the modelling stage and not tested in the lab. In particular, the parameters calibration was done by a manual trial-and-error procedure until an acceptable matching between simulated and recorded displacements fields, i.e. magnitude and distribution, was reached.

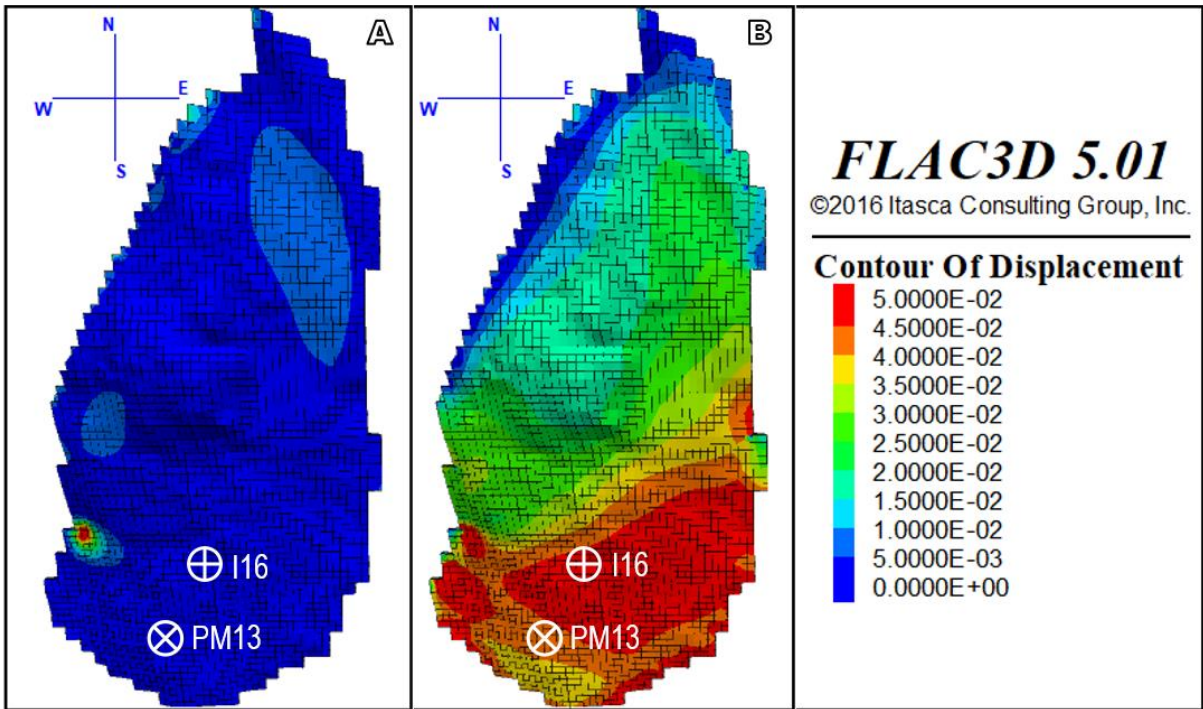


Figure 5-10 Displacements pre (A) and post (B) an extreme rainfall event, i.e. slip surface dry (A) and wet (B)

The displacements along the North-South section passing through the inclinometer I16 are presented in Figure 5-11.

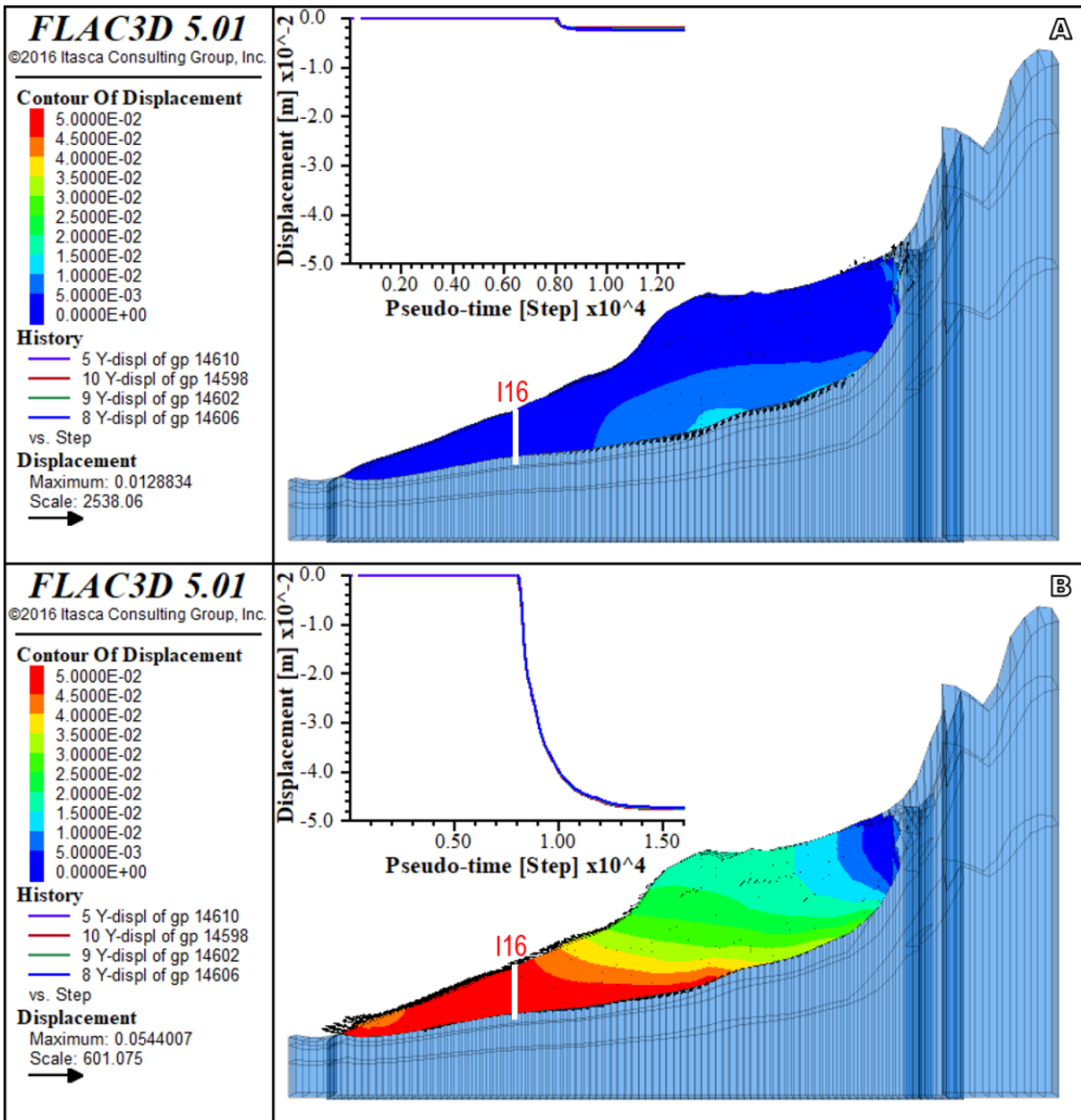


Figure 5-11 Section including I16 as reference, displacements pre (A) and post (B) an extreme rainfall event, i.e. slip surface dry (A) and wet (B)

Displacement profile at I16 axis is shown in Figure 5-12. The simulated displacements match with those measured at inclinometer I16 (ex S2N) [58]. The so-called S2N inclinometer was drilled nearby the nowadays-active I16. Periodic readings of S2N allow knowing a full-depth deformation profile instead of the subsequent I16, in which an in-place inclinometer has been installed in the supposed slip surface.

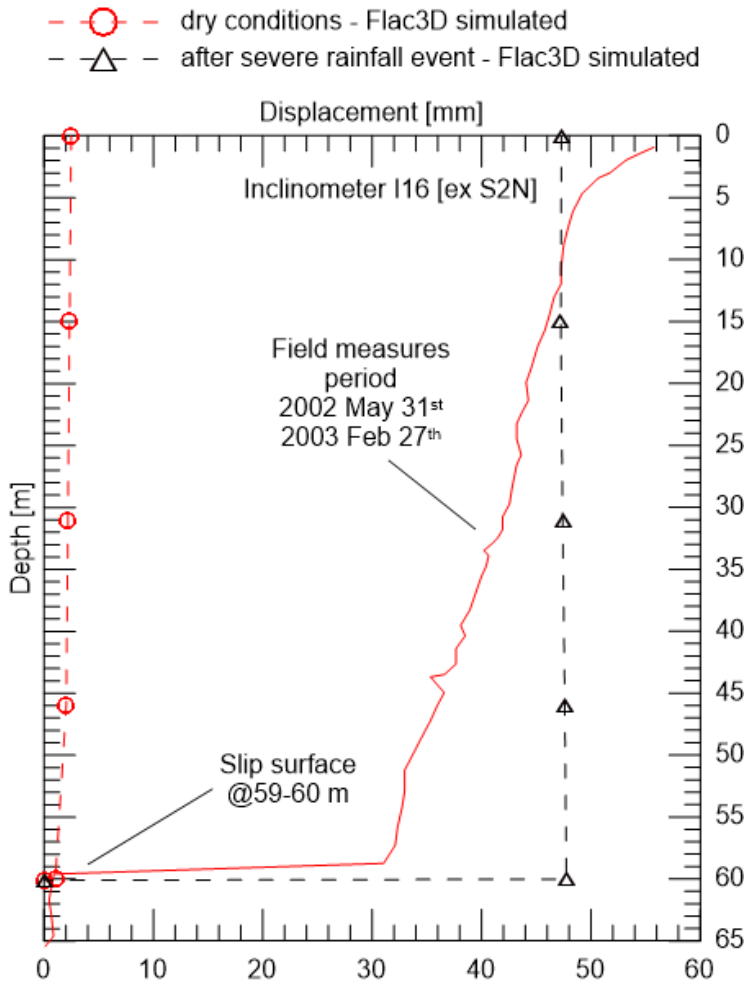


Figure 5-12 Simulated displacement profiles at I16

The model was calibrated matching the displacements recorded during an activation phase (Figure 5-12).

The obtained material properties are representative of an active landslide state. Parameters representative of a limit state equilibrium were defined too (Figure 5-10A, Figure 5-11A).

The alternation of active and dormant phases is shown in Figure 5-13. Each activation phase can be subdivided in an initial acceleration followed by some months of inertial movement until the complete stop. The year time in witch acceleration are concentrated is late autumn and spring when intense, warm precipitation events are coupled with intense snowmelt. The acceleration magnitude ranges in function of the cumulated rainfall and snowmelt. In case of long periods without rain, as in 2015, the activity is suspended.

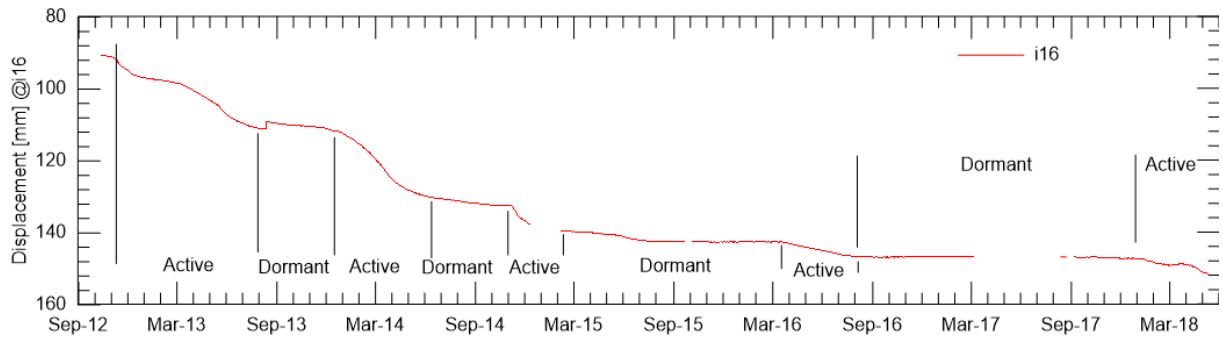


Figure 5-13 Activation phases

The parameters from back-analysis look confident with those expected. In chapter 4, the properties degradation of the slip surface material was explained. For the abovementioned reasons, this numerical model can be used as support in the countermeasures design.

## 6 CONCLUSIONS

The study presents a complex slope instability threatening a strategic infrastructure in Carnic Alps.

The final aim of the present research is increasing the serviceability level of the San Lorenzo road tunnel. This objective cannot be reached by stopping the displacements via consolidation works mainly because of the volume of the unstable rock mass. For this reason a series of countermeasures are proposed as conclusion of the document. Those remediation and mitigation works are suggested following the evidence of chapters 3, 4 and 5.

Geomorphological and hydrological settings explained in chapter 2 allowed to define geometry and kinematic of the landslide. The site climate is reported and the main events highlighted. In the end of the chapter, the tunnel project history was summarized.

More than ten years of monitoring data are shown in chapter 3. The weather station and inclinometers data series analysis allowed the identification of the triggering factors of Passo della Morte landslide. Furthermore, several field surveys and investigations carried out during this research were presented in order to lead to a better slope model definition. The structural health monitoring system was shown, it became possible to correlate landslide activity and lining damage. The decision of installing four new extensometers into the drainage tunnel was described.

The results of the laboratory tests presented in chapter 4 furnish a detailed characterization of the mechanical properties associated to the rock materials involved in the project. In the end of the section, the preliminary results of an X-ray diffraction test are shown in order to highlight the presence of a water sensitive component in the chaotic silty clay formation.

The numerical simulations are presented in chapter 5, those analysis play a key role in the final countermeasures planning. Modelling allows identifying the fundamental role played by the water sensitive material founded in the sliding surface. A 3D Finite Difference code has been used for the simplified simulations of the instable slope. A series of numerical simulations are carried out with Flac3D in order to test the model reliability. Furthermore, a sensitivity analysis was completed testing model parameters and settings. In the end, a landslide activation following a severe rainfall event is simulated through the degradation of the slip surface properties. This hypothesis should reproduce the rheological change of the material when in contact with water.

### 6.1 PROPOSED COUNTERMEASURES

A decade after the drainage tunnel construction, its effectiveness in the neighborhood of the East portal can be demonstrated. Firstly, the water table level in piezometer P23 decreased of about 51 cm per year (Figure 6-1). Secondly, as a direct effect of the groundwater table lowering, the landslide 2 has been almost stabilized [33]. At the moment, the upper part of the landslide 2 is moving at the same rate of Passo della Morte landslide.

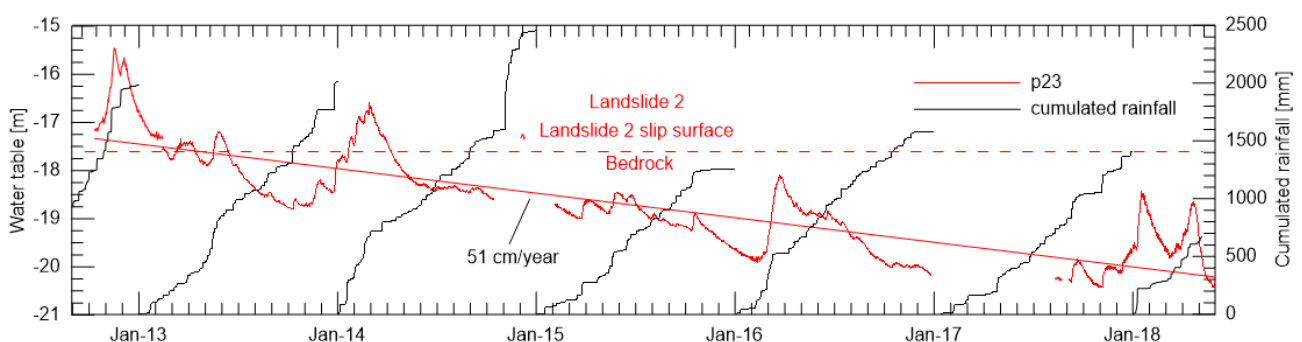


Figure 6-1 Drainage tunnel effect: water table level at P23, landslide 2 area

Considering the mentioned effectiveness of the drainage tunnel and the hydro-geological field evidences, an extension of the drainage tunnel up to the overthrust dolomite seems fundamental to reduce duration and intensity of the water seepage into the San Lorenzo tunnel. A schematic section view of the drained area is shown in Figure 6-2.

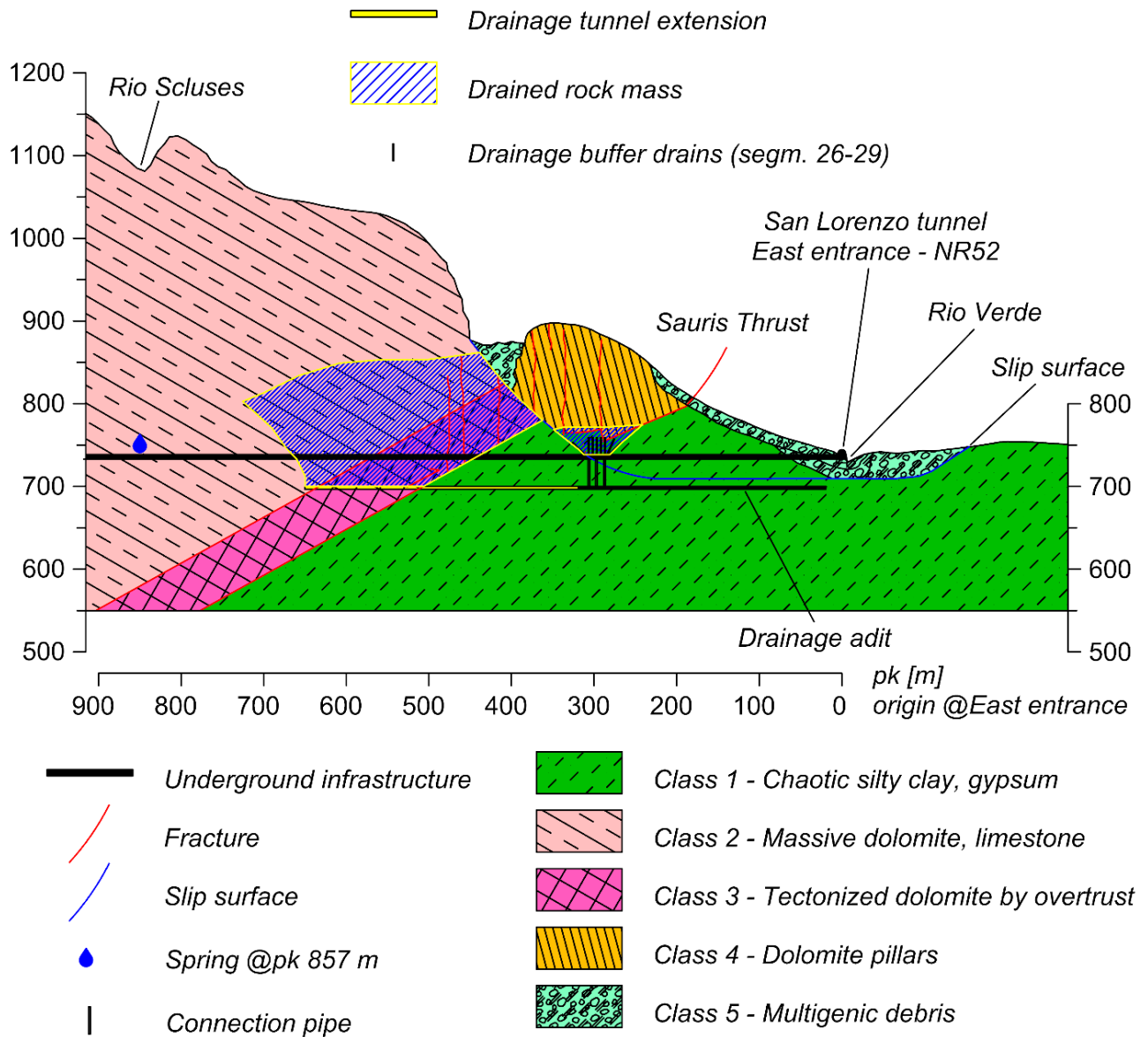


Figure 6-2 Dewatering expected effectiveness of the drainage tunnel extension

In Figure 6-3 the proposed countermeasure works is depicted. This design includes an extension of the drainage tunnel reaching the aquifer hosted in the severely fractured dolomite. Two large diameter wells are also proposed to complete the dewatering of the landslide (CNR ID 2) at the East entrance and finally a series of 40 m long drains from the East front of the drainage tunnel are designed to catch the groundwater in the coarse material of the Rio Verde paleo-streambed.

In the end, a series of radial drains between segments 26 and 29 should catch part of the water infiltrating from the dolomite pillars area to the slip surface.

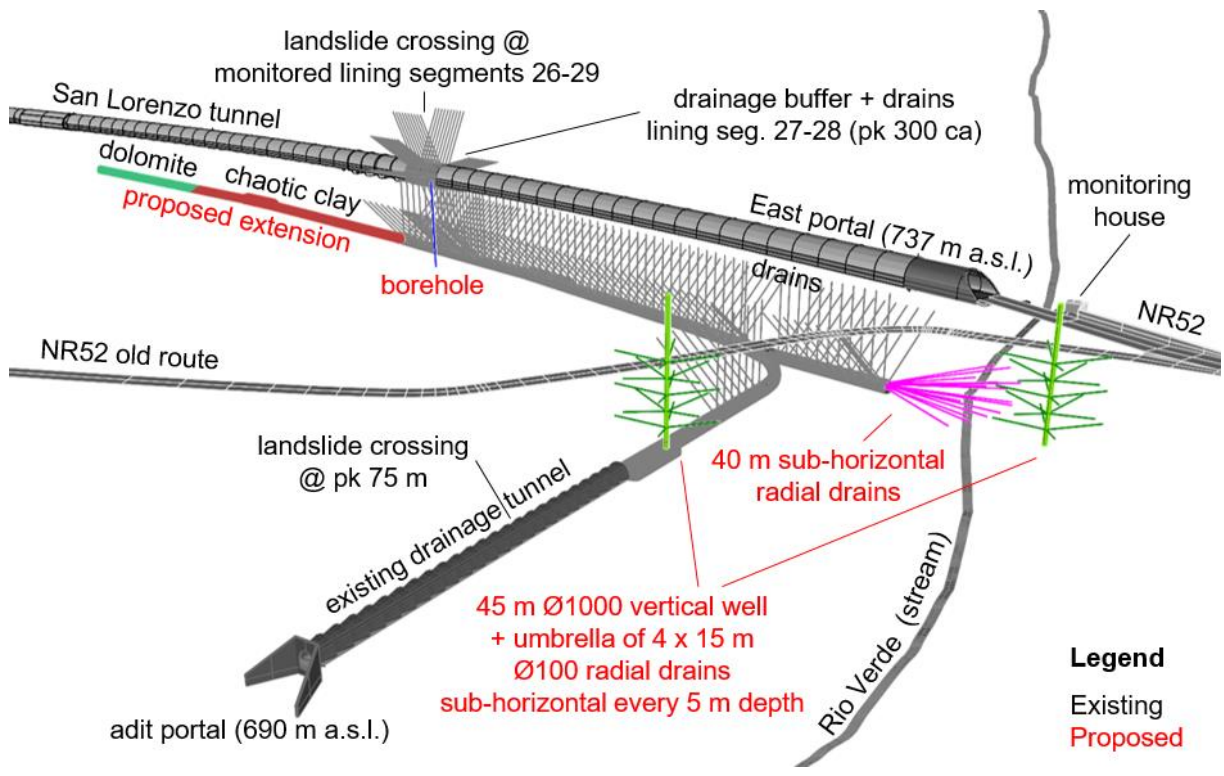


Figure 6-3 Proposed countermeasure works

The proposed countermeasures works will not solve definitely the San Lorenzo tunnel problems but they will improve the expected life of the infrastructure and its serviceability level.

## 7 REFERENCES

- [1] Wikipedia. "Diga di Sauris" 2018. [Online]. Available: [https://it.wikipedia.org/wiki/Diga\\_di\\_Sauris](https://it.wikipedia.org/wiki/Diga_di_Sauris).
- [2] G. Marcato, "Valutazione della pericolosità da frana in località Passo della Morte", Unpublished PhD Thesis, University of Modena and Reggio Emilia, 2007.
- [3] M. Panizza, M., Pasuto, A., Silvano, S., Soldati, "Landsliding during the Holocene in the Cortina d'Ampezzo Region, Italian Dolomites", *Rapid mass movement as climatic evidence for Holocene times. Paläoklimaforschung/Palaeoclimate Research*, vol. 19, pp. 17–31, 1997.
- [4] Comune di Forni di Sotto, "Storia di Forni di Sotto," 2018. [Online]. Available: <http://www.comune.fornidisotto.ud.it/index.php?id=3323>.
- [5] F. Guzzetti, "Landslide fatalities and the evaluation of landslide risk in Italy", *Eng. Geol.*, vol. 58, pp. 89–107, 2000.
- [6] A. Cavallin and B. Martinis, "Studio geologico della grande frana di Borta (Ampezzo)", *Alto*, vol. LVII, 1974.
- [7] A. P. Dykes, E. N. Bromhead, S. M. Hosseyni, and M. Ibsen, "A geomorphological reconnaissance of structurally-controlled landslide in the Dolomites", *International Conference on Vajont - 1963-2013 - Thoughts and analyses after 50 years since the catastrophic landslide*, no. 6, pp. 133–140, 2013.
- [8] G. Grillo, "Una targa per i morti del Bivera", *Messaggero Veneto*, Trieste, p. 34, 26-Sep-2006.
- [9] G. Pisa, "La geologia dei monti a Nord di Forni di sotto (Carnia occidentale)", *Giorn.Geol.*, vol. Ser 2, 38, no. II, pp. 543–688, 1972.
- [10] S. Marazzi, *SOIUSA - Suddivisione orografica internazionale unificata del Sistema Alpino*. 2005.
- [11] G. Bressan, A. Snidarcig, and C. Venturini, "Present state of tectonic stress of the Friuli area (Eastern Southern Alps)", vol. 292, pp. 211–227, 1998.
- [12] C. Venturini and G. B. Carulli, "Neoalpine structural evolution of the Carnic Alps central core (Mt. Amariana, Mt. Plauris, Mt. San Simeone)", *Mem. della Soc. Geol. Ital.*, vol. 57, 2002.
- [13] G. . Carulli, A. Cozzi, G. L. Salvador, E. Pernarcic, F. Podda, and M. Ponton, "Geologia delle Prealpi carniche", Edizioni del Museo Friulano di Storia Naturale, Udine, 2000.
- [14] D. Codeglia, N. Dixon, G. Bossi, and G. Marcato, "Alpine landslide risk scenario: run-out modelling using a 3D approach", *Rend. della Soc. Geol. Ital.*, pp. 14–17, 2017.
- [15] D. Codeglia, N. Dixon, G. John, and G. Marcato, "Analysis of acoustic emission patterns for monitoring of rock slope deformation mechanisms", *Eng. Geol.*, vol. 219, pp. 21–31, 2017.
- [16] A. Scuri, "Analisi cinematica, idrogeologica e proposte di intervento per il dissesto in sinistra idrografica del Rio Verde, in località Passo della Morte (UD)", Unpublished M.Sc.thesis, University of Padova, 2013.
- [17] G. Monegato, C. Ravazzi, M. Donegana, R. Pini, G. Calderoni, and L. Wick, "Evidence of a two-fold glacial advance during the last glacial maximum in the Tagliamento end moraine system (Eastern Alps)", *Quat. Res.*, vol. 68, no. 2007, pp. 284–302, 2007.
- [18] McColl ST , Davies TRH , McSaveney MJ, "Glacier retreat and rock-slope stability : debunking debuttering", Association for Engineering Geology and the Environment , Auckland , Aotearoa , 5-10 September 2010, 2010.

- [19] F. Cervi, L. Borgatti, G. Dreossi, G. Marcato, M. Michelini, and B. Stenni, "Isotopic features of precipitation and groundwater from the Eastern Alps of Italy : results from the Mt . Tinisa hydrogeological system", *Environ. Earth Sci.*, vol. 76, no. 12, pp. 1–17, 2017.
- [20] G. Sinigardi, G. Bossi, A. Scuri, G. Marcato, and L. Borgatti, "Geological and numerical models as a tool to manage landslide risk: The Passo della Morte case study (UD, Italy)", *Rend. Online Soc. Geol. Ital.*, vol. 34, pp. 46–53, 2015.
- [21] DICAM, "Relazione Idrogeologia Passo della Morte", Unpublished report, Bologna, 2015.
- [22] C. Venturini, "Note illustrative della carta geologica d'Italia al 1:50.000 foglio 031 Ampezzo", ISPRA - Servizio Geologico d'Italia, p. 232, 2007.
- [23] Vicenzetto, "Indagine geognostica Vicenzetto 035CM02", ANAS unpublished report, Trieste, 2002.
- [24] M. Mattioli, "Analisi dei dissesti per frana che coinvolgono le opere d'arte stradali in prossimità del corso del Rio Verde sulla S.S. n° 52 'Carnica' (Forni di Sotto, UD). Studio idrogeologico per la valutazione dei possibili interventi di mitigazione", Unpublished M.Sc. thesis, University of Bologna, 2015.
- [25] F. Petronici, L. Borgatti, F. Cervi, and L. Piccinini, "Hydrogeological monitoring and modelling in the S . Lorenzo road tunnel area ( Passo della Morte , Udine ) for the design of countermeasure works", *Rend. Online Soc. Geol. Ital.*, vol. 39, pp. 93–96, 2016.
- [26] G. Sinigardi, "Mitigation of landslide risk along S.R. 52 "Carnica" (Forni di Sotto, UD). Analysis of possible countermeasure works", Unpublished M.Sc. thesis, University of Bologna, 2014.
- [27] Cruden, D.M., and Varnes, D.J., "Landslide Types and Processes", Special Report , Transportation Research Board, National Academy of Sciences, 247:36-75, no. January, 1996.
- [28] S. Pellizza, "Relazione B, geotecnica della galleria di San Lorenzo", ANAS unpublished report, Torino, 2002.
- [29] V. Marzi, "Collaudo della variante ANAS di Passo della Morte", ANAS unpublished report, 2014.
- [30] Società Geotecnica Italiana, "Interventi per la sicurezza della galleria di Passo della Morte", ANAS unpublished report, 1998.
- [31] G. Bossi, L. Schenato, G. Marcato, "Structural Health Monitoring of a Road Tunnel Intersecting a Large and Active Landslide", *Ap. Scien.*, vol.7, no.12, 2017.
- [32] D. Codeglia, "Internship final report", CNR unpublished report, 2009.
- [33] G. Marcato, G. Bossi, A. Pasuto, L. Schenato, and S. Frigerio, "Relazione Finale convenzione CNR-ANAS", ANAS unpublished report, Trieste, 2014.
- [34] L. Noferini, M. Pieraccini, D. Mecatti, G. Macaluso, C. Atzeni, M. Mantovani, G. Marcato, A. Pasuto, S. Silvano, and F. Tagliavini, "Using GB-SAR technique to monitor slow moving landslide", *Eng. Geol.*, vol. 95, pp. 88–98, 2007.
- [35] E. Hoek, T. G. Carter, and M. S. Diederichs, "Quantification of the Geological Strength Index Chart", *47th US Rock Mech. Symp.*, 13-672, 2013.
- [36] R. M. Holt, M. Brignoli, and C. J. Kenter, "Core quality : quantification of coring-induced rock alteration", *Int. J. Rock Mech. Min. Sci.*, vol. 37, pp. 889–907, 2000.
- [37] ISRM, "Suggested methods for determining sound velocity," in *The complete ISRM suggested methods for rock characterization, testing and monitoring: 1974-2006*, R. Ulusay

and J. A. Hudson, Eds. 2007, pp. 113–120.

- [38] E. A. Eissa and A. Kazi, "Relation between static and dynamic Young's moduli of rocks", *Int. J. Rock Mech. Min. Sci.*, vol. 25, no. 6, pp. 479–482, 1988.
- [39] J. Martínéz-martínéz, D. Benavente, and M.A. Garcia-del-Cura, "Comparison of the static and dynamic elastic modulus in carbonate rocks", *Bull.Eng.Geol. Environ.*, vol. 71, pp. 263–268, 2012.
- [40] S. Elkhatny, M. Mahmoud, and I. Mohamed, "Development of a new correlation to determine the static Young's modulus", *J. Pet. Explor. Prod. Technol.*, vol. 8, no. 1, pp. 17–30, 2018.
- [41] M. C. Spreafico, "Lateral spreading and associated slope processes in fractured rock slabs", Unpublished PhD thesis, University of Bologna, 2015.
- [42] E. Hoek, D. Wood, and S. Shah, "A modified Hoek-Brown failure criterion for jointed rock masses" in *International ISRM Symposium on rock characterization*, Chester, UK, September, 1992.
- [43] E. Hoek, C. Carranza-Torres, and B. Corkum, "Hoek-Brown failure criterion – 2002 Edition," in *5th North American Rock Mechanics Symposium*, vol. 1, pp. 267–273, 2002.
- [44] ISRM, "Suggested methods for determining the uniaxial Compressive Strength and deformability of rock materials" in *The complete ISRM suggested methods for rock characterization, testing and monitoring: 1974-2006*, R. Ulusay and J. A. Hudson, Eds. 2007, pp. 151–156.
- [45] N. A. Al-shayea, "Effects of testing methods and conditions on the elastic properties of limestone rock," vol. 74, pp. 139–156, 2004.
- [46] ISRM, "Suggested methods for duggedged methods for determining point load strength" in *The complete ISRM suggested methods for rock characterization, testing and monitoring: 1974-2006*, R. Ulusay and J. A. Hudson, Eds. 2007, pp. 121–132.
- [47] ISRM, "Suggested methods for deteremining block punch strength index (BPI)" in *The complete ISRM suggested methods for rock characterization, testing and monitoring: 1974-2006*, R. Ulusay and J. A. Hudson, Eds. 2007, pp. 141–149.
- [48] H. Ā. Gercek, "Poisson' s ratio values for rocks", *Int. J. Rock Mech. Min. Sci.*, vol. 47, no. 6, pp. 974–982, vol. 44, pp. 1–13, 2007.
- [49] ISRM, "Suggested methods for determining the strength of rock materials in triaxial compression" in *The complete ISRM suggested methods for rock characterization, testing and monitoring: 1974-2006*, R. Ulusay and J. A. Hudson, Eds. 2007, pp. 157–164.
- [50] Rocscience, "RocData", Toronto, Canada, 2015.
- [51] J. Claesson and B. Bohloli, "Brazilian test : stress field and tensile strength of anisotropic rocks using an analytical solution", *Int. J. Rock Mech. Min. Sci.*, vol. 39, pp. 991–1004, 2002.
- [52] ISRM, "Suggested methods for determining tensile strength of rock materials" in *The complete ISRM suggested methods for rock characterization, testing and monitoring: 1974-2006*, R. Ulusay and J. A. Hudson, Eds. 2007, pp. 177–180.
- [53] M. A. Perras and M. S. Diederichs, "Journal of Rock Mechanics and Geotechnical Engineering Predicting excavation damage zone depths in brittle rocks", *J. Rock Mech. Geotech. Eng.*, vol. 8, no. 1, pp. 60–74, 2016.
- [54] Itasca consulting group, "Flac 3D v5.01", Indianapolis, United States, 2016.
- [55] B. Abbasi, D. Russell, and R. Taghavi, "FLAC 3D mesh and zone quality", report, 2009

- [56] Ministero dell'Ambiente, "Geoportale cartografico nazionale." [Online]. Available: <http://www.pcn.minambiente.it/viewer/>.
- [57] A. K. Alzo'ubi, C. D. Martin, and D. M. Cruden, "Influence of tensile strength on toppling failure in centrifuge tests", *Int. J. Rock Mech. Min. Sci.*, vol. 47, no. 6, pp. 974–982, 2010.
- [58] Vidoni, "Risultante movimenti per punti tubo S2N", ANAS unpublished report, 2003.

# 8 APPENDIX

## 8.1 CONDUITS AND DRAINAGE TUNNEL WATER DISCHARGE

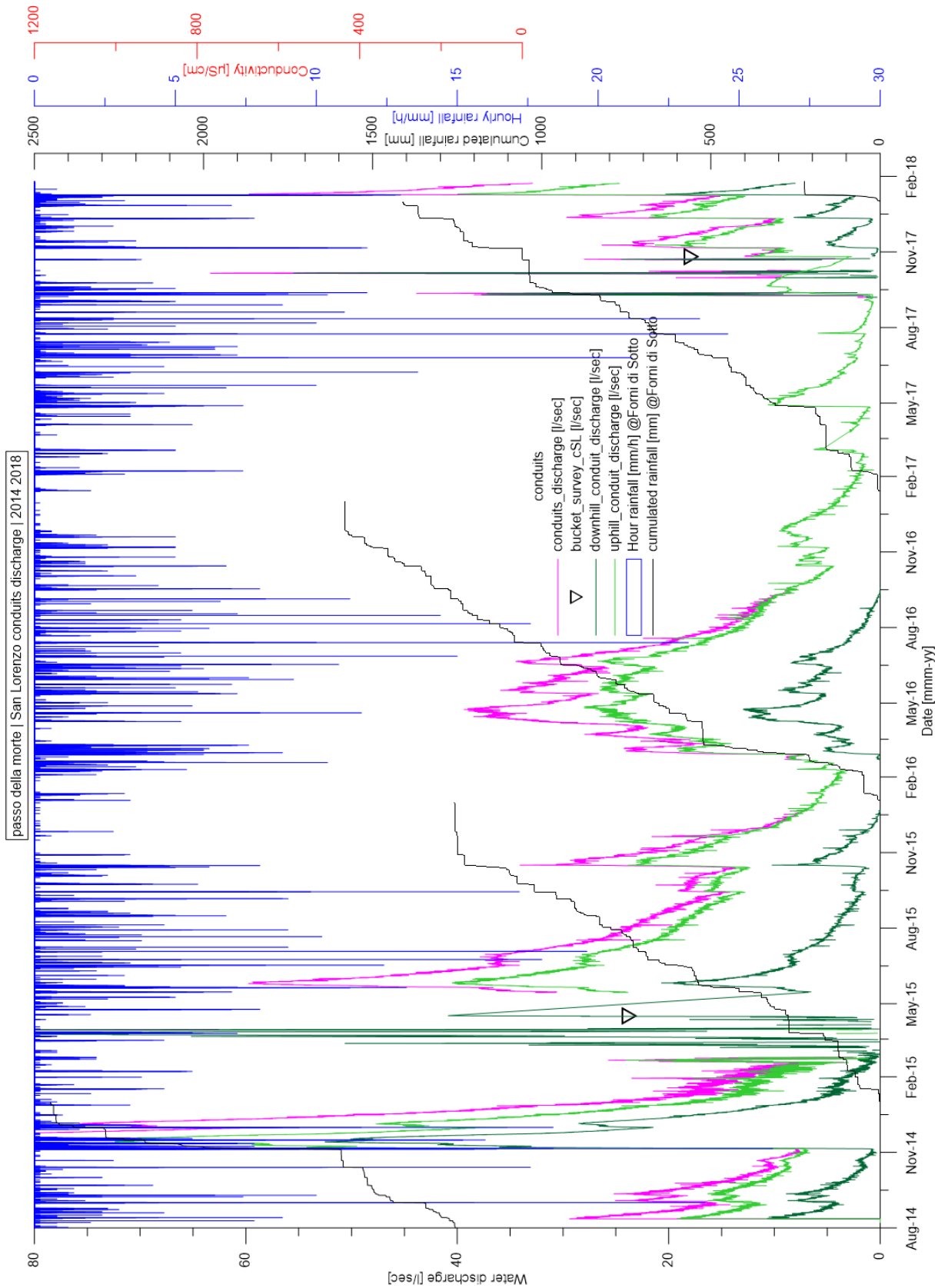


Figure 8-1 Conduits discharge (2014-2018)

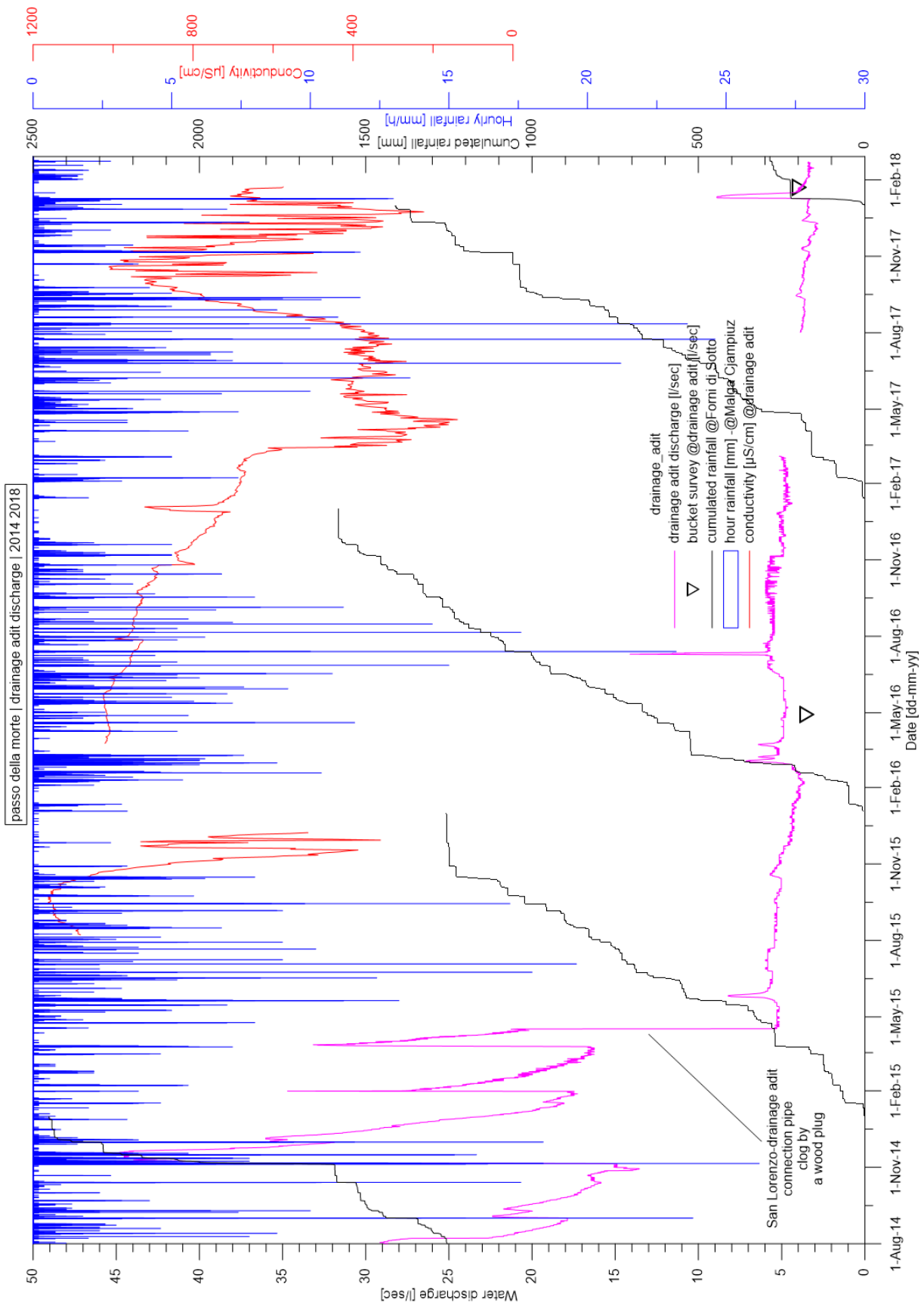


Figure 8-2 Drainage adit discharge (2014-2018)

## 8.2 INSTRUMENTATION INSTALLED SINCE 1999

Table 8-1 Instrumentation installed, since 1999

ID ANAS abandoned	ID CNR	Installation [yyyy-mm-dd]	Sensor	Depth [m]	Representativeness	Active
I 1	I 1	1999-04-21	inclinometer	72	poor	
I 2	I 2	1999-04-21	inclinometer	76	good	
I 3	I 3	1998-10-30	inclinometer	93	good	
I 4	I 4	1998-10-30	inclinometer	35	good	
I 5	I 5	1999-03-03	inclinometer	46	good	
I 5 bis	I 6	1999-11-04	inclinometer	50	good	
I 6	I 7	1999-03-03	inclinometer	58	good	
I 8	I 8	1999-11-03	inclinometer	75	good	
S1N	I 17	2001-06-14	inclinometer	53	good	
			in place inclinometer	24	poor	
			in place inclinometer	34	poor	
S 2	I 9	1998-08-04	inclinometer	20	no	
S2 bis	I 10	1998-08-04	inclinometer	41	no	
S2 N	I 16	2001-06-12	inclinometer	65	poor	
			in place inclinometer	20	poor	
			in place inclinometer	57	poor	
S 3	I 14	1998-08-04	inclinometer	65	poor	
S3 N	I 15	2001-06-13	inclinometer	38	poor	
			in place inclinometer	17	poor	
			in place inclinometer	30	poor	
S4 N	I 13	2001-06-13	inclinometer	80	good	
			in place inclinometer	20	poor	
			in place inclinometer	61	poor	
G2 I	I 11	2001-06-15	inclinometer	70	poor	
			in place inclinometer	20	poor	
			in place inclinometer	25	poor	
G4 I	I 12	2001-06-15	inclinometer	100	poor	
			in place inclinometer	24	poor	
			in place inclinometer	35	poor	
S 5	I 18	2003-04-18	inclinometer	80	data not available	x
AM12	I 19	2005-05-04	inclinometer	250	poor	
AM14	I 20	2005-05-05	inclinometer	250	poor	
AM15	I 21	2004-08-15	inclinometer	100	good	
AM4 A	T1	2003-04-30	TDR	80	data not available	
AM5 A	T2	2003-04-18	TDR	80	data not available	
AM6	T3	2003-04-08	TDR	80	data not available	
S1	P1	2002-06-06	piezometer	80	poor	
S2	P2	2002-06-06	piezometer	60	poor	
S3	P3	2002-06-06	piezometer	37	poor	
S4 P	P4	2002-06-06	piezometer	67	data not available	x
G1 P	P5	2002-04-10	piezometer	49	poor	
G3 P	P6	2002-04-08	piezometer	70	poor	
G3 P bis	P7	2002-04-09	piezometer	10	poor	

G5 P	P8	2002-03-26	piezometer	51	poor	
G5P bis	P9	2002-03-26	piezometer	9	poor	
G6 P	P10	2002-04-04	piezometer	44	poor	
G6 P bis	P11	2002-04-04	piezometer	32	poor	
P1	P12	2000-08-03	Casagrande piezometer		poor	
P2	P13	2000-08-03	Casagrande piezometer		poor	
P3	P14	2000-08-03	Casagrande piezometer		poor	
P5	P15	2000-08-03	Casagrande piezometer		poor	
P6	P16	2000-08-03	Casagrande piezometer		poor	
P7	P17	2000-08-03	piezometer		poor	
Pz1	Pz1		pressure gauge		data not available	
Pz3	Pz3		pressure gauge		data not available	
Pz5	Pz4		pressure gauge		data not available	
AM3	P18	2003-06-19	piezometer	40	data not available	x
AM4	P19	2003-06-19	piezometer	50	data not available	x
AM5	P20	2003-06-19	piezometer	50	data not available	x
S5 N	P21		piezometer	50	data not available	x
AM8	P20	2004-08-02	piezometer	70	data not available	x
Cl1	Cl1	2003-08-16	clinometer		poor	
Cl2	Cl2	2003-08-16	clinometer		poor	
Cl3	Cl3	2003-08-16	clinometer		poor	
FS1	Fs1	2003-11-06	crackmeter		poor	
FS2	Fs2	2003-11-06	crackmeter		poor	
FS3	Fs3	2003-11-06	crackmeter		poor	
FS4	Fs4	2003-11-06	crackmeter		poor	
DEC.1	E1	2003-03-24	extensometer		good	x
DEC.2	E2	2003-03-24	extensometer		good	
DEC.3	E3	2003-03-24	extensometer		poor	
CENT.1	E4	2003-03-24	extensometer		poor	
CENT.2	E5	2003-03-24	extensometer		good	
CENT.3	E6	2003-03-24	extensometer		good	

**If not specifically mentioned, in the text the instrumentation name is referred to ID CNR**



## 8.4 X RAY DIFFRACTION

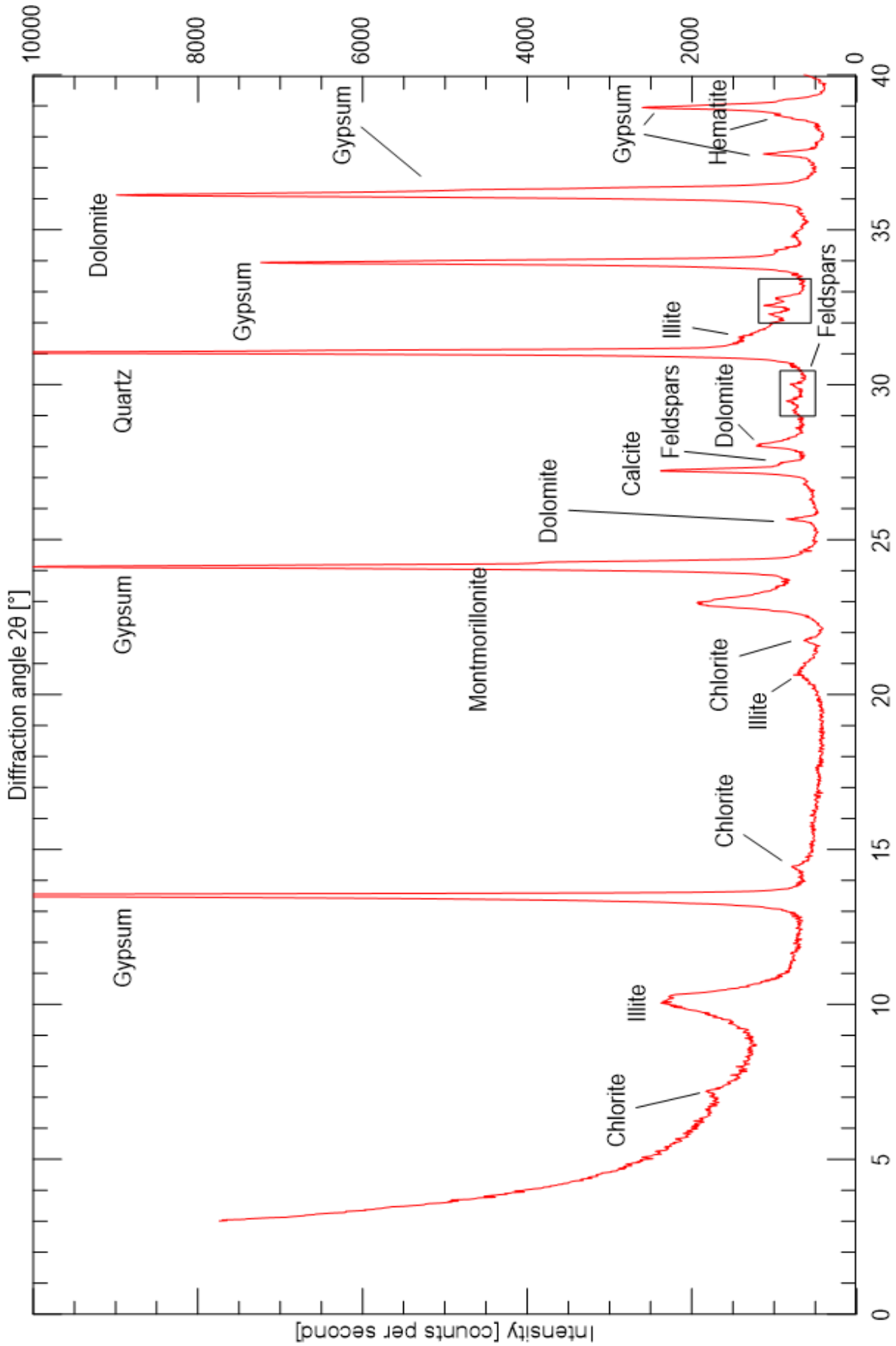


Figure 8-4 X ray diffraction on G4I sample

## 8.5 SAN LORENZO MONITORING HOMEPAGE

Benvenuto in Galleria San Lorenzo

monpulse.it/sanlorenzo/

Galleria San Lorenzo Home Contatti Chi Siamo Data Zoom Galleria Cunicolo HeatMap MaxDisp Annual trend coopsette

### Benvenuto coopsette

Questo sezione illustra le funzionalità di monitoraggio strutturale della galleria "San Lorenzo", SS52 "Carnica" - Comune Forni di Sotto (UD)

[Al monitoraggio galleria](#)

Questo sezione illustra le funzionalità di monitoraggio del cunicolo drenante a servizio della galleria

[Al monitoraggio cunicolo](#)

### Diagnostica

Stato batterie datalogger				Webcam
Posizione	Data	Tensione [V]	Status	Ingresso galleria
Galleria	2018-07-27 14:32:01	6.577		
Esterno	2018-07-27 14:32:04	7.176		

Figure 8-5 Home-page of the CNR-ANAS monitoring online portal

## 8.6 SENSITIVITY ANALYSIS DISPLACEMENTS

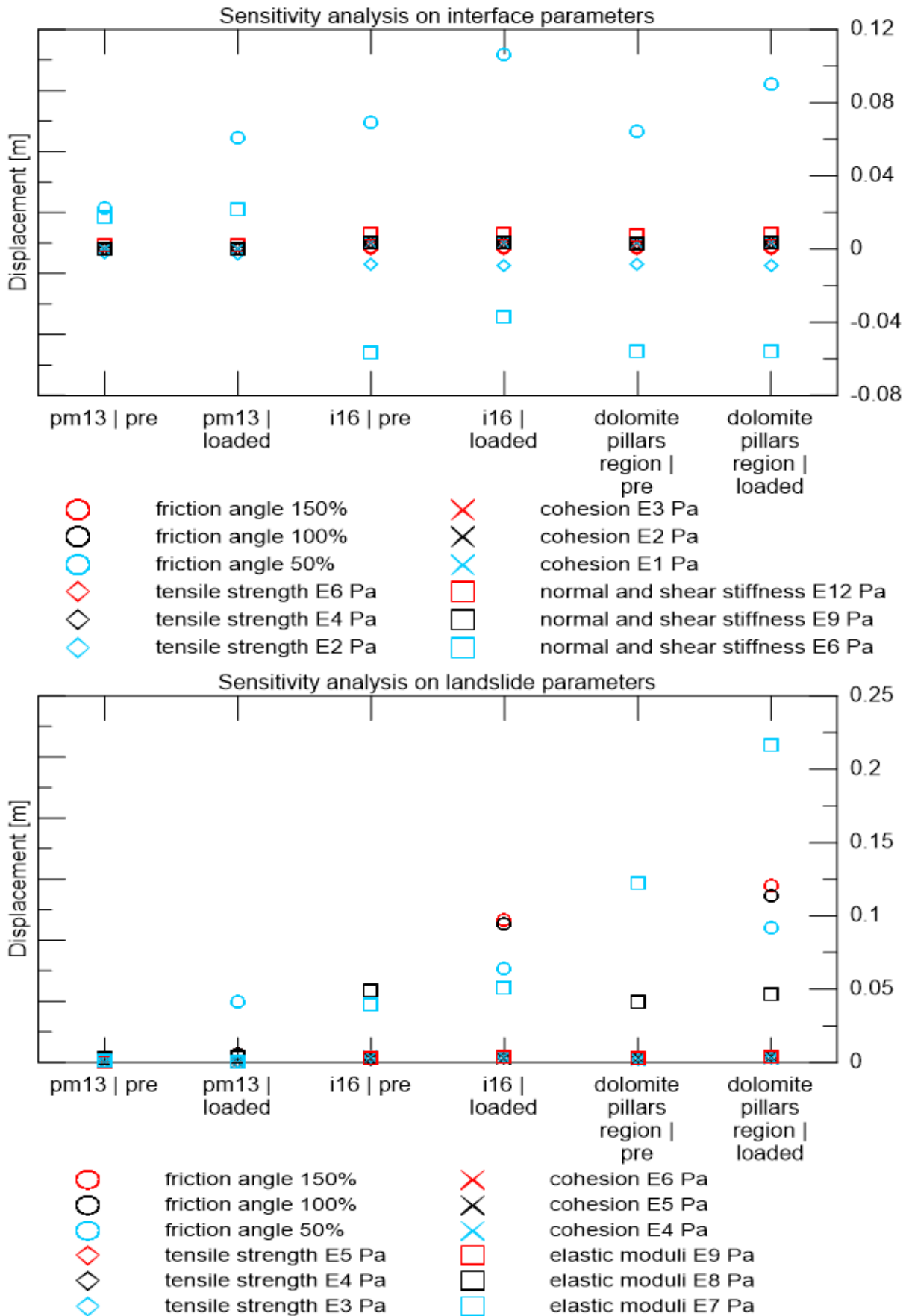


Figure 8-6 Sensitivity analysis absolute displacements. Top-down: on slip surface (interface) and landslide body properties

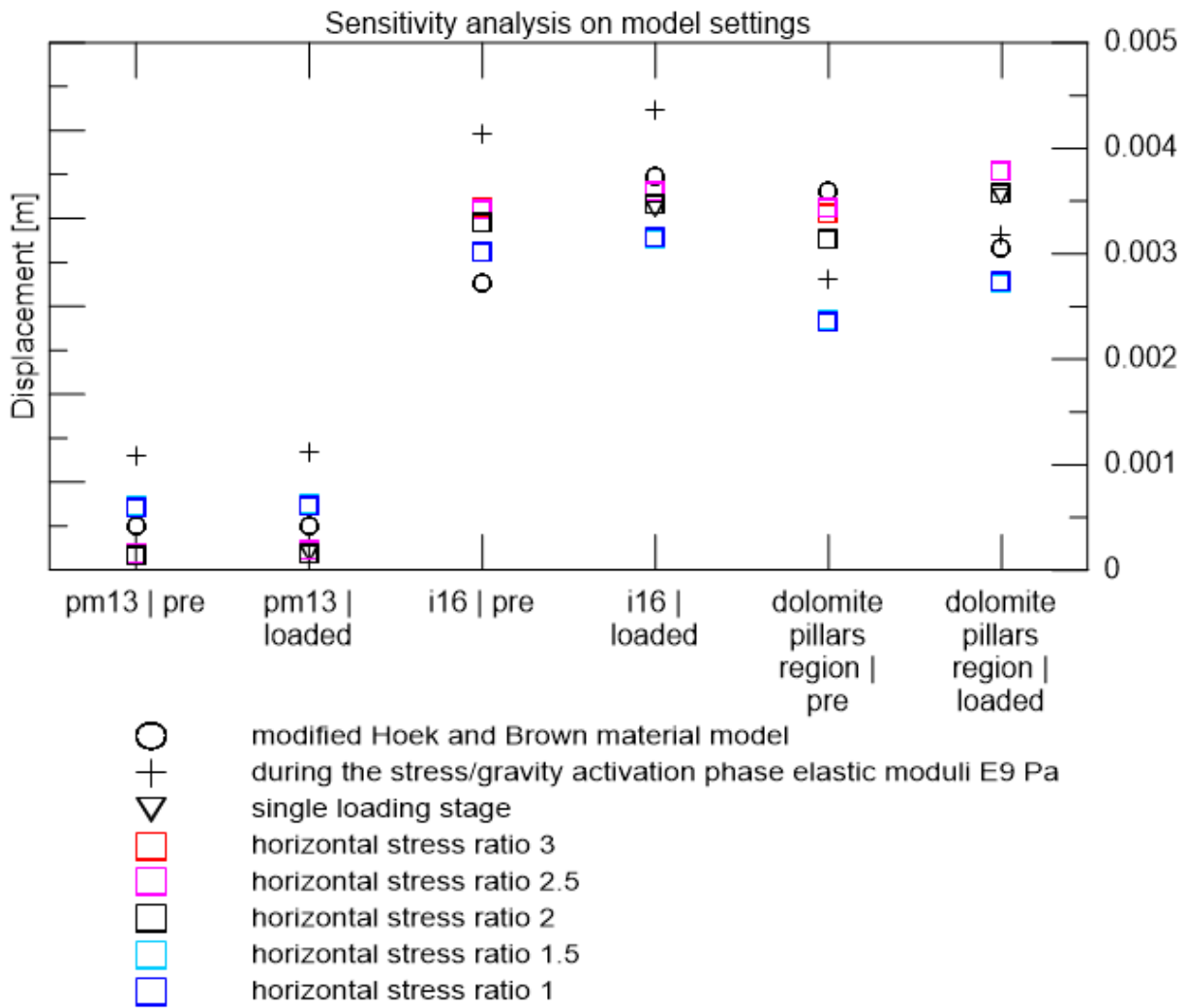


Figure 8-7 Sensitivity analysis absolute displacements on model settings variation